Implementation of OMS-Based Scour Prediction and Real-Time Monitoring of Scour Processes for Alabama Bridges

FINAL REPORT

Prepared by

Jose G. Vasconcelos, Ph.D.
J. Brian Anderson, Ph.D., P.E.
Murilo H. P Tarozzo
T. Excie Guillot
Luis F. Castaneda Galvis

Department of Civil Engineering
Auburn University

Submitted to

Alabama Department of Transportation
Montgomery, Alabama

APRIL 2025

Highway Research Center
Harbert Engineering Center
Auburn University, Alabama 36849

1. Report No. ALDOT 931-053	**2. Government Accession No.**	**3. Recipient Catalog No.**
4 Title and Subtitle Implementation of OMS-Based Scour Prediction and Real-Time Monitoring of Scour Processes for Alabama Bridges		**5 Report Date** March 2025 **6 Performing Organization Code**
7. Author(s) Jose G. Vasconcelos, Ph.D., J. Brian Anderson, Ph.D., P.E., Murilo Tarozzo, T. Excie Guillot, Luis F. Castaneda Galvis		**8 Performing Organization** Highway Research Center, Auburn University
9 Performing Organization Name and Address Highway Research Center Department of Civil Engineering 238 Harbert Engineering Center Auburn, AL 36849		**10 Work Unit No. (TRAIS)** **11 Contract or Grant No.**
12 Sponsoring Agency Name and Address Alabama Department of Transportation 1409 Coliseum Boulevard Montgomery, AL 36130-3050		**13 Type of Report and Period Covered** 14 **Sponsoring Agency Code**
15 **Supplementary Notes**		

16 Abstract

This research compares the current methods used by ALDOT in developing bridge pier scour calculations, based on FHWA HEC-18, with alternative methods using the Observational Method for Scour and propose methods for pier scour real time monitoring. The work performed entailed the development of pier scour depth estimates in four Alabama bridges using a range of hydrological and hydraulic approaches. Various peak flow estimation methods—Regional Regression Equations (RRE), Flood Frequency Analysis (FFA), and HEC-HMS 4.9 with SCS Curve Number—were used, with results analyzed through HEC-18 and the Observational Method for Scour (OMS). Hydraulic modeling to compute scour velocities was conducted with HEC-RAS 6.1/6.2, incorporating 1D and 2D approaches. The research determined that RRE, commonly used by ALDOT, frequently did not correspond to the most conservative peak flow rate predictions. Also, it was found that 2D approaches were better at capturing velocity distributions resulting in more representative pier scour depth predictions. OMS yielded scour estimates that were smaller than HEC-18 by at least 20% across the studied bridges. Additionally, long-term scour monitoring using sonar sensors proved to be a simple, low-cost, deployable, and reliable strategy, though requiring periodic visits for simple maintenance. Such approaches can be seen as part of monitoring efforts that could be applied in bridge structures that could be more at risk of excessive scour to ensure their safety.

17 Key Words Hydrologic modeling, pier scour, bridges		**18 Distribution Statement** No restrictions.	
19 Security Classification (of this report) Unclassified	**20 Security Classification (of this page)** Unclassified	**21 No. of pages** 147	**22 Price** None

DRAFT Final Report

Implementation of OMS-Based Scour Prediction and Real-Time Monitoring of Scour Processes for Alabama Bridges

Submitted to

The Alabama Department of Transportation

Prepared by

Jose G. Vasconcelos, Ph.D.
J. Brian Anderson, Ph.D., P.E.
Murilo H. P. Tarozzo
T. Excie Guillot
Luis F. Castaneda Galvis

MARCH 2025

DISCLAIMERS

The contents of this report reflect the views of the authors, who are responsible for the facts and the accuracy of the data presented herein. The contents do not necessarily reflect the official views or policies of the Alabama Department of Transportation or the Auburn University Highway Research Center. This report does not constitute a standard, specification, or regulation. Comments contained in this paper related to specific testing equipment and materials should not be considered an endorsement of any commercial product or service; no such endorsement is intended or implied.

NOT INTENDED FOR CONSTRUCTION, BIDDING, OR PERMIT PURPOSES

Jose G. Vasconcelos, Ph.D.
J. Brian Anderson, Ph.D., P.E.
Research Supervisors

Acknowledgements

This project was sponsored by the Alabama Department of Transportation (ALDOT). Material contained herein was obtained in connection with a research project "Implementation of OMS-Based Scour Prediction and Real-Time Monitoring of Scour Processes for Alabama Bridges" ALDOT Project 931-053, conducted by the Auburn University Highway Research Center. The funding, cooperation, and assistance of many individuals from each of these organizations are gratefully acknowledged.

Executive Summary

Bridge scour, a phenomenon characterized by the erosion and removal of sediment from the vicinity of bridge foundations, is a significant concern throughout the United States. The Alabama Department of Transportation is aware of these issues and has methods to estimate and monitor these processes across Alabama bridges. ALDOT has adopted the approach based on the Federal Highway Administration HEC-18 document, and in some cases, the perception is that the estimated scour depths are too conservative. This research was motivated by the need to evaluate alternative methods for computing bridge pier scour, as well as to assess methods for monitoring scour evolution in bridges. To achieve these goals, this research evaluated various hydrological and hydraulic calculation methods, as well as the Observational Method for Scour (Briaud et al., 2009; Govindasamy et al., 2013), as an alternative to HEC-18. In addition, this research has developed, deployed, and monitored scour in multiple bridges in Alabama using sonar-based instrumentation.

There are various hydrologic and hydraulic approaches to calculating the peak flow that can be used to determine the water depth and velocity in the vicinity of a bridge, which are key variables used in bridge scour estimates. The extent to which hydrological and hydraulic alternative methods influence pier scour estimates is not well understood, as systematic investigations are mostly absent. This research evaluated pier scour on four Alabama bridges, considering various combinations of hydrological and hydraulic approaches. Peak flows were computed using the current approach adopted within ALDOT (i.e., based on Regional Regression Equations, RRE) and through estimates yielded by hydrological distributed models using HEC-HMS 4.9. Flood Frequency Analysis (FFA) estimates were obtained when USGS stream gage data was available. The peak flows for a 100-year event in each method were coupled with different hydraulic modeling approaches to determine the flow velocity near the bridge pier. Four approaches were used, applying 1D and 2D HEC-RAS modeling, including the method adopted by ALDOT based on 1D velocity estimates and the WSPRO equations. The two key findings for this stage of the work were: 1) RRE does not always provide the most conservative peak flow estimates; and 2) velocity estimates from 2D models are more representative and accurate for bridge pier scour calculations.

These computations were used to develop a comparison between HEC-18 and OMS bridge pier scour estimates for all the considered bridges. A key distinction between the methods is that OMS is typically used for future scour estimates of existing bridges, whereas HEC-18 is generally applied to estimate scour in proposed bridges. Thus, a procedure for implementing OMS, considering the data available to ALDOT, was developed to perform this comparison. Upon considering all the tested hydrological and hydraulic methods in HEC-18 and comparing these scour estimates with those of OMS, it was determined that the HEC-18 scour depths fell within the same range as the OMS estimates. This suggests that, at least for the selected bridges, HEC-18 scour estimates can be considered reliable and representative of the scour conditions these structures may experience.

Additionally, this research included long-term monitoring of pier scour processes on these bridges, utilizing sonar sensors. The instrumentation strategy, developed around the use of Sonar, proved to be simple, easy to deploy, and reliable. The strategy requires some prior work on the programming aspect of the sensors, as well as planning for deployment. The sonar sensors results occasionally returned noisy data, especially during flood events; however, the data trends of scour occurrence can still be seen, with a proper post-processing method and periodic manual verifications A few practical issues must also be accounted for, such as periodic sensor cleaning and debris removal, to ensure accurate monitoring. However, during the period when the bridges were monitored, no actual major flood occurred, which limits the observed scour magnitude. It is believed that sonar-based monitoring approaches have the potential to be beneficial for bridges at a higher risk of excessive scour, informing any necessary corrective actions to ensure their safety.

TABLE OF CONTENTS

LIST OF TABLES

LIST OF FIGURES

1. Introduction

1.1. Overview and Problem Statement

Bridge scour is a highly relevant and complex issue that involves interactions between soil and water at bridge constructions and in the vicinity of pier structures. During large floods, stream velocity and related shear stresses increase, causing scour that can compromise the bridge's safety and ultimately lead to catastrophic failure. Briaud et al. (2011) state that bridge scour is the leading cause of bridge failure in the United States, accounting for approximately 60% of all failures.

From the 1990s, guidelines began to consider scour as an integral component of bridge design. During scour evaluation, a bridge is considered scour critical when its foundations are determined to be unstable for the calculated or observed scour conditions (Hunt, 2009). Of the more than 500,000 highway bridges in the United States, over 20,000 have been deemed scour critical (Gee, 2008). With various research efforts across the US aimed at better understanding this critical issue, bridge failure episodes are now less frequent. Nevertheless, the design of safe and cost-effective bridges across the State of Alabama remains a top priority for ALDOT.

The Federal Highway Administration developed and improved guidelines to estimate bridge scour, with the purpose of guiding the design of new bridges and bridge replacement, as well as evaluating the vulnerability of existing bridges to scour. These guidelines are the "Hydraulic Engineering Circular No. 18", also referred to as HEC-18, with the latest version by Arneson et al. (2012). HEC-18 guidelines are designed to ensure that scour estimates are representative, but not underestimated. This is confirmed by Briaud (2018), who noted that the HEC-18 equations minimize any underprediction of scour. However, the perception among bridge inspectors and practitioners is that HEC-18 predictions are too conservative, to the extent that they are considered wasteful. The perception is also that predictions present significant scatter, as is indicated in Figure 1. On the other hand, scour estimation methods that consider observation of past scour can support a better understanding of scour processes and possibly lead to more economical design of bridge foundations.

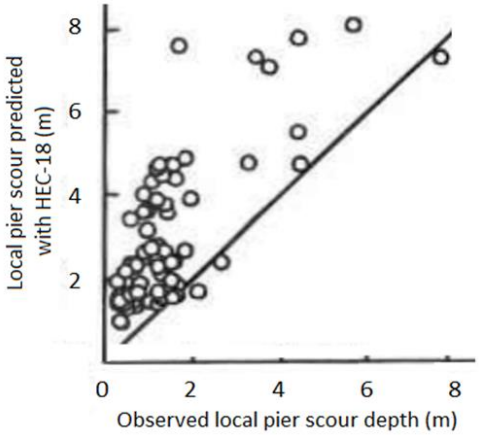

Figure 1. Comparison between observed and HEC-18 scour depths predictions (adapted from Landers and Muller, 1996)

Another observational approach linked to bridge scour diagnosis is in-stream monitoring. Real-time scour monitoring has been used by different departments of transportation across the US (Henneberg, 2018; NWIS, 2020) to assess its severity, as is illustrated in Figure 2. Such assessments often rely on the deployment of sonars at selected bridge piers, along with measurements of stream stage and velocity.

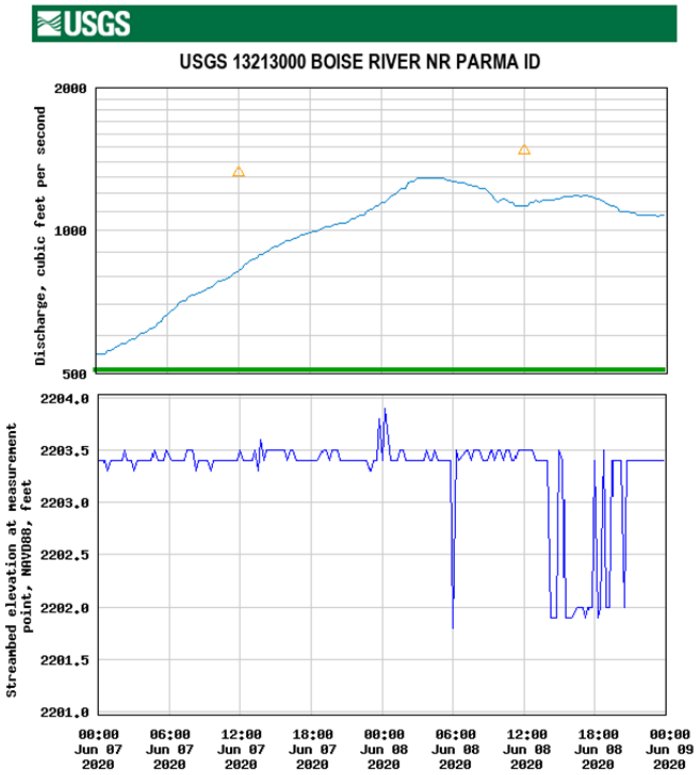

Figure 2. USGS measurements of stream flow rate and streambed elevation changes at Boise River for the Idaho Department of Transportation

The Observational Method for Scour (OMS) was developed at Texas A&M University (Briaud et al., 2009; Govindasamy et al., 2013) as an alternative method for estimating scour depths that are more closely aligned with those observed by bridge inspectors in the field. The application of OMS at a bridge site involves measuring actual scour, understanding bridge geometry, and analyzing flow history. Briaud (2018) pointed out that in a study in Texas involving twelve bridges classified as scour critical according to HEC-18, six of these were found to be stable. Such findings are valuable from the standpoint of overall safety and asset management. Briaud et al. (2018) applied HEC-18 and OMS in comparable conditions and determined that OMS also yields results with less scatter, as is shown in Figure 3.

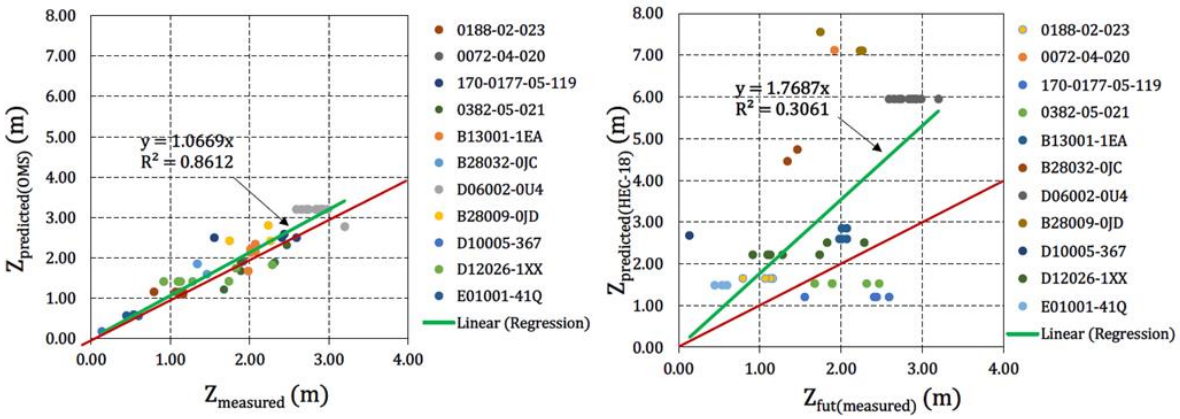

Figure 3. Application of OMS and HEC-18 to predict bridge scour for 11 bridges in Texas and Massachusetts

These past studies also highlighted some limitations of OMS, such as difficulties associated with predicting future scour in layered soils. While OMS cannot be directly applied to new bridges, its use on existing bridges is nevertheless useful for the design of foundations for new bridges. As Briaud et al. (2018) pointed out, a new bridge design may be implemented near an existing bridge where OMS was applied, such as in a replacement project.

In summary, the technology for real-time monitoring of bridge scour has developed significantly in recent years and has been applied in different states, providing insights into the severity of scour processes. In addition, OMS has been shown to be a more accurate tool for performing scour estimates in existing bridges, and it can provide valuable insights into the design of new bridges under certain conditions.

1.2. Research Objectives

Based on the above, the following research objectives were proposed:

1. Develop a procedure for the application of OMS in Alabama that considers the data availability for bridge geometry, soils, and scour measurements within ALDOT;
2. Develop a pilot study to cost-effectively gather real-time scour data in Alabama bridges and determine the best sensor installation strategies; and
3. Compare HEC-18, OMS, and field-collected scour data to understand how flows and soil characteristics influence the differences between predicted and measured scour depths.

1.3. Report Structure

The structure of this Final Report follows the research tasks that were delineated in the research proposal:

- Chapter 1: Introduction and Research Objectives.
- Chapter 2: Literature Review
- Chapter 3: Methodology for scour evaluations by HEC18 and OMS, including hydrological and hydraulic modeling
- Chapter 4: Instrumentation Strategy for Monitoring of Pier Scour in Alabama Bridges
- Chapter 5: Deployment of Scour Monitoring Instrumentation
- Chapter 6: Data and Results from the Long-term monitoring deployed in the five selected bridges in Alabama.
- Chapter 7: Results from Scour Evaluations using HEC18 and OMS methodology.
- Chapter 8: Research Conclusions and Recommendations for Future Work.

1.4. Selected Bridges

The selected Alabama bridges for this research were:

- Over Blue Creek, on Meriwether Trail, near Lapine, Montgomery Co. (BIN 010738)
- Over Little Double Bridges Creek, on County Road 606, near Enterprise, Coffee Co. (BIN 015002)
- Over Conecuh River, on County Road 2243, near Goshen, Pike Co. (BIN 013310)
- Bridge over French Creek, on Arcola St, near Demopolis, Marengo Co. (BIN 007070)
- Bridge over Chewacla Creek, on I85 Northbound Lane, near Tuskegee, Macon Co. (BIN 008598) – recently selected for sonar-based scour monitoring.

Figure 4 to Figure 9 show the five instrumented bridges selected for investigation in the state of Alabama, along with their respective cross-sections. All these cross sections were obtained with the web-based tool AASHTOware Bridge Management System, also referred to as BIN.

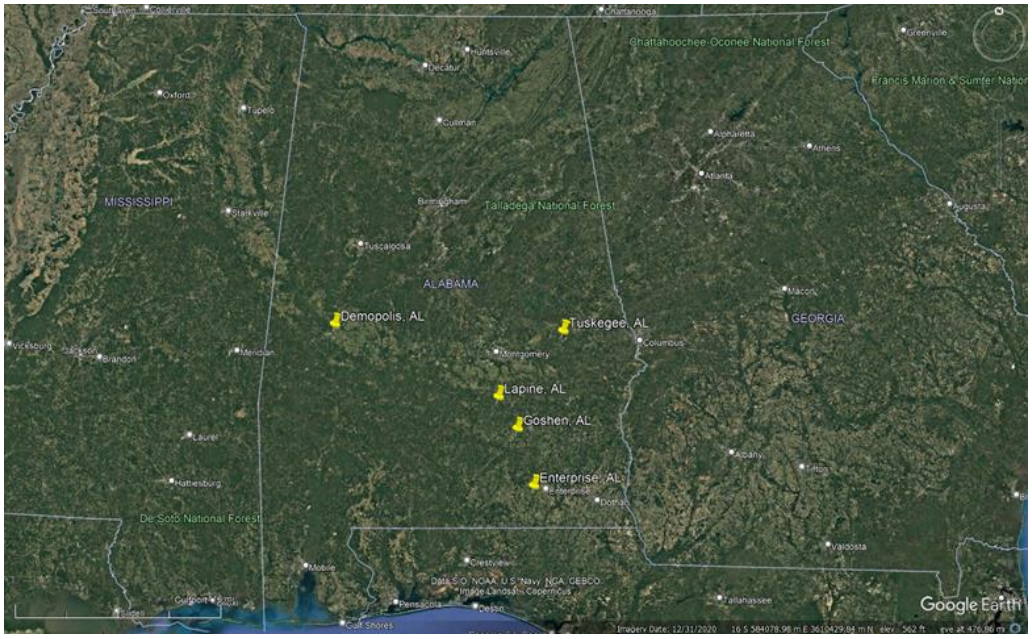

Figure 4. Selected bridges for instrumentation (source: Google Earth)

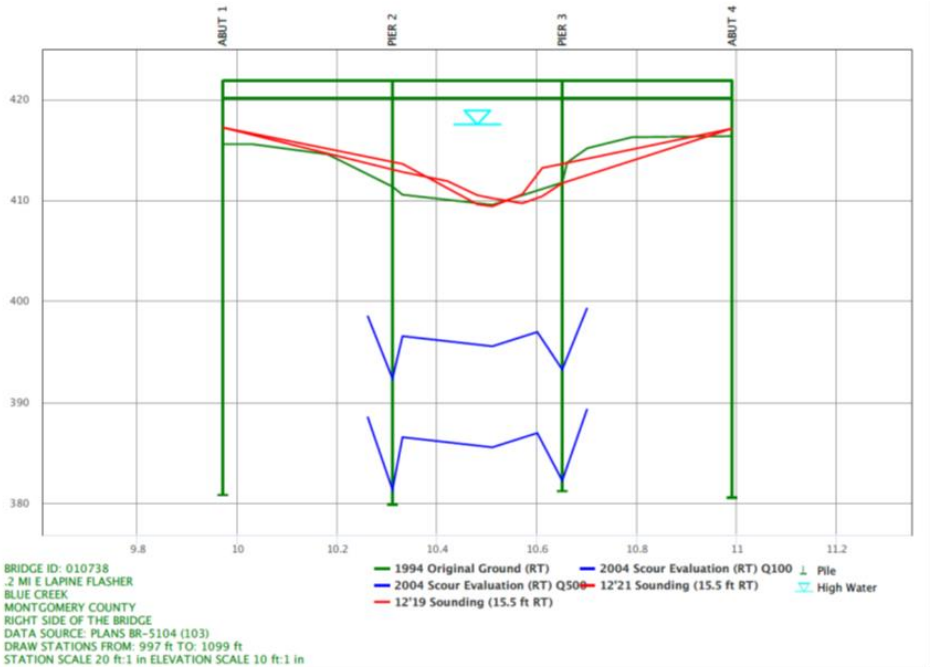

Figure 5. Cross-section of BIN 010738, Lapine, AL. Water flows in the direction into the page (AASHTOWare, 2024).

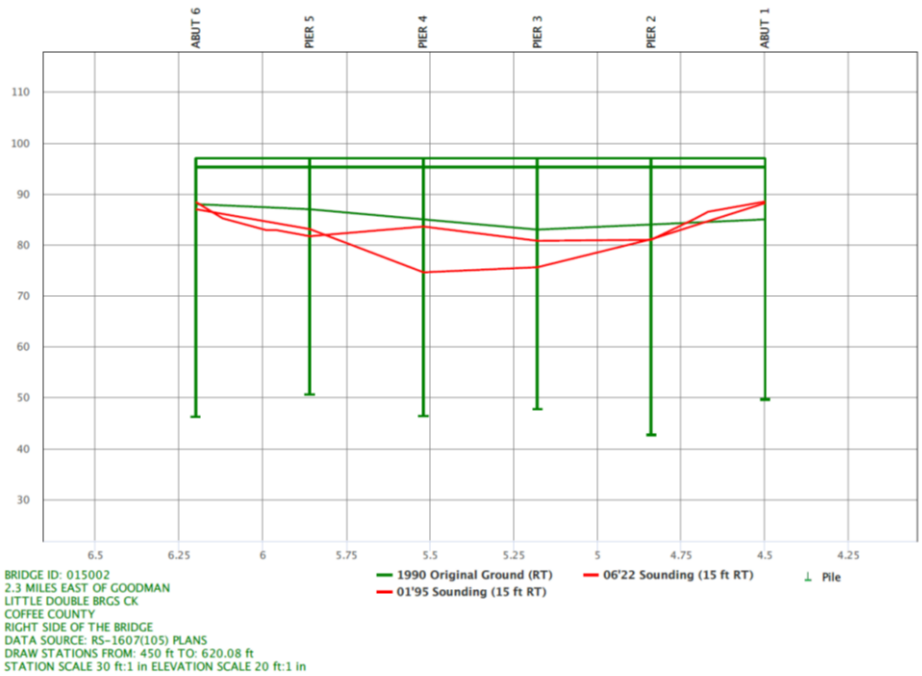

Figure 6. Cross-section of BIN 015002, Enterprise, AL. Water flows in the direction into the page (AASHTOWare, 2024).

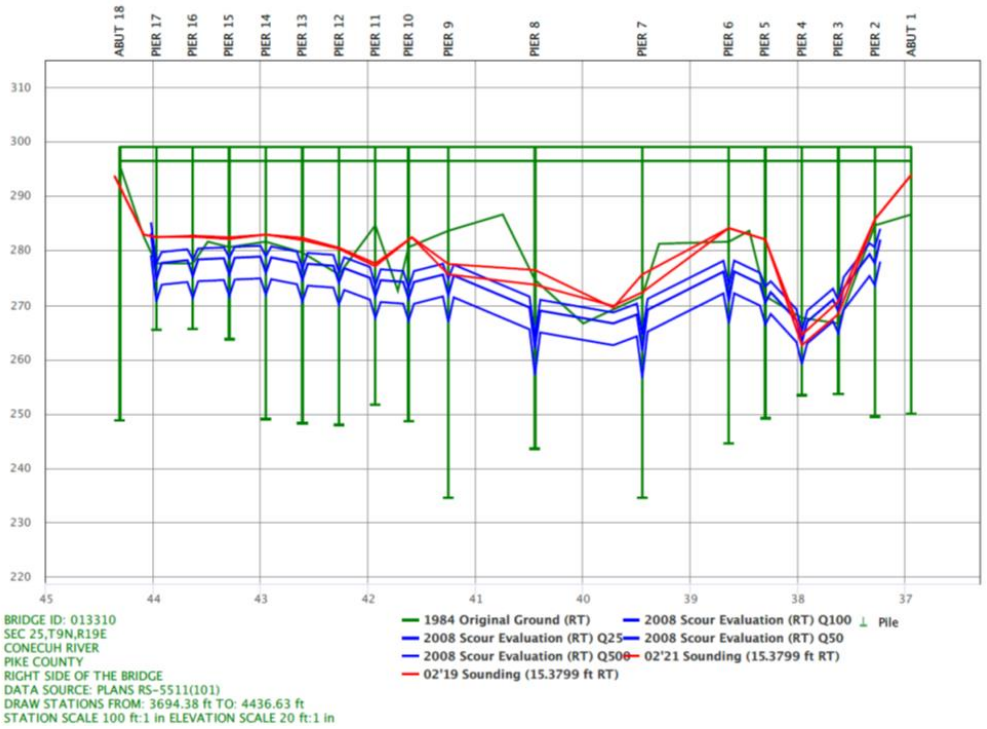

Figure 7. Cross-section of BIN 013310, Goshen, AL. Water flows in the direction into the page (AASHTOWare, 2024).

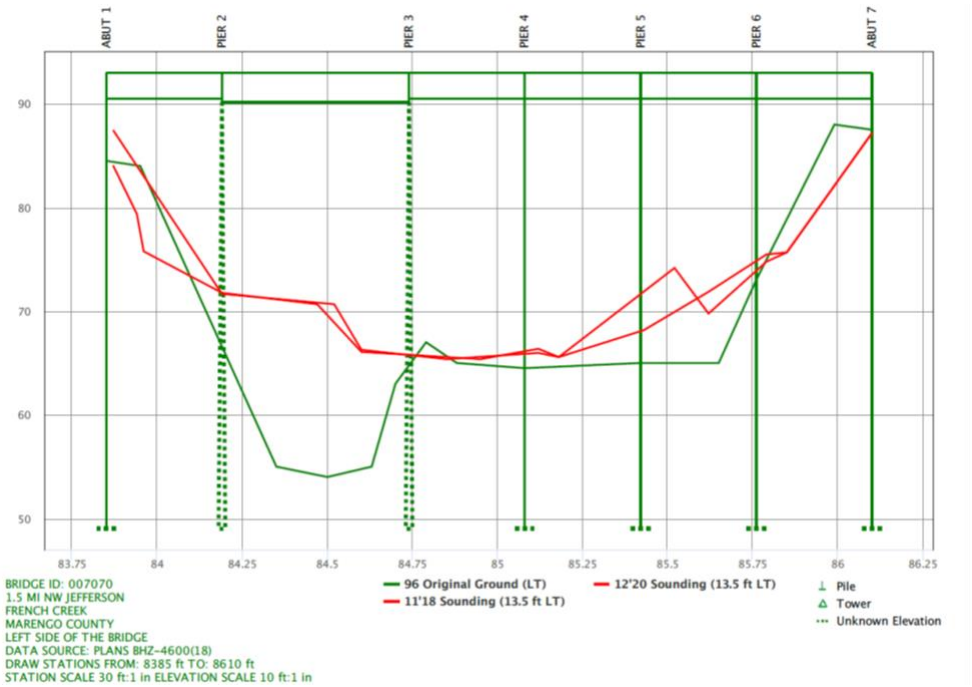

Figure 8. Cross-section of BIN 007070, Demopolis, AL. Water flows in the direction into the page (AASHTOWare, 2024).

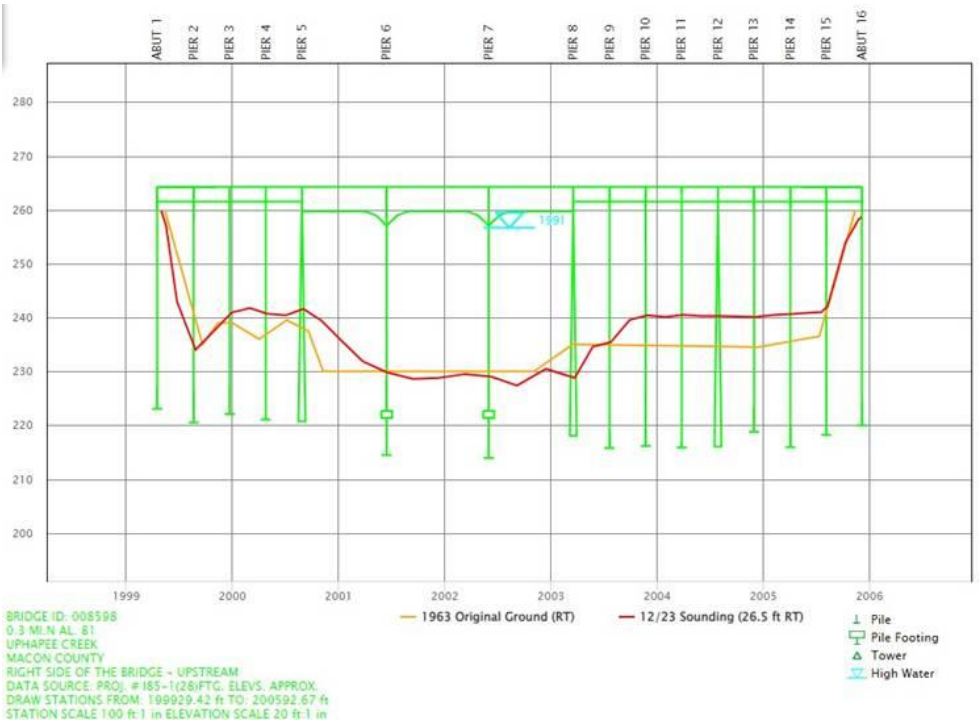

Figure 9. Cross-section of BIN 008598, Tuskegee, AL. Water flows in the direction into the page (AASHTOWare, 2024).

2. Literature Review

This section contains the literature review done for this research project. It comprises Hydrological and hydraulic modeling, as well as bridge scour fundamentals and calculations. It also includes a section on bridge scour laboratory investigation and field monitoring.

2.1. Hydrological and Hydraulic Modeling

Peak flow estimates are frequently utilized in the design of conveyance systems in open channels. There are different methods for estimating peak flows, depending on whether the watershed is gauged or ungauged. In gauged sites, it is common to use Flood Frequency Analysis (FFA), considering that there exists an inverse relationship between the magnitude of an extreme event and its frequency of occurrence, as noted by Chow et al. (1988). In ungauged sites, methods such as Regional Regression Equations (RRE) are used to calculate peak flows, complementing hydrological modeling results. The difference between these methods in ungauged watersheds is that the latter consider abstractions or losses, which are linked to physical processes such as infiltration (Green & Ampt, 1911), interception (Goudriaan & Monteith, 1990), evaporation (Penman, 1948; Priestley & Taylor, 1972), and evapotranspiration (Monteith & Unsworth, 2013). In addition, there is a method for calculating direct runoff and quantifying abstractions developed by the Soil Conservation Service (SCS) (Mockus, 1972), known as the SCS method for abstractions, which is based on land cover, land use, area, and hydrological conditions.

This research compares peak flow predictions using FFA, RRE, and hydrological models for gauged sites, as well as RRE and hydrological models for ungauged sites. The subsequent section presents a brief description of the hydrological methods used in this study.

2.1.1. Flood Frequency Analysis (FFA)

The primary aim of conducting a frequency analysis on hydrologic data is to establish the relationship between the occurrence of severe events and their corresponding magnitudes, utilizing probability distributions. Typically, the values used in this approach refer to the annual maximum discharge, denoting the highest instantaneous peak flow observed at any given point throughout the year. It is assumed that consecutive measurements of this variable across different years are statistically independent (Chow, 1953).

The observed data should typically be adjusted to an extreme value (EV) probability distribution, considering the goodness-of-fit product of the null hypothesis that the data are distributed as expected. If the goodness-of-fit test indicates that the data do not follow the expected distribution, then an alternative extreme value probability distribution may need to be considered. This adjustment ensures that the observed data accurately represent the extremes, allowing for more accurate analysis and predictions. The most common extreme value distributions are the Gumbel extreme value distribution and the log-Pearson Type III distribution. The log-Pearson Type III distribution is a three-parameter gamma distribution with a logarithmic transform of the independent variable (Chow et al., 1988).

Flynn et al. (2006) describe PeakFQ, a software application developed by the United States Geological Survey (USGS) that integrates the principles outlined in Bulletin 17B (B17B) of the Interagency Advisory Committee on Water Data (IACWD, 1982). Following B17B, annual peak-flow data must be fitted to a log-Pearson Type III distribution using the Expected Moments Algorithm (EMA) (Cohn et al., 1997) and a generalized version of the Grubbs-Beck test for low outliers (Cohn et al., 2013).

2.1.2. Regional Regression Equations (RRE)

Regression equations are used to estimate peak flows at ungagged or limited sites. The United States Geological Survey (USGS) has created and compiled regional regression equations, which are incorporated in computer software called the National Streamflow Statistics software (NSS) (Ries III et al., 2007), which is the foundation for StreamStats (Ries III et al., 2004) and allows quick estimation of peak flows throughout the US.

Brown et al. (2009) mention that the rural equations were developed for all states based on a series of studies conducted by the USGS, State Highway, and other agencies. Those equations are based on watershed and climatic characteristics within specific regions of each state that can be obtained from topographic maps, rainfall reports, and atlases. These regression equations are generally referred to as Equation (1).

$$RQ_T = a\, A^b\, B^c\, C^d \qquad (1)$$

Where:
RQ_T= peak flow associate with a recurrence interval T
a= Regression constant
b, c, d= Regression coefficients
A, B, C= Basin characteristics

Brown et al. (2009) describe how the USGS developed seven-parameter nationwide urban regression equations to convert rural peak flows to urban peak flows. The urban equations are based on data from 269 basins across 56 cities and 31 states. These equations have been systematically evaluated and shown to provide relatively accurate estimates of peak flows with recurrence intervals ranging from 2 to 500 years. However, these estimates may still contain errors of up to 35-50% when compared to field measurements. Those errors can be too significant for bridge scour estimates.

In Alabama, various documents are used to estimate the frequency and magnitude of floods. Most of them are focused on the size of the watershed's characteristics, stream size (small and large), and the magnitude of the analyzed event. Those documents can be categorized into three types of references related to peak flow (Anderson, 2020; Hedgecock, 2004; Hedgecock & Lee, 2010), low flow, and annual flow statistics (Feaster et al., 2020), which are used to estimate annual exceedance probability flows at ungauged locations. They were developed by using current geospatial data, new analytical methods, and annual peak flow (Anderson, 2020). In those reports, Alabama is divided into four flood regions, as shown in Figure 10, which were delineated based on a review of residual plots, previous reports, eight-digit hydrologic unit code maps, geologic maps, and physiographic maps (Anderson, 2020).

Figure 10. Locations of the Flood regions in Alabama (Anderson, 2020)

2.1.3. Hydrological Models

Hydrological models were developed to simulate and understand the movement and distribution of water in various natural systems, including watersheds, rivers, and groundwater aquifers (Chow et al., 1988). Different types of hydrological models differ in their approaches to simulating and predicting hydrological processes. The empirical models are primarily based on historical data and observations, and do not explicitly consider the underlying physical processes that govern hydrology. On the other hand, the physical-based models are designed to represent the fundamental physical processes that govern the movement of water in the hydrological cycle. These models consider principles of fluid dynamics, conservation of mass, energy, and momentum (Maidment, 1993). These hydrological models can be classified into two categories: lumped and distributed models. Their difference lies in that lumped models simplify the watershed into a single unit (Chow et al., 1988), while distributed models consider the spatial variability of hydrological processes (Beven, K. J., & Kirkby, M. J.,1979)

Chen, Y. (2018) defines distributed hydrological models as a type of hydrological model that divides the terrain of an entire studied basin into numerous cells and then characterizes the hydrological processes, including interception and evapotranspiration, snowmelt, infiltration, and runoff formation and movement, at both the cell and basin scales. Some examples include SWWM (Rossman, 2010), SWAT (Neitsch et al., 2009), and HEC-HMS (Feldman, 2000). In this study,

the hydrological peak flow was determined using HEC-HMS, and a brief description of these models is presented below.

The Hydrologic Engineering Center (HEC) from the U.S. Army Corps of Engineers developed the Hydrologic Modeling System software, which intends to reproduce hydrological analysis procedures such as event infiltration, unit hydrographs, and hydrologic routing loss models, direct runoff models, hydrologic routing models, naturally occurring confluences and bifurcations, water-control strategies, and an automated calibration package. HEC-HMS also includes procedures necessary for continuous simulation including evapotranspiration, snowmelt, and soil moisture accounting (Feldman, 2000).

In this study, the models were event-based simulations; therefore, the effect of evapotranspiration was not considered. In addition, to compute the abstractions, a method known as the SCS curve number, developed by the Natural Resources Conservation Service (NRCS), was used. This method calculates the peak flow as a function of drainage basin area, potential watershed storage, and the time of concentration (Mockus, 1972). The rainfall runoff separates total rainfall into direct runoff, retention, and initial abstraction to yield using Equation (2) (Brown et al., 2009).

$$Q_D = (P - 0.2 \cdot S_R)^2 \,/\, (P + 0.8 \cdot S_R) \tag{2}$$

Where:
Q_D = Depth of direct runoff (in)
P = depth of 24-hour precipitation (in)
S_R= Potential maximum retention (in)

The potential maximum retention SR is calculated with Equation (3).

$$S_R = (1000/CN - 10) \tag{3}$$

Where:
CN = Curve Number.

CN depends on the Land cover and the hydrological soil groups. The value considered in Equation (3) corresponds to AMC II or normal antecedent moisture conditions. The antecedent moisture conditions (AMC) refer to the level of saturation that the soil has when rainfall begins. Exist three different levels of Antecedent Moisture Conditions as is shown in Table 1:

Table 1. CN's correction by antecedent runoff condition (AMC)

Antecedent Moisture Conditions	**Antecedent Moisture Condition (5-days before)**	**CN Equation**
I	Less than 0.5 in	$CN_I = \frac{4.2 * CN_{II}}{10 - 0.058 * CN_{II}}$
II	0.5 to 1.1 in	CN_{II}
III	Above 1.1 in	$CN_{III} = \frac{23 * CN_{II}}{10 + 0.13 * CN_{II}}$

The antecedent moisture conditions (AMC) were a key part of the hydrological simulations used in this study. This is because different AMC conditions were simulated in each watershed to find the worst-case scenario for bridge scour calculations.

A calibration process, illustrated in Figure 11, was conducted in this research following Feldman (2000), which is based on the search for optimized values for modeling parameters:

- The process begins with data collection, and each step requires a different type of data collection. For instance, rainfall-runoff models require rainfall data and flow time series. Routing models require inflow and outflow data from the routing reach.
- The program utilizes initial parameter estimates and observed boundary conditions to develop models for watershed runoff hydrographs and channel outflow hydrographs. The goal is to compare the model's fit with the real hydrologic system. If the fit is not satisfactory, the program adjusts the parameters and repeats the process. The optimal parameter values are reported when the fit is satisfactory, which can be used for flood runoff analyses, such as runoff or routing computations, as shown in diagrams used by HEC-HMS.

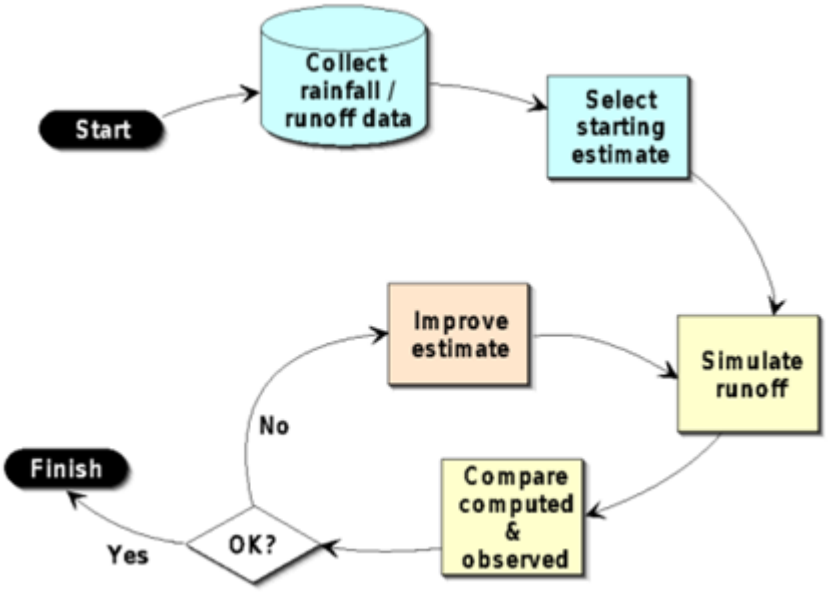

Figure 11. Calibration process diagram used by HEC-HMS. Feldman (2000)

Feldman (2000) explains how HEC-HMS compares a computed hydrograph to an observed one by computing goodness-of-fit indexes. It utilizes algorithms to determine model parameters that yield the optimal value of an objective function. The goal is to find reasonable parameters that minimize the objective function's minimum value. The objective functions that HEC-HMS can evaluate in the calibration process are the sum of absolute errors, the sum of squared residuals, the percent error to peak, and the peak-weighted root mean square error function. In this research, the objective function evaluated was percent error in peak and is shown in Equation (4).

$$Z = 100\left(q_{(s(peak))} - q_{(O(Peak))}\right)/q_{(O(Peak))} \quad (4)$$

2.1.4. Governing Equations 1D vs 2D models

Brunner and CEIWR-HEC (2016) introduce the governing principles that govern the flow of water in streams, which are the principles of continuity and conservation of momentum. These principles are theoretically described as partial differential equations. Those principles are

employed in the derivation of unsteady flow equations in one and two dimensions, commonly referred to as shallow water equations. These assumptions include the assumption that water behaves as an incompressible fluid, the pressure distribution follows hydrostatic principles, the vertical acceleration can be considered negligible, the bed slope is relatively mild (less than 10%), the boundary friction can be accounted for using flow resistance laws such as Manning's equation for steady flows, and the Boussinesq approximation is valid, thereby disregarding forces resulting from variations in water density.

One-Dimensional Equations (1D)

Brunner et al. (2020) present the flow equations for the 1D continuity and momentum equations concerning depth (h) and velocity (u) (See Equations (5) and (6)), and the symbols used for motion and mass conservation equations are shown in Figure 12. Those equations are only applicable to 1D flows, and a variation for 2D flows is presented further ahead.

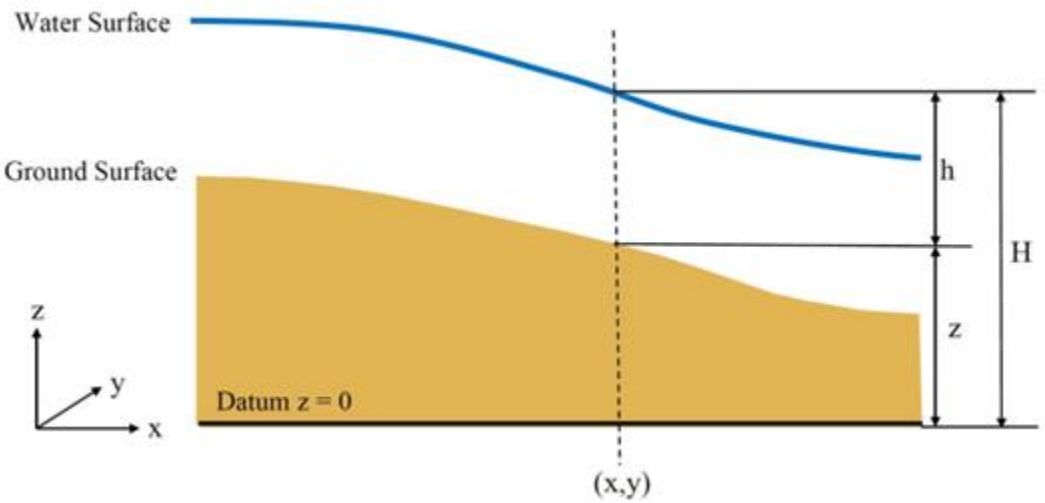

Figure 12. Symbols used. Equations for motion and mass conservation (Brunner et al., 2020)

$$\frac{\partial}{\partial t}(h) + \frac{\partial}{\partial x}(hu) = q \tag{5}$$

$$\frac{\partial u}{\partial t} + u\frac{\partial u}{\partial x} + g\frac{\partial h}{\partial x} = g(S_0 - S_f - S_h) \tag{6}$$

Where:
u = velocity in the x direction
h = depth of water
g = gravity
t = time
x = distance in the direction of flow (x plane)
q = Lateral inflow term (source/sink)
S_0 = Bed slope
S_f = Friction slope, as defined in Manning's equation.
S_h = added force term (Minor Losses)

Two-Dimensional Equations (2D)

Brunner et al. (2020) present a version of the two-dimensional vertically and laterally average continuity (Equations (7) and (8)) and vertically averaged momentum (Equations (9) and (10)) and laterally averaged Momentum (Equations (11) and (12)) can be written in partial differential equation form, concerning depth (h) and velocity (u, v, U, V) as is shown below.

$$\frac{\partial H}{\partial t} + \frac{\partial (hu)}{\partial x} + \frac{\partial (hv)}{\partial y} = q \tag{7}$$

$$\frac{\partial UB}{\partial x}\, x + \frac{\partial WB}{\partial z} = qB \tag{8}$$

$$\frac{\partial u}{\partial t} + u\frac{\partial u}{\partial x} + v\frac{\partial u}{\partial y} = -g\frac{\partial H}{\partial x} + v_t\left(\frac{\partial^2 u}{\partial x^2} + \frac{\partial^2 u}{\partial y^2}\right) - c_f u + fv \tag{9}$$

$$\frac{\partial v}{\partial t} + u\frac{\partial v}{\partial x} + v\frac{\partial v}{\partial y} = -g\frac{\partial H}{\partial x} + v_t\left(\frac{\partial^2 v}{\partial x^2} + \frac{\partial^2 v}{\partial y^2}\right) - c_f v + fu \tag{10}$$

$$\frac{\partial UB}{\partial t} + U\frac{\partial UB}{\partial x} + W\frac{\partial U\mathrm{B}}{\partial z} = -g\frac{\partial BH}{\partial x} + \frac{B}{\rho}\frac{\partial P}{\partial x} + \frac{1}{\rho}\frac{\partial B\tau_{xx}}{\partial x} + \frac{1}{\rho}\frac{\partial B\tau_{xz}}{\partial z} \tag{11}$$

$$\frac{1}{\rho}\frac{\partial P}{\partial z} = -g\frac{\partial H}{\partial z} \tag{12}$$

Where:
v = velocity in the y direction
y = distance in the lateral direction (y plane)
H = water surface elevation (z + Depth)
v_t = horizontal eddy viscosity coefficient
c_f = bottom friction coefficient
f = Coriolis parameter
U = laterally averaged velocity in x direction
W = laterally averaged velocity in z direction
B = width
P = laterally averaged pressure
t_{xx},t_{xz} = turbulent stresses in the xx and xz directions, respectively
q = lateral inflow per unit volume

While 2D formulations are more complex than 1D, there are key limiting assumptions and from 1D models, which can lead to erroneous results in rivers with high hydraulic complexity :

- Single flow direction, flow path, and limited ability to represent flow splits
- Difficulty in determining adequate spaces for consecutive cross-section calculation

- Difficult in determining ineffective flow areas, flow contraction, and flow expansion coefficients at bridges
- Oversimplification of boundary conditions and roughness parameters

On the other hand, 2D models have distinct assumptions and limitations, including:

- No vertical velocity components for velocity, flow diffusion, and flow turbulence
- Somewhat simplified boundary conditions can lead to errors
- Turbulence accounting using eddy viscosity can result in unrealistic patterns
- Issues with model stability and convergence.

Brunner et al. (2020) also discusses the computational differences between 1D and 2D unsteady flow modeling. In the context of the HEC-RAS model, which is the model used in this report, the following discussion contrasts 1D and 2D unsteady flow modeling:

- **Water Surface and Velocities:** The primary difference lies in the fact that 1D models compute a single water surface elevation at each cross-section. In contrast, 2D models compute unique water surfaces for every cell or face, with detailed water surfaces and velocities varying based on the number of cells used.
- **Friction Losses:** In 1D models, friction losses are calculated by multiplying an averaged friction slope (S_f) by the distance between cross sections. For 2D models, the friction slope is also calculated at each face of the cells; however, it is typically not averaged over the cell because the flow direction is two-dimensional.
- **Conveyance Calculations:** Conveyance in 2D models is computed separately for each cell face, whereas in 1D models, conveyance is calculated for the main channel (Brunner et al., 2020) as a separate flow area. This can result in different findings, with the highest discrepancies typically found in areas with steep banks.
- **Contraction and Expansion Losses:** In 1D models, losses due to contraction and expansion are determined by multiplying empirical coefficients by velocity head, while 2D models include pressure forces and spatial acceleration terms.
- **Ineffective Flow Areas:** Since 1D models require conveyance across sections, they often result in "ineffective flow" areas. 2D models calculate recirculation zones automatically, but turbulence modeling and coefficients can influence their size and water velocity.

2.1.5. Modeling Bridges in HEC-RAS

Brunner (2016) explains that HEC-RAS has four different methods for computing losses through bridges in 1D: the Energy Equation, Momentum Balance, Yarnell Equation, and FHWA WSPRO method. This research compares two methods using 1D models, the Energy Equation and the WSPRO method.

- Energy equation: This approach considers a bridge as a natural river cross-section. It involves removing the area below the water surface and raising the wetted perimeter to the points where the water meets the structure. The approach employed in this method incorporates Manning's n values to account for friction losses, as well as contraction and expansion coefficients to address transition losses.
- The WSPRO method is an iterative solution that calculates the water surface profile through a bridge by solving the energy equation. It is performed from the exit cross section (1) to the approach cross-section (4), with the energy balance being performed in steps from the exit section (1) to the cross section just downstream (2) of the bridge, inside of

the bridge at the downstream end (BD), inside of the bridge at the upstream end (BU) to just upstream of the bridge (3), and from just upstream of the bridge (3) to the approach section (4). An illustration of the channel profile and the cross sections used for modeling losses through the bridges are shown in Figure 13 and Figure 14.

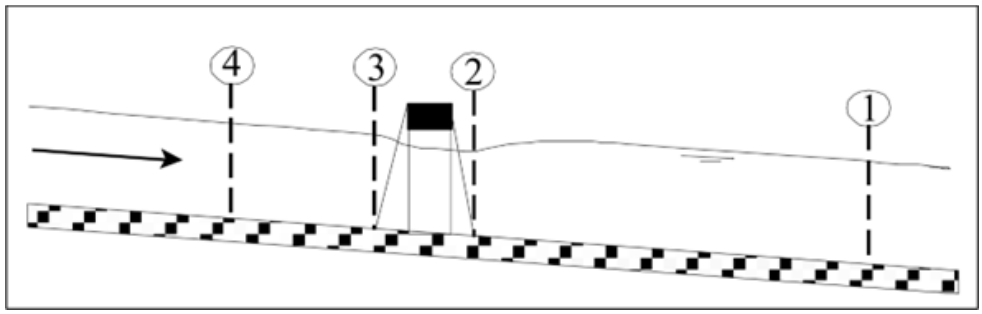

Figure 13. Channel Profile and cross section locations (Brunner and CEIWR-HEC, 2020)

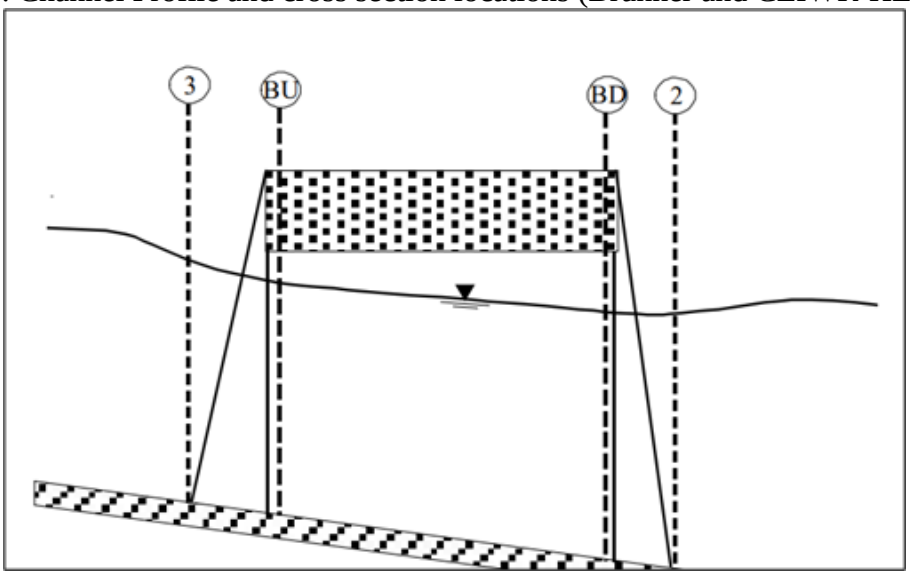

Figure 14. Cross Sections Near and Inside the Bridge (Brunner and CEIWR-HEC, 2020)

Conversely, there are two different ways to model compute losses through bridges in HEC-RAS 2D (Hydrologic Engineering Center, 2023):

- SA 2D connection in HEC-RAS features a tool that enables the modeling of roadway crossing bridges and culverts within 2D flow areas. This tool can handle the full range of flow regimes, from low flow to pressure flow, combined pressure flow, and flow going over the top of the bridge deck or roadway. The HEC-RAS software takes the user input bridge data and modeling approaches, then develops a family of rating curves for the bridge, just as it does for 1D modeling. However, for 2D modeling, the bridge's curves are used to calculate the water surface difference across the bridge for each set of cells used to model the bridge. This water surface difference is then equated to a force. That force is distributed and put into a special version of the momentum equation for each set of cells spanning the bridge centerline. Instead of calculating friction forces, pressure forces, and spatial acceleration forces, these forces are obtained directly from the bridge curves. Then, the 2D equations are solved as they are typically solved at any cell or face in the model. (Brunner and CEIWR-HEC, 2020)

- 2D Terrain modification with raised piers To model piers in bridges by means of raising the terrain elevation in HEC-RAS, Terrain Modification tool in RAS Mapper can be applied. This tool can be used to improve the terrain data by adding channel information, adding high ground (such as a road), adding features that impede flow (such as piers), or otherwise modifying the terrain elevations. Then, the 2D equations are solved as they would be at any cell or face in the model (Hydrologic Engineering Center, 2023).

2.2. Bridge Scour Estimates

Bridge scour is the result of modifications to water flow patterns, such as bends or constrictions, which can increase water turbulence. (Richardson et. al., 1993). There are three main components of total scour in bridges: long-term aggradation and degradation, contraction scour at the bridge, and local scour at the pier or abutments (Richardson & Davis, 2001). Those components are described below:

- Aggradation and degradation are long-term changes in the elevation of the streambed, affecting the river section where the bridge is located. Aggradation is the deposition of eroded material upstream of the bridge, while degradation lowers the streambed and contributes to overall scour.
- Contraction scours occur when a bridge's placement constricts the stream flow region, often during flood events. This can cause increased flow velocities and higher shear stresses, potentially leading to erosion.
- Local scour is a phenomenon that occurs near a specific bridge pier, abutment, spur, or embankment, causing sediment removal as a result of vortices created by flow-obstructing objects.

2.2.1. Parameters related to Bridge Scour estimates

Critical shear stress refers to the minimum shear stress required to initiate erosion in cohesionless soils. In other words, it is the threshold at which the soil particles start to detach and move. Understanding the critical shear stress is crucial because it helps determine the stability of the soil and its resistance to erosion. If the shear stress acting on the soil exceeds the critical shear stress, erosion will occur. On the other hand, if the shear stress is below the critical shear stress, no erosion will take place. Arneson et al. (2012) define shear stress as the force per unit area applied to the channel boundary by flowing water:

$$\tau = K_b . \gamma . R . S_f \quad (13)$$

Where:
τ = Design shear stress, lb/ft^2 (N/m2)
K_b = Bend coefficient (dimensionless)
γ = Unit weight of water, lb/ft^3
R = Hydraulic radius (area divided by wetted perimeter), ft (m)
S_f = Slope of the energy grade line, ft/ft (m/m)

Another important parameter is the critical velocity, which is the lowest velocity required to begin sediment transport and erosion at a pier. When the flow velocity reaches critical velocity, sediment particles from the bed can be displaced and transported (Richardson & Davis, 2001).

Considering these factors, bridge scour can happen through two different mechanisms limited to sediment motion: (1) when the water is clear, which means that there is no movement of sediment in the bed of the approach channel, and (2) when there is sediment motion in the approach flow. Under clear water conditions ($V_c > V$), sediment remains stationary in the bed of the approach channel because the bed shear stress is lower than or equal to the critical bed shear stress required for sediment motion to occur. On the other hand, under live bed conditions ($V_c < V$), there is a generalized movement of the bed sediment caused by a higher bed shear stress that exceeds the critical threshold (Arneson et al., 2012).

In addition, another important parameter to consider is the erosion rate. Briaud et al. (1999) found that the erosion rate in scour processes depends on the critical shear stress, the soil and water temperatures, the chemical makeup of the soil and water, the soil water content, the plasticity index, the soil unit weight, the soil undrained shear strength, and the average grain size. Briaud et al. (2011) presents a graph, shown in Figure 15, which related the critical shear stress to the particle grain size as a function of D_{50} (mm) and the critical shear stress (N/m^2). This V-shaped graph also illustrates that particle size controls the erosion threshold of coarse-grained soils, while particle size does not correlate with the erosion threshold of fine-grained soils. This effect is attributed to the cohesive nature of fine-grained soils, specifically silt and clay (Anerson et al., 2012).

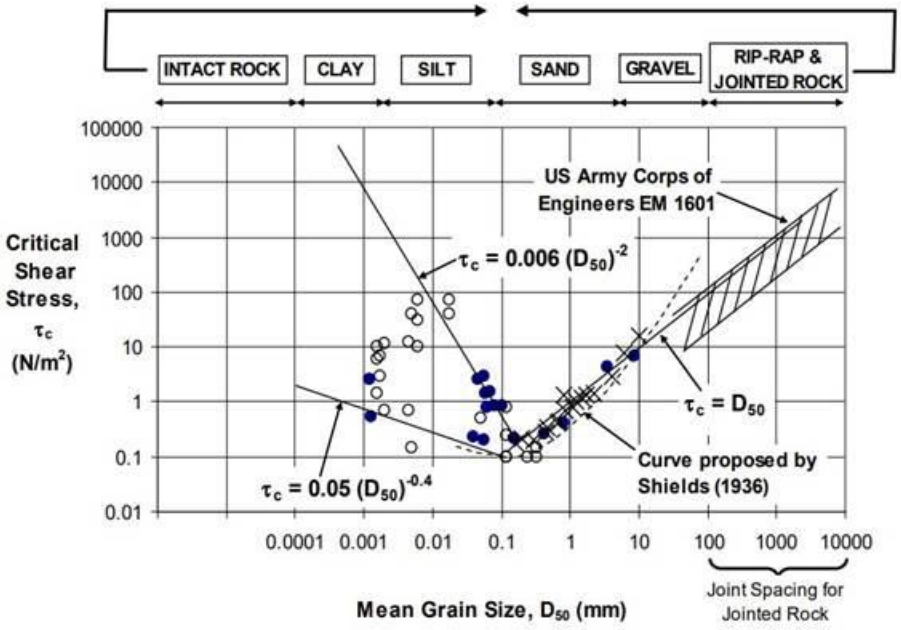

Figure 15. Critical shear stress vs particle grain size (Briaud et al. 2011)

Typically, in scour analysis, it is assumed that the soil is uniform. Nevertheless, in reality, the soil can involve multiple layers with characteristics that can vary significantly with depth. For this situation, a multilayer analysis can be conducted (Pokharel, S., 2017; Briaud et al., 2011). This type of analysis assumes different layers in the channel bottom bed with specific thicknesses (y_i). Each layer, with a different D_{50}, can be removed for flood events with a constant velocity over a specified period (t_i). When the scour depth Y_{si} exceeds the thickness Y_i, the following layer (Y_{i+1}) is involved, eroding its thickness during a specific time (t_{i+1}). Geotechnical borings provide the necessary stratigraphic information, particle size distribution, and D_{50} for each stratum required for this multilayer analysis. This type of analysis is common in cohesive soils, where the

erosion rate of the material can support long periods and several flood events (Anerson et al., 2012). It is important to note that D_{50} varies across the cross-section and the stratigraphic profile, which significantly impacts the scour estimates.

2.2.2. Practical guidelines for Sour Calculations

There are several reference documents related to Bridge scour and are mentioned below.

- *HEC 18 Evaluating Scour at Bridges (2012):* This document state of knowledge and practice for the design, evaluation, and inspection of scour-critical bridges includes policy and regulatory basis for the FHWA Scour Program, risk-based evaluations, developing Plans of Action (POAs), countermeasure design philosophy (new vs. existing bridges), and a section on contraction scour in cohesive materials (Anerson et al., 2012)
- *HEC 20 Stream Stability at Highway Structures (2012):* This document contains recommendations for identifying stream instability issues at highway stream crossings. The HEC-20 manual discusses geomorphic and hydraulic elements that influence stream stability, providing a step-by-step analysis technique for assessing stream stability issues. (Lagasse et al., 2012).
- *HEC 23 Bridge Scour and Stream Instability Countermeasures: Experience, Selection and Design Guidance (2009):* The objective of this document is to ascertain and provide design principles for mitigating bridge scour and stream instability, as observed in the practices adopted by different State departments of transportation (DOTs) within the United States (Lagasse et al., 2009).
- *HDS 7 Hydraulic Design of Safe Bridges (2012):* This guidance provides technical information and recommendations on the hydraulic design of bridges. Bridges should be constructed to be as safe as possible while keeping costs low and minimizing the impact on property and the environment. This guidance also addresses regulatory issues, specialized methodologies for bridge hydraulic modeling, hydraulic model selection, the impact of bridge design on scour and stream instability, and sediment transport (Zevenbergen et al., 2012).
- *Observation method for estimating future scour depth at existing bridges (2013): This method utilizes charts that extrapolate or interpolate measured scour depths at the bridge to determine* the corresponding scour depth for a specified future flood event. It was designed to be used as a first-order assessment in conjunction with a routine bridge inspection program (Briaud et al., 2011; Govidasamy et al., 2013)

2.2.3. Worst-Case scour scenario

Sharp et al. (2021) describe two definitions for the worst-case scour scenario: one created by FHWA, which recommended the use of 100-year and 500-year exceedance discharges as the scour design flood and scour check flood, and the second proposed by AASHTO LRFD, which recognizes that the worst-case scour depth may not occur at the highest flow rate that the scour design flood or scour check flood may have (i.e., Q_{100} and Q_{500} events). As a result, the scour design flood may include some flood magnitudes less than Q_{100}, resulting in increased scour at the bridge. If that is the case, the standards permit the discharge to be used as the scour design flood. Similarly, if a flood event less than the Q_{500} creates the worst-case scour depth at the bridge, it should be used as the scour check flood. Another way to put it is that the scour design flood should be the worst-case scour estimate for all floods up to and including Q_{100}.

The FHWA included risk-based approaches in its bridge program goals, including the scour program, in a 2010 recommendation to the United States Congress. This analysis examines

the significance of the structure, the necessity of reliable crossings, and the economic implications of a collapse. All bridges were previously planned for scour using Q_{100} flood events, which were then double-checked using Q_{500}, prior to the advent of risk-based approaches. The recommended minimum scour design and check flood frequencies based on hydraulic design flood frequencies defined by FHWA in HEC-18 (Anderson et al., 2012) are shown in Table 2.

Table 2. Hydraulic design, scour design and scour design check flood frequencies

Hydraulic design Flood Frequency, QD	**Scour design Flood Frequency, Qs**	**Scour design check Flood Frequency, Qc**
Q10	Q25	Q50
Q25	Q50	Q100
Q50	Q100	Q200
Q100	Q200	Q500

Briaud et al. (2011) proposed a methodology to determine the scour rate in cohesive soils. This method enables users to predict scour depths as a function of time. This method is based on two parameters: the maximum scour depth and the maximum shear stress. Those methods require determining the scour depth using a given set of sequential daily discharge values. In addition, Briaud et al. (2011) also developed a method for preparing daily discharges based on previously recorded hydrographs (Q100 and Q500) to predict possible scour depths in the future. To calculate the daily discharges, Montecarlo assumed that the hydrograph was modeled as a stochastic process. The methodology uses a theoretical distribution (log-normal) and the future daily stream flow as the exponential of a normally distributed variable. At the same time, Briaud et al.. (2011) developed another approach based on Q_{100} and Q_{500}, utilizing the cumulative density function (CDF) of the log-normal distribution of Q evaluated at Q_{100} and Q_{500} to calculate daily stream discharges. It is worth noting that these methods are particularly useful for predicting scour in cohesive soils. This study is based on the premise that the maximum scour will happen for an event with an exceedance probability of 1% or a 100-yr return period.

2.2.4. Pier scour

Pier scour is a type of local scour that occurs around individual bridge piers and abutments. Downward flow is induced at the upstream end of bridge piers, resulting in very localized erosion near the structure (Hamill, 1999). This research is focused on pier scour comparison, so more emphasis will be placed on this type of scour. To contextualize the phenomenon of pier scours, it is important to describe the flow field on a single pier. Pier scour is caused by vortices resulting from objects obstructing the flow. In this process, the downward flow is induced at the upstream of the bridge pier leading to a localize erosion in the vicinity of the structure; horseshoes vortices are then created at the base of the pier due to the acceleration of the flow around the nose of the pier and the subsequent flow movement at the edge of the scour hole. Finally, wake vortices are created when the flow at the side of the pier is separated (Prendergast & Gavin, 2014).

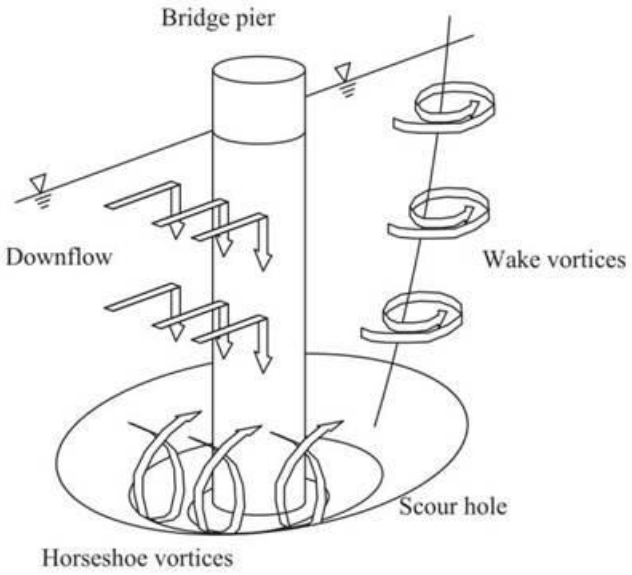

Figure 16. Flow around a single pier (Prendergast and Gavin, 2014)

Despite the lack of field data, local scour at piers has been thoroughly studied in the laboratory. Most studies have been conducted on simple piers, such as Ettema (1976, 1980), Sheppard, (1999); Melville and Coleman (2000); Richardson and Davis (1995, 2001) and Sheppard and Renna (2010) and Anerson et al., (2012), others conducted in complex piers as such as Jones and Sheppard (2000), Salim and Jones (1995,1996, 1999) and Sheppard, (2001), and some in cohesive materials as Briaud et al., (2009, 2011) and others in coarse bed as Lagasse et. al., (2012). Additionally, there are methods based on scour observations, such as the Observational Method for Scour (Govindasamy et al., 2013). This research focuses on HEC-18 calculations (Anerson et al., 2012) and the Observational Method for Scour (OMS) (Govindasamy et al., 2013). Therefore, their origins and formulations are presented below.

2.2.5. HEC- 18 equations for pier scour

Liu et. al (1961) and Chang and Yevdjevich (1962) conducted studies in the Colorado State University on the hydrodynamic and physical description of contraction and local scour; and prepared a logical outline of future research procedures into the study of the local scour phenomenon, those equation products of that work are known as Colorado State University Equations. Those equations were based on preliminary studies conducted by Einstein (1950), Laursen (1956), and Chabert and Engeldinger (1956).

Studies performed by Jones (TRB, 1983) show that the Colorado State University Equation (CSU) covered the condition for most equations developed for local pier scour. Using the recommendations from this study, the FHWA recommended the CSU equation in the interim procedures accompanying FHWA's Technical Advisory T5140.20 (1988). The CSU equation was also recommended, with some changes, in earlier editions of HEC-18. In addition, studies conducted by Mueller (1996) compared 22 scour equations with field measurements and concluded that the HEC-18 (CSU) equation was suitable for design, as it rarely underestimated measured scour depths but frequently overpredicted the actual scour. Figure 17 compares scour equations for variable depth ratios (y/a) according with Jones (TRB, 1983).

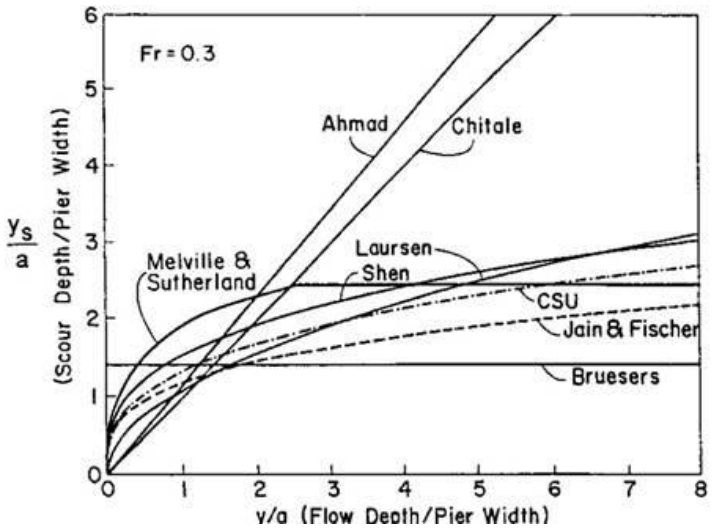

Figure 17. Comparison of scour equations for variable depth ratios (y/a) according with Jones (TRB, 1983)

The HEC-18 pier scour equation is also based on the CSU equation and is recommended for both live-bed and clear-water pier scour in cohesionless soils. Figure 18 shows the Pier scour sketch according to HEC-18, and its respective Equation (14) (Anerson et al., 2012).

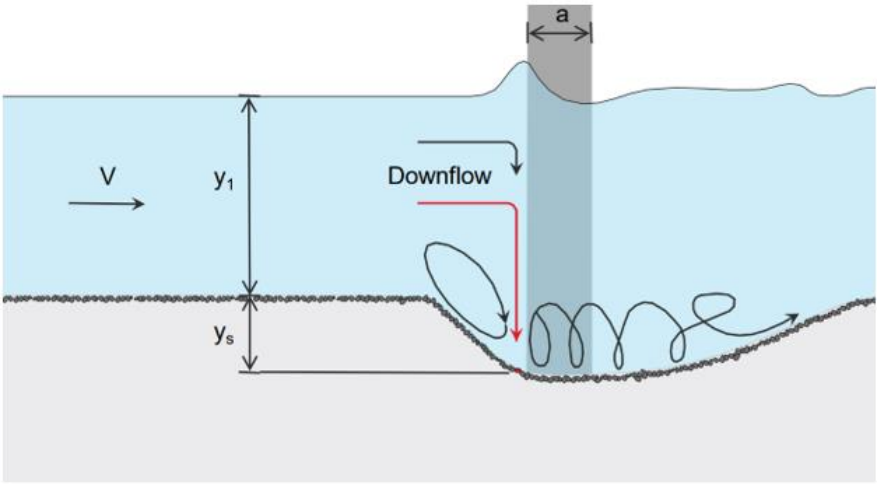

Figure 18. Pier scour sketch (Anerson et al., 2012)

$$\frac{y_s}{y_1} = 2.0\, K_1 K_2 K_3 \left(\frac{a}{y_1}\right)^{0.65} Fr_1^{0.43} \qquad (14)$$

Where:

y_s = Scour depth (ft)

y_1 = Flow depth directly upstream of the pier (ft)

K_1, K_2, and K_3 are correction factors for pier nose shape, for angle of attack of flow, and for bed condition, respectively.

a = Pier width (ft)

Fr_1 = Froude Number directly upstream of the pier = $V_1/(gy_1)^{1/2}$

V_1 = Mean velocity of flow directly upstream of the pier (ft/s)

g = Acceleration of gravity (32.2 ft/s^2)

Arneson et al. (2012) define it as a rule of thumb that the maximum scour depth for round nose piers aligned with the flow is: $y_s \leq 2.4$ times the pier width (a) for $Fr \leq 0.8$, $y_s \leq 3.0$ times the pier width (a) for $Fr > 0.8$.

2.2.6. Observational Method for Scour (OMS)

OMS, presented by Briaud et al. (2009), Briaud et al. (2011), and Govindasamy et al. (2013), is a method for estimating the future scour depth of existing bridges without site-specific erosion testing. It was developed as a first-order assessment for bridge inspection programs, such as those conducted by the Texas Department of Transportation (TxDOT). The method uses observations at existing bridges to determine the scour depth for a future flood event. This information is obtained from scour depth observations and charts that relate the future scour depth ratio (Z_{fut}=Z_{mo}) to the future velocity ratio (V_{fut}=V_{mo}). Govindasamy et al. (2013) present OMS's four methodological steps:

1. Determine Maximum Observed Scour Depth (Z_{mo}) This value is obtained directly from routine bridge inspection reports and other measurement records.
2. Determine the maximum flow velocity the bridge has been subjected to since its construction (V_{mo}). To estimate V_{mo} and, consequently, V_{fut}, there are two possible cases, depending on whether flow data are available from gauge stations. Suppose flow data is available, after obtaining an annual instantaneous flow peak series at the bridge or nearby. In that case, a flood frequency analysis is performed to determine the flow corresponding to the selected future peak flow magnitude (Q_{fut}). Then, Q_{mo} must be determined, as the maximum deserved peak flow has occurred at the station since the day of the bridge construction. However, if flow data is not available, V_{mo} and V_{fut} must be inferred from flow data near the bridge by developing maps of historical flow recurrence intervals to determine the maximum flow observed at the bridge (RIQ_{mo}) and by the relationship between RIQ_{mo} and Q_{mo}/Q_{fut}. Alternatively, the estimated V_{mo}/V_{fut} can be determined by converting Q_{mo}/Q_{fut} using hydrological and hydraulic tools such as HEC-HMS and HEC-RAS (Brunner, 2020) or TAMU-FLOW (Briaud et al., 2009)
3. Determine scour depth for a future flood This step requires the use of charts that relate Z_{fut}/Z_{mo} to V_{fut}/V_{mo}, which in turn obeys the relationship shown in Equation (15).

$$Z_{fut} = Z_{mo} \times f(V_{fut}/V_{mo}) \quad (15)$$

4. Compare the future scour depth to the allowable (threshold) scour depth of the foundation. This step Z_{fut} is now compared with the allowable scour depth ($Z_{threshold}$). If Z_{fut} is less than $Z_{threshold}$, the bridge is considered to have minimal risks and should undertake regular monitoring. Otherwise, the bridge is considered requiring further analysis

2.2.7. Scour and Geotechnical Parameters

Erosion rates in scouring processes are influenced by several factors, including hydraulic shear stress, soil and water temperature, soil and water chemical composition, soil water content, plasticity index, soil unit weight, undrained shear strength, and mean grain size (Briaud et al., 1999). Cohesive and cohesionless soils are eroded at different rates. In the first case, erosion can occur particle by particle or block by block, and its resistance to erosion is determined by a combination of weight and interparticle forces (electromagnetic and electrostatic), which are

characteristic of cohesive soils (Arneson et al., 2012). In cohesive soils, the rate of erosion increases slowly; however, not all types of cohesive soils erode at the same rate. Therefore, erosion is a function of the soil properties. Table 3 summarizes the factors influencing the erodibility of cohesive soils (NCHRP 2004).

In cohesionless soils (coarse-grained), erosion occurs particle by particle. Therefore, the resistance to erosion is influenced by the weight of the particles. There is a critical shear stress, τ_c, below which no erosion occurs and above which erosion begins. Briaud et al. (2001) defined that the critical shear stress (in N/m^2, or Pa) for cohesionless soils is proportional to the mean grain size D_{50} (expressed in mm):

$$\tau_c \left(\frac{N}{m^2}\right) \alpha\ D_{50}(mm) \tag{16}$$

Therefore, when hydraulic conditions exceed the critical limit of the soil, it erodes at a rate that depends on the increment of the hydraulic load (Arneson et al., 2012). Figure 19 shows the relationship between the erosion rate and the flow velocity as a function of the USCS (Unified Soil Classification System).

Table 3. Factors influencing the erodibility of cohesive soils (NCHRP 2004). Asterisk denotes unknown

When this parameter increases	**Consequence to Erodibility**
Soil water content	*
Soil unit weight	decreases
Soil plasticity index	decreases
Soil undrained shear strength	increases
Soil void ratio	increases
Soil swell	increases
Soil mean grain size	*
Soil percent passing sieve #200	decreases
Soil clay minerals	*
Soil dispersion ratio	increases
Soil cation exchange capacity	*
Soil sodium absorption ratio	increases
Soil pH	*
Soil temperature	increases
Water temperature	increases
Water chemical composition	*

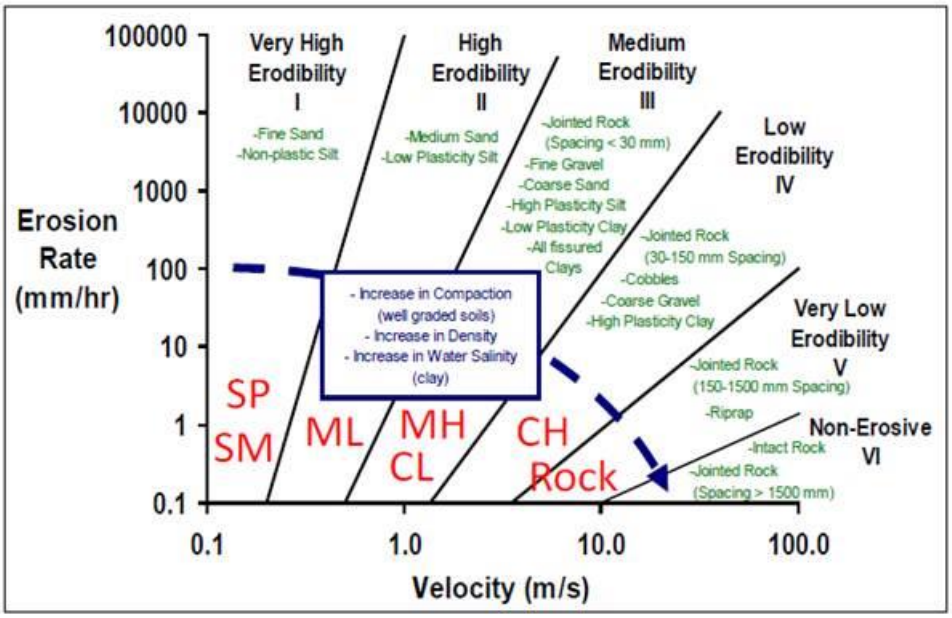

Figure 19. Erosion rate vs. velocity for a wide range of geomaterials (Briaud et al. 2011).

2.3. Scour Monitoring

Due to the cyclic nature of the scour process, determining its magnitude is complicated. Maximum scour can occur near the peak of a flood, but scour holes could refill with sediment as floodwaters recede (Arneson et al., 2012). Several studies and relationships have been published since 1990 to estimate local scour at bridge foundations (NCHRP 2011).

2.3.1. Erodibility rate relationship measured at laboratory

A series of devices has been used in the laboratory to measure erodibility. Some of the ones used in the laboratory are piston-type devices, which measure the erosion of a sample material exposed to flowing water under controlled conditions. In this technique, the soil is pushed out of the sampling tube due to the erosion created by the water flowing over it at a constant velocity. The data of velocity and erosion rate were compiled, and shear stress was thus calculated (Arneson et al., 2012).

Other devices used to measure erodibility in the laboratory include rotating-type and submerged Jet-Type Devices. In the first method, shear stress is created by rotating a cylinder filled with water that surrounds a cylindrical soil sample. The increments of the rotational speed and erosion rates are measured and used to develop the erodibility rate relationship. The submerged Jet-Type device is used to apply a water jet to a submerged soil. The depth of the surface scour is measured while the velocity of the water delivered over the soil interface is varied. The data are used to develop a relationship between the erodibility rate and the material.

2.3.2. Real-time Monitoring

Visual monitoring during a flood or inspection after it cannot provide sufficient information to determine if the bridge is safe (HEC-23, 2009). Different techniques pose different challenges and problems. According to Hunt (2009), many bridge owners, for instance, express that the maintenance needs of scour monitoring systems are commonly far greater than previously predicted. Factors such as instrument longevity, vandalism, and debris in water flow, among

others, are common issues that must be considered when selecting a monitoring system. Additionally, many systems require a great amount of installation effort, time, and personnel and/or are very expensive.

Given the importance of real-time monitoring, several instruments have been developed to measure the evolution of the scour hole. These instruments can be categorized as sonars (or fathometers), buried or driven rods, single-use devices, and sounding rods (HEC-23 2009).

- Magnetic Sliding collars:

According to Ahamed (2020), Magnetic Sliding Collars consist of a magnetic collar that is driven by a rod or mast to the streambed. When the streambed erodes, the collar slides down the rod into the hole. The information on the depth of the collar is stored and related to the advance of scour. When the collar slides around the rod, the switches inserted at defined distances along the rod are magnetically activated, providing the position of the collar.

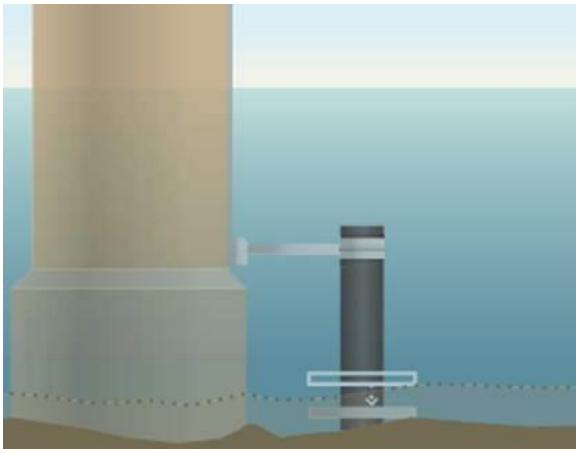

Figure 20. Sliding collar (Fondriest Environmental, 2021)

- Time domain reflectometers:

An electromagnetic pulse (wave) is sent through two pipes buried vertically in the streambed. Each time the pulse is sent down, a portion of the pulse's energy is reflected to the source once it encounters a change that represents the soil-water interface. Based on the monitored round-trip travel time of the pulse, the distance is calculated, providing information on any changes in the riverbed elevation.

Fisher et al. (2013) found that TDR is highly sensitive to changes in temperature and salinity, which affect the dielectric constant of water and lead to measurement errors. While TDR devices performed well in freshwater environments, their accuracy significantly decreased in brackish or saline conditions (above 0.5 PPT), where the waveform features became indistinct. However, TDR was resistant to turbidity, making it a suitable option for monitoring in highly sediment-laden waters. The findings suggested that TDR systems could be used effectively if temperature and salinity variations are accounted for in real-time adjustments.

- Ground Penetrating Radar (GPR):

According to Sreedhara et al. (2015), Ground-Penetrating Radar (GPR) is an effective tool for measuring scour, particularly in post-flood assessments when water levels are low. It enables data collection around bridge structures using portable or inflatable boat-mounted systems

(Boehmler & Olimpio, 2000). By transmitting electromagnetic pulses, GPR identifies subsurface interfaces based on reflected signals, providing continuous streambed profiles (Forde et al., 1999). It can detect existing, infilled, and historical scour holes, making it valuable for long-term scour analysis (Olimpio, 2000). However, GPR equipment is costly, and the collected data may be contaminated by noise (Webb et al., 2000).

- Float-out devices:

Float-out devices are sensors buried in the streambed that float to the surface when scour reaches a critical depth, activating a transmitter (Ahamed, 2020). The transmitter must be buried at a pre-defined depth in the streambed. When the scour reaches that depth, the buried device floats to the stream surface, and the transmitter is activated. The receiver, located near the bridge, detects the radio signal which contains the identification number of the device. The disadvantage of this system is that it is single-use. Once it floats out, it needs to be buried again if more measurements are needed.

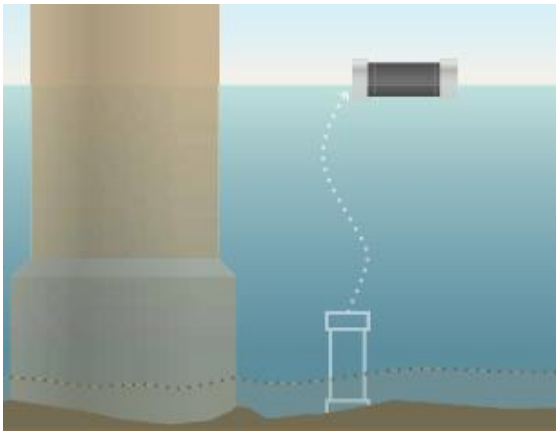

Figure 21. Float-out devices (Fondriest Environmental, 2021)

- Sounding rods:

According to Ahamed (2020), sounding rods are gravity-based mechanical instruments that slide as the streambed erodes, recording elevation changes.

- Fiber-Bragg Grating Devices:

According to Prendergast and Gavin (2014), these sensors use strain measurements along cantilever rods to detect scour progression. The bending of exposed rods generates strain signals that correlate with scour depth. These devices are low-cost and can track scour progression over time; however, their accuracy depends on the sensor spacing. They are also highly sensitive to vibrations from water flow or traffic, which can lead to unreliable readings.

- Buried or Driven Rods:

Buried or Driven rods provide reference points for measuring scour depth but require manual inspection (Ahamed, 2020).

- Electrical Conductivity Devices

According to Prendergast and Gavin (2014), these systems detect scour based on the difference in electrical conductivity between water and sediment. By measuring the current

between two probes, they determine the scour depth. While useful, they share a common limitation with other submerged sensors—underwater installation costs and maintenance challenges.

- Smart Rocks:

Smart Rocks are passive monitoring devices embedded with magnetic sensors or other tracking elements, allowing for real-time scour monitoring around bridge piers. They can be placed around piers, and their movement can be tracked using magnetometers or external sensors, allowing for data on the depth and progression of scour to be obtained without requiring direct underwater inspection (Chen et al., 2018; Tola et al., 2023).

Chen et al. (2018) first demonstrated the feasibility of this method, showing that magnet-equipped smart rocks could be effectively used for scour depth estimation. Tola et al. (2023) expanded on this concept by testing both direction-known and direction-unknown smart rocks, verifying their ability to track vertical displacements within scour holes. However, one major challenge identified is measurement accuracy, as environmental magnetic field variations can introduce noise and distortions in the readings.

Zhang et al. (2019) introduced a method where a magnetometer-equipped unmanned aerial vehicle (UAV) is flown over the water to locate smart rocks beneath the riverbed. This system enables engineers to track the movement of smart rocks without requiring divers or permanent underwater sensors. Tola et al. (2023) confirmed the reliability of this approach, demonstrating that UAV-assisted tracking achieved a location accuracy of less than 36 cm, as validated by total station measurements.

- Tiltmeters:

Tilt sensors detect angular changes in structures due to scour-induced instability (Ahamed, 2020). Briaud et al (2011) state that a big problem with this method is that it can provide movement data that may or may not be related to scour.

- Vibration-based Monitoring Systems:

Fisher et al. (2013) investigated vibration-based monitoring system in their work. This system operates by detecting scour through changes in turbulent pressure fluctuations. The system consists of an array of sensors installed along a buried pipe, with each sensor equipped with a flexible disk that responds to fluctuations in flow turbulence. The authors found that this method was insensitive to variations in temperature, salinity, and suspended sediment concentration, making it highly adaptable to different river environments. Even when the flow direction misaligned with the sensor, the system continued to perform well, maintaining a strong contrast between energy content in flowing water and buried sediment.

Kazemian et al. (2023) provide a detailed review of vibration-based scour monitoring techniques. The authors explain that vibration-based scour monitoring relies on changes in a bridge's structural vibration properties to infer the progression of scour. As scour removes sediment from around a bridge foundation, stiffness decreases, leading to measurable changes in natural frequencies, mode shapes, damping ratios, and spectral density. By deploying accelerometers on the bridge or embedding vibrating rods near the foundation, engineers can continuously track these vibration changes. Unlike traditional methods, vibration-based monitoring does not require underwater installation, making it more resilient to harsh environmental conditions and reducing maintenance costs. The authors summarize several key laboratory experiments that have validated the use of vibration-based monitoring. These include

studies by Shinoda et al. (2008) and Yao et al. (2010), which demonstrated that scour causes a significant decrease in the natural frequencies of bridges, a key indicator of foundation weakening.

More recent studies, such as those by Boujia et al. (2018) and Kariyawasam et al. (2020), have refined these techniques by examining mode shape variations and utilizing centrifuge modeling to simulate full-scale conditions. Field deployments, such as those by Ko et al. (2010b) in Taiwan and Briaud et al. (2011) in Texas, confirmed that frequency shifts correlate with real scour events, demonstrating the viability of vibration-based scour detection in real-world conditions. Kazemian et al. (2023) stated that vibration-based scour methods still require optimization in terms of distinguishing scour effects from environmental influences, ensuring long-term data reliability, and enhancing real-time detection. Advances in machine learning, multi-parameter analysis, and wireless sensors are improving accuracy and accessibility. Kazemian et al. (2023) conclude that, with continued technological progress, vibration-based monitoring provides a cost-effective and real-time solution for detecting scour and preventing bridge failures.

Tola et al. (2023) focus on vibration-based methods and their potential for real-time scour detection. It reviews other existing scour monitoring approaches, discusses their limitations, and highlights recent advancements in structural health monitoring (SHM) using vibration-based sensors. The study examines how natural frequency changes, mode shapes, and damping variations can be utilized to evaluate scour progression and predict foundation stability. Additionally, the paper includes experimental and numerical studies that validate vibration-based monitoring as a promising alternative to traditional scour detection methods.

2.3.3. Sonars' approach to monitoring bridge scour

This approach is more detailed in this report, as it corresponds to the method used in the present research, including efforts in other states that have applied sonar technology to monitor bridge scour. This type of equipment is mounted on the pier face to measure the distance to the streambed based on the time it takes for a sound wave to travel from the transducer to the streambed and return. The data is collected by a data logger, which can be programmed to take measurements at determined intervals. These instruments can collect data on the scour and refill processes (HEC-23, 2009).

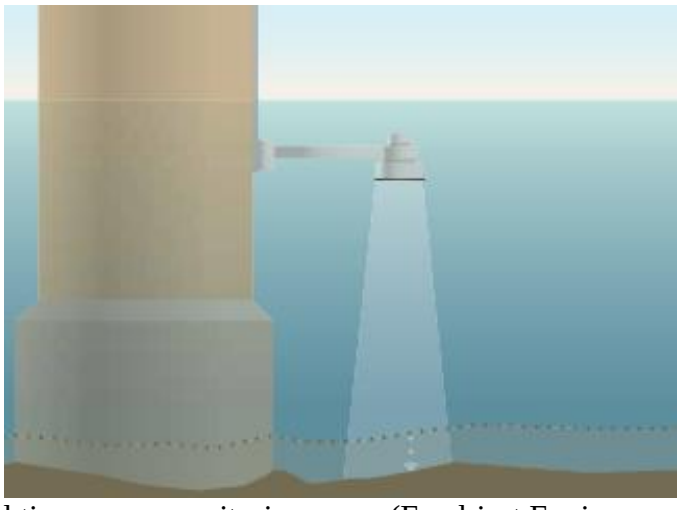

Figure 22. Real time scour monitoring sonar (Fondriest Environmental, 2021)

Mueller and Landers (1999) provide a comprehensive review of echo sounders and velocity-based measurements for hydrographic and sediment transport studies. Echo sounders determine streambed elevation by measuring the time for an acoustic pulse to travel to the streambed and back. They function best in deep, low-velocity streams, but performance deteriorates in shallow, turbulent, or sediment-laden waters. Echo sounders fall into three categories: non-recording, analog recording, and digital recording. While non-recording sounders provide only numerical depth values, recording sounders offer continuous cross-sectional records. Theoretical considerations, including beamwidth, frequency, and digitization techniques, affect measurement accuracy. Narrower beams, achieved through the use of high-frequency or larger transducers, enhance resolution but increase the instrument's size. Threshold and peak detection methods refine accuracy, although errors persist near obstructions, such as bridge piers. Digital-output echo sounders, used in hydrographic surveys, generate large datasets and employ RS-232, NMEA-0183, and parallel interfaces. Their performance depends on frequency, signal processing, and vessel motion compensation. Multibeam and scanning sonar enable rapid, high-resolution bathymetric mapping, which is essential for assessing bridge scour. Velocity measurements rely on current meters, electromagnetic meters, and Acoustic Doppler Current Profilers (ADCPs). ADCPs, which use the Doppler shift, provide three-dimensional velocity profiles but struggle near water surfaces and streambeds due to interference. Bottom tracking helps measure vessel velocity, but moving sediment can introduce errors. Experiments comparing 300-kHz and 1,200-kHz ADCPs reveal that lower frequencies penetrate mobile sediments, ensuring accurate bottom tracking, whereas higher frequencies misinterpret sediment motion as bed movement. The 600-kHz ADCP offers a balance for deep- and shallow-water applications. Real-time DGPS integration improves vessel tracking, though magnetic declination errors persist. Future advancements, such as Acoustic Correlation Current Profilers (ACCPs), may refine three-dimensional velocity measurements in turbulent zones, including bridge piers and abutments.

De Falco and Mele (2002) explore the use of sonar technology for monitoring scour and sediment transport around bridge piers. The study employed high-frequency sonar devices installed at Mezzana Corti and Borgoforte bridges, with six sonar sensors strategically positioned to track real-time scour depth variations and sediment movement. These devices provided continuous monitoring, allowing for a detailed temporal analysis of scour evolution under different hydraulic conditions. The sonar data revealed that scour depth changes dynamically in response to flow velocity and sediment transport, particularly during floods. Sonar measurements correlated well with manual depth readings and sediment sampling, highlighting their accuracy. The study demonstrated that sonar technology is highly effective in detecting scour progression and sediment deposition, making it valuable for infrastructure safety assessments. Among the advantages, sonar systems offer high-resolution, real-time data, allowing bridge engineers to monitor scour remotely and improve maintenance strategies. However, challenges include signal interference from suspended sediments, turbulent flow effects, and the need for periodic calibration to maintain accuracy. In conclusion, sonar-based monitoring is a powerful tool for evaluating bridge scour and sediment transport, providing continuous, precise, and efficient assessment of riverbed changes that are crucial for ensuring infrastructure safety.

Walker and Hughes (2005) report on scour monitoring methods at three bridge sites in Wisconsin, conducted in cooperation between the United States Geological Survey (USGS), the Wisconsin Department of Transportation (WisDOT), and local highway departments. The study aimed to evaluate manual and automated monitoring techniques for tracking streambed elevation changes caused by scour. The first bridge was instrumented with manual wire-weight gages, the

second with Datasonics PSA-916 sonar transducers, and the third with a sonar transducer and a depth sensor, both linked to a Campbell Scientific CR10 data logger for real-time data transmission. The study compared the effectiveness of these methods. Manual monitoring proved to be a cost-effective approach, particularly suitable for documenting long-term trends in streambed elevation. However, it was labor-intensive and did not allow for continuous, real-time data collection. In contrast, the automated sonar-based method provided real-time monitoring, making it particularly useful for tracking episodic scour events and supporting emergency decision-making. Despite its advantages, this method came with higher costs and presented challenges related to equipment durability. Sonar transducers were frequently damaged by ice and debris, requiring careful installation and maintenance. Additionally, calibration and validation, along with manual check measurements, were necessary to ensure data accuracy. The study concluded that both monitoring methods produced reliable measurements of streambed elevation. Manual monitoring was more economical and effective for long-term trend analysis, whereas automated sonar monitoring was crucial for real-time scour detection and monitoring. However, the researchers emphasized the importance of designing durable transducer mounts to minimize the risk of damage from environmental factors.

Conaway and Brabets (2011), in a USGS effort, examine the impact of channel migration and streambed scour on Bridge 339 along the Copper River Highway in Alaska. Over the decades, the river's discharge has shifted from western bridges to eastern ones, with Bridge 339 carrying up to 49 percent of the total flow in 2010, exceeding its design capacity by a factor of four. This shift has led to severe erosion, road closures, and instability in infrastructure. Scour monitoring, using pier-mounted sonars, recorded up to 33 feet of streambed erosion, necessitating emergency measures such as rip-rap placement. Pier 2 experienced significant oscillations due to high flow velocities, requiring continuous monitoring. Flow measurements indicate that Bridge 339 remains vulnerable to further scour, and ongoing river migration could exacerbate the conditions. Given the unpredictable nature of the river, maintaining the safety and functionality of the Copper River Highway will require proactive intervention and adaptive management to address the ongoing hydrologic hazards in this dynamic environment.

Fisher et al. (2013) identifies several limitations affecting sonar performance, including temperature, salinity, turbidity, and debris. Since the speed of sound in water varies with temperature and salinity, sonar measurements showed relative errors of up to 6% due to temperature changes and 3% due to salinity effects. Additionally, sonar devices were found to be highly sensitive to suspended sediments and turbid flows, with increased turbidity leading to inaccurate readings or an inability to detect the bed level. The study also noted that air bubbles and debris could disrupt sonar signals, resulting in false echoes and system failures. These findings reinforced the need for supplementary monitoring methods to validate sonar readings, especially in highly dynamic environments.

According to Topczewski et al. (2016), more sophisticated forms of sonars include 2D mechanical scanning sonar and 3D mechanical scanning sonar. 2D sonar captures high-resolution cross-sectional images of bridge pier walls, while 3D sonar maps scour holes and tracks changes in the riverbed over time. A 900 kHz 2D sonar was used in preliminary surveys on the Vistula River in Poland to identify critical scour areas. For long-term monitoring, a stationary 3D sonar recorded the evolution of scour depth over 1.5 months, revealing significant changes near the main river current. Sonar echograms enabled real-time analysis, demonstrating their reliability and accuracy. The study concludes that scanning sonar is the most effective tool for scour assessment,

with 3D sonar being ideal for long-term tracking and preliminary surveys essential for system placement.

Shen et al. (2018) lists the fundamentals of the sonar method, as well as the various types of 2D and 3D sonar technologies available, and the factors affecting the dependability of sonar data. The field testing and outcomes are also described. The field-testing study looked at 1) underwater feature identification, 2) performance in harsh settings, 3) data collection and reporting time, 4) equipment expenses, and 5) manpower needs. Sonar technology was shown to be capable of detecting larger-scale features of interest, such as scour holes, debris, and moderate-to-large-sized voids and protrusions. Sonar technology was identified as an effective way to quickly locate macro-objects in all situations, especially in unfavorable conditions.

Zheng et al. (2018) uses multi-beam echo sounders (MBES) to assess bridge scour and riverbed morphology in the Yangtze River Estuary. Using a Teledyne RESON SeaBat 7125, the authors conducted high-resolution sonar surveys (1 × 1 m grid) to map scour depths and erosion patterns around bridge foundations. MBES provided detailed 3D models, revealing scour depths up to 19.0 m and channel erosion rates of 0.33 m/year. The technique outperformed traditional single-beam sonar, enabling precise tracking of morphological changes influenced by tidal cycles and sediment transport. The study highlights MBES as a crucial tool for bridge safety monitoring, emphasizing its ability to capture wide-area riverbed deformations and enhance long-term infrastructure assessment in dynamic estuarine environments.

Ahamed (2020) developes a sonar-based real-time scour monitoring system enhanced by machine learning. Laboratory tests and results from the literature showed that sonar depth sensors in sediment-laden, fast-flowing water often produce noisy data – with many outliers and missing readings – due to turbulence and suspended sediments. Ahamed (2020) addressed this issue by employing Machine Learning (ML) algorithms, specifically Long Short-Term Memory networks, a type of recurrent neural network, to process the sonar signals. The ML-based signal processing method automatically identifies and removes outlier measurements, predicts scour depths for missing or erroneous data points, and fuses data from multiple sonar sensors to improve reliability. According to the author, this approach significantly outperforms traditional statistical filtering methods in handling the noisy time-series data. The cleaned and fused sonar measurements closely tracked the true scour depth in real-time, making the system less unreliable in flood conditions.

Hou et al. (2022) focuses on combining sonar data with a deep convolutional network to enhance scour hole detection accuracy. This machine learning integration enabled the automated identification and measurement of scour depth, thereby reducing manual interpretation errors. The model was trained to distinguish scour-related features from other underwater elements, allowing for the precise measurement of scour holes. However, Tola et al. (2023) note that this method performs poorly in high turbidity conditions, the presence of air bubbles, and turbulent flow.

San Martin et al. (2023) discusses sonar-based scour monitoring, particularly in supercritical flow conditions. They highlight the use of fathometers (echo sounders) and ultrasonic sensors, which provide real-time scour depth measurements but may be affected by high flow velocities and suspended sediment. Previous studies, such as those by Sturm et al. (2004) and Wu et al. (2012), successfully used sonar to track scour evolution. In their case study at the Rucúe Bridge in Chile, they installed an Airmar Echorange SS510 ultrasonic scour sensor, which recorded scour depth every 10 minutes with a precision of 1 cm. The study finds sonar to be superior to traditional methods, such as numbered bricks, offering continuous monitoring and improved accuracy. However, turbulence and sediment concentration can still impact performance, requiring further refinement in field applications.

Fosness and Schauer (2024) present a study conducted by the U.S. Geological Survey (USGS) in cooperation with the Idaho Transportation Department (ITD). The study focused on monitoring pier scour in real time at three scour-critical bridge sites in Idaho from 2020 to 2022. Real-time sonar sensors were installed at three bridges to measure bed elevation changes every 15 minutes. The study locations included the Payette River near Letha (Bridge ID 19935), the Boise River near Parma (Bridge ID 27415), and the Saint Joe River at Calder (Bridge ID 30730). Observed scour depths at all three sites were generally less than 20% of the estimated minimum pile tip depth, meaning no severe foundation exposure occurred during the study. The collected data were compared with the Coarse Bed and HEC-18 scour equations. The Coarse Bed equation provided more reasonable predictions than HEC-18 but still tended to underestimate scour in some cases. Below-average streamflows in 2020 and 2021 have likely contributed to lower-than-expected scour, with only 2022 experiencing above-average peak flows. The study employed quality assurance techniques, including manual depth verification and data filtering, to eliminate errors caused by debris, ice, and sonar malfunctions. Despite these efforts, some data gaps occurred due to equipment issues and environmental factors. The study demonstrated that real-time monitoring is a valuable tool for bridge safety assessments and can be effectively integrated into scour risk management strategies. The authors recommend expanding monitoring efforts to include more bridges and longer study periods to improve data reliability. They also suggest using alternative scour equations in conjunction with real-time data to refine scour predictions. Additionally, they propose considering the rapid deployment of real-time scour monitoring for critical bridges.

Currently, the USGS and the South Carolina Department of Transportation (SCDOT) have partnered to monitor and mitigate bridge scour in South Carolina bridges (SCDOT, 2024). To address this, sonar-based sensors, stream gages, and cameras have been installed on ten bridges across South Carolina, providing real-time data on river levels and scour depth. These monitoring systems are essential, especially in locations influenced by tides, such as the Wando and Cooper Rivers, where discharge computations are also conducted. Technicians conduct biannual cross-section surveys and manual tape-down measurements to validate sensor data. Acoustic Doppler Current Profilers (ADCPs) are used in deep or inaccessible sections of rivers. Maintenance of sensors can be challenging due to environmental conditions and physical obstructions. Data undergoes a rigorous validation process before being approved.

Beebee et al. (2023) examines scour at 20 bridge sites across Alaska. Conducted in cooperation with the Alaska Department of Transportation and Public Facilities (ADOT&PF), the study aims to assess the potential for scour-related bridge failures, particularly in locations where prior quantitative scour analysis is lacking. The evaluation incorporates geomorphic assessments, flood history analysis, and hydraulic modeling. The study used two-dimensional hydraulic models (SRH-2D) to estimate scour conditions more accurately than traditional one-dimensional methods. The study considered contraction scour, abutment scour, and pier scour, with vertical contraction scour observed at one site where floodwaters reached the bridge superstructure. The results indicate that most of the studied bridges are located in stable stream channels. However, two sites were classified as less stable or unstable due to factors such as mining activity and changing flow distributions. Hydraulic modeling revealed that floodplain overflow at some locations reduces scour risk by distributing floodwaters away from bridge foundations.

The study by Henneberg (2018) investigates real-time streambed scour monitoring at two bridges over the Gunnison River in western Colorado. Conducted in collaboration with the Colorado Department of Transportation, the study aimed to assess bridge stability by measuring

streambed elevations during snowmelt and runoff periods in 2016 and 2017. Traditional monitoring methods pose safety risks; therefore, the study introduced an innovative real-time monitoring system utilizing echosounders and data collection platforms. The research focused on two bridges: Bridge I–04–K on U.S. Highway 50 and Bridge I–03–A on Colorado Highway 141. Echosounders were installed to detect scour around bridge piers. Results showed that minor scour and fill occurred at Bridge I–04–K in 2017 but not in 2016, aligning with peak streamflow events. Meanwhile, Bridge I–03–A showed no significant scour, although underwater inspections revealed pre-existing undermining along the pier wall. Cross-sectional surveys were conducted, and statistical tests confirmed significant changes in streambed elevation over a two-year period. The study concludes that real-time monitoring is effective for scour detection, improving safety and bridge management. Future monitoring efforts could expand using wireless telemetry and standardized data protocols to enhance data collection.

2.3.4. Previous Bridge Scour Research Conducted at Auburn University

Auburn University developed studies to evaluate scour in bridges because the Hydraulic Engineering Circular 18 (HEC-18) predictions, in certain cases, present unrealistic estimates of bridge scour, particularly in cohesive soils. Walker (2013) notes that the scour behavior of granular soils is typically well understood, and the Federal Highway Administration has established design criteria. However, the work emphasized that the case of cohesive soils is different and complex, making it difficult to establish and develop universal methods for predicting erosion.

Wright (2014) develops a scour test using the Erosion Function Apparatus (EFA) to determine the erosion function for six different soil layers throughout southern Alabama. The erosion function has been modified to account for the effects of sample swelling during testing. Based on EFA test results, a correlation was found between erodibility and traditional geotechnical parameters. It has been observed that the erodibility of these clay layers depends on the "N-value" of the Standard Penetration Test (SPT), the site's moisture content, and the percentage of soil that passes through the 200th sieve.

Anderson et al. (2015) tests ten soil formations using an updated Erodibility Function Apparatus (EFA) equipped with an ultrasonic sensor capable of quantifying erosion. EFA testing was performed to determine erosion function and to determine which strata demonstrated resistance to erosion. The study determines that three of the ten tested formations had a scour moisture content of less than 22% and a mean grain size of less than 0.008 mm.

Pokharel's (2017) study emphasizes uncertainties of HEC-18 results and demonstrates the variability of the input parameters and calculated scour depth. Although the research suggests that the critical shear stress of HEC18 scouring is related to the average particle size (D_{50}), in reality, it is also influenced by several other factors, particularly in cohesive soils. Six clay soil samples were used to compare the critical shear stress and critical velocities obtained by HEC-18 with those previously obtained from the Erosion Function Apparatus (EFA), demonstrating the unreliability of HEC-18 regarding the soil property. A multi-layer method was proposed to calculate the total feasible scour depth, and D_{50} was used layer by layer to test the depth.

Vasconcelos et al. (2018) presents results from field and numerical simulations of bridge aggradation at the Soapstone Branch in Dale County, Alabama, a tributary of the Little Choctawhatchee River. The study aimed to explain the origin of ongoing processes in the basin and avoid bridge replacement, considering the various competing processes occurring in the basin, and provide alternative solutions that will improve conveyance at Dean Road Bridge. The research included fieldwork to assist in the calibration of hydrological and hydraulic modeling.

Additionally, the study revealed that the altered slope of the stream near the bridge increased shear stress in the streambed, thereby reducing the likelihood of accumulation near the bridge.

2.3.5. Bridge Scour Research Involving Field Observations

In this literature review, hydraulic investigations on bridge scour are classified into those that involve field work and those that include only laboratory results. Robinson and Thompson (1995) review streambed scour data at 1,338 federal-aid bridges in southeastern Indiana in 1991. The inspections were part of a seven-year study conducted by the US Geological Survey and the Indiana Department of Transportation, which evaluated 5,600 bridge sites across the state. Site conditions were recorded using measurements and observations of leftover scour made during low-flow discharges. These remnant-scour data were utilized to create an observed-streambed-scour index as a screening tool for determining the scour severity.

Atkins and Hedgecock (1996) collects scour data at 15 sites along Alabama streams during high-flow conditions. The streamflow recurrence intervals ranged from less than 2 to 10 years. This study revealed that scour depths at bridge piers varied from 0.3 to 5.8 feet. To estimate scour depths at the sites, the study employed the Colorado State University (CSU) local scour equation, as indicated in the Federal Highway Administration's Hydraulic Engineering Circular No. 18. The estimates from the equation were, on average, over four times larger than the measured scour depths.

Wilson (1995) evaluates scour data gathered at 22 bridge sites in Mississippi between 1938 and 1994. The drainage area of the bridge-scour sites ranged from 60.8 to 5,720 square miles, with slopes ranging from 0.00011 to 0.00163 feet per foot in the vicinity of each site. Pier-scour depths were measured to be between 0.6 and 20.4 feet. Total scour depths were measured at minimum bed elevations ranging from 5.2 to 29.8 feet. Measured recurrence periods of discharge ranged from less than 2 to 500 years. By relating the pier-scour depth divided by the normal pier width to the approach-flow depth divided by the normal pier width, an envelope-curve equation for Mississippi pier-scour data was created. Using this envelope-curve equation and the scour-prediction equation now suggested in the Federal Highway Administration Hydraulic Engineering Circular No. 18 (1994), measured pier-scour depths were compared to computed pier scour depths (HEC-18).

Hopkins and Robinson (1997) collect data at 5,587 federally funded bridges in Indiana in collaboration with the United States Geological Survey and the Indiana Department of Transportation. These data are stored in a computerized data bank at the US Geological Survey in Indianapolis, Indiana, and may be used to measure Streambed scour and channel instability. The five groups of data items are General Site Characteristics, observed and Calculated Scour Characteristics, Bridge Characteristics, Stream Characteristics, and debris characteristics. The element name, samples of data from Bridge Number 89-54 over Lick Creek in Wayne County, Indiana, and a brief description of each element are included in data for each group.

Landers and Müller (1996) employs a dataset of pier scour field measurements comprising 139 local scour observations in live-bed and clear-water situations. Pier scour measurements were taken at 44 bridges in 12 states, totaling 90 bridge piers. In logarithmic space, the effect of pier width on scour depth is linear. In logarithmic space, the effect of pier width on scour depth is linear. Comparisons of computed and actual scour depths reveal that none of the chosen equations accurately predict scour depth for all tested situations. Some of the equations performed well as conservative design equations; however, they significantly overpredicted many observed scour depths.

Jackson (1996) examined scour data obtained between 1989 and 1994 to check if pier and contraction scour occurred at 22 bridge sites in Ohio. Pier scour depths calculated using several pier scour prediction equations were compared to measured pier scour depths, and the accuracy of the prediction equations was assessed. The observed pier scour relationships were compared to analogous relationships produced in the lab. The depth of the contraction scour was determined by measuring mean streambed elevations. Mean streambed elevations at the approach segment were used to determine channel stability. The occurrence of historical scour was investigated at all sites using ground-penetrating radar.

Lee and Hedgecock (2008), in a collaboration between the US Geological Survey and the Alabama Department of Transportation, observed clear-water contraction scour at 25 bridge locations in Alabama's Black Prairie Belt of the Coastal Plain. These bridge locations included 54 hydraulic structures, 37 of which had demonstrable scour holes. Scour depths measured varied from 1.4 to 10.4 feet. For each bridge, theoretical clear-water contraction-scour depths were calculated and compared with observed scour depths.

Conaway (2006) monitors streambed scour in real-time at several Alaskan bridge sites. The research collected four years of bed elevation data from the Knik River in Palmer, Alaska, and discovered a yearly cycle of channel aggradation and degradation to an equilibrium level, punctuated by shorter episodes of aggradation and degradation. Conaway discovered that the annual vertical bed-elevation change exceeds 6 meters, resulting from a complex interaction among sediment supply, discharge, and the effects of instream hydraulic structures. A combination of hydraulic variables measured in real-time during high flows, data collected from pier data sonar, and calculated variables from a multi-dimensional hydrodynamic model was used to evaluate seven predictive equations for live-bed contraction scour and two abutment scour calculations. A multi-dimensional hydrodynamic model was computed with hydraulic variables measured in real-time.

Straub and Over (2010) conducts research with the purpose of this report to present the results of testing the SRICOS-EFA method for estimating the scour depth of cohesive soils in Illinois streams. Fifteen sites were chosen for testing. Streamflow data were retrieved from historical data records or estimated, then disaggregated to an hourly time step, if necessary, using the methods described in this report. Channel geometry, including the measurement of historic scour, and bridge information were retrieved from historical data files or collected during this study. EFA tests were conducted on soil samples from each site to facilitate the completion of SRICOS scour prediction. In addition, scour prediction methods defined in HEC-18 (Richardson & Davis, 2003) for non-cohesive soils were applied at each site to forecast scour. This research presented a reduction factor technique for adjusting HEC-18 scour projections based on SRICOS and observed scour.

Govindasamy et al. (2013) applies the Observed Method for Scour (OMS), which is further detailed in this literature review. This study included 16 bridges in Texas, 10 of which were scour-critical. According to the OMS approach, six of the ten bridges were deemed to be stable. They developed a new hydraulic-hydrologic analysis approach that could be applied in other areas with sufficient flow gauges. They used nine case histories to validate OMS and found that the predicted and measured values were in good agreement.

Additionally, Straub et al. (2013) presents the findings of research on ultimate pier and contraction scour procedures for cohesive soils on 30 Illinois bridge locations. The ultimate cohesive and non-cohesive approaches are compared, as well as the cohesive soil reduction factor method and measured scour data from the Illinois Department of Transportation (IDOT). Also

provided are the findings of a comparison of past IDOT laboratory and field data on the unconfined compressive strength of soils (Qu). Both ultimate cohesive and reduction-factor techniques employ unconfined compressive strength, and understanding how data from field methods relates to laboratory methods is crucial for making informed decisions about the approaches. The non-cohesive method predicts the most scour, followed by the reduction-factor method, and finally, the ultimate cohesive method predicts the least amount of scour.

Benedict and Caldwell (2014) conducts field assessments of bridge scour in collaboration between the USGS and the South Carolina Department of Transportation to better understand regional scour patterns. The researchers took measurements of clear-water abutment, contraction, and pier scour, as well as live-bed contraction and pier scour, at about 200 riverine bridges. These analyses revealed bridge-scour envelope curves for estimating scour potential associated with all components of scour at riverine bridges in South Carolina, as well as significant insights into regional scour patterns.

Henneberg (2018) develops a study for the Colorado Department of Transportation to assess the structural stability of two bridges. These studies were conducted during and immediately after peak flows, utilizing real-time instrumentation to measure streambed elevations during snowmelt-runoff periods (May through June) in 2016 and 2017. Surveys were conducted in the spring of 2016 before snowmelt runoff, the spring of 2017 before snowmelt runoff, and the fall of 2017. To find significant differences across surveys, streambed elevations from cross-section surveys at both bridges were analyzed using two-tailed, paired t-tests and Wilcoxon rank-sum tests. Both tests revealed substantial changes in mean streambed heights for the cross-sections and around the monitored piers at two bridges.

Chedid (2018) evaluates the Borehole Erosion Test, a new in-situ erosion test (BET). During wet rotary drilling, the increase in borehole diameter over time is measured for a particular flow velocity. The BET produces a profile of soil erodibility along the entire depth of the borehole. BET experiments in clay and sand are conducted at Texas A&M University's National Geotechnical Experimentation Sites. To calculate the shear stress fields during the test, the BET is simulated using Computational Fluid Dynamics (CFD).

2.3.6. Laboratory and Analytical Research on Bridge Scour

Briaud et al. (1999) proposes the method Scour Rate In Cohesive Soils (SRICOS), which is intended to predict scour depth over time around a cylindrical bridge pier. SRICOS method requires sampling soil at the bridge pier and testing it in an erosion function apparatus (EFA) to obtain the scour rate versus the hydraulic shear stress curve. After that, the maximum shear stress at the bridge pier needs to be estimated, and then it is possible to obtain the initial scour rate by applying the maximum shear stress at the scour rate curve previously developed. The maximum depth of scour can thus be calculated, and the complete scour depth curve versus time can finally be developed through an empirical hyperbola equation obtained from flume tests. The scour depth prediction can be done by reading the scour depth generated by the corresponding flood duration. This model is the recommended approach to estimate scour in cohesive soils in the current version of HEC-18. Among the limitations of SRICOS are the necessity to compare its results with full-scale scour measurements and the fact that SRICOS was developed for the simplest case of a circular pier; therefore, bridges with more complex geometries would likely result in different scour depths over time. This limitation was addressed in the subsequent version of SRICOS presented in Briaud et al. (2004).

Chen et al. (2000) investigates mathematical models that could be used to solve problems involving bridge scour. "The pier scour was first investigated using numerical models. These models have not yet matured to the point where they can be trusted. As a result, this research was abandoned. Expert systems offer an alternative technique for evaluating challenges associated with bridge scour. They might include formal approaches, such as CAESAR (Catalog and Expert Evaluation of Scour Risk and River Stability), or informal indices, such as INDOT's probable streambed scour index.

In FHWA's Hydraulic Engineering Circulars (HECs) 18, 20, and 23, Jones and Richardson (2003) provides the equations and procedures for determining local scour depths, which are used in the design and evaluation of most bridges. They did, however, emphasize that physical model studies are often required for the design or evaluation of scour around bridges with complex foundations or canal conditions. In HEC 18, complex piers are described as piers composed of two or more parts (pier shaft, pile cap or footing, and piles) that are exposed to flow due to design, long-term deterioration, or contraction scour.

Molinas (2004) summarizes the findings of an experimental research study titled "Effects of Gradation and Cohesion on Bridge Scour," conducted at Colorado State University from 1991 to 1996. As a product of this work, over 250 new pier scour data sets were obtained. A new equation was developed that expresses pier scour in terms of the dimensionless excess velocity factor, flow depth, pier diameter, and a correction factor for coarse fractions present in the mix.

Lee et al. (2004) conducts research in which three full-scale laboratory models of a prototype bridge on the Chattahoochee River in Cornelia, Georgia, were built for comparison with continuous scour and velocity measurements taken in the field. The whole river bathymetry, as well as the bridge pier bents and abutments, were included in the laboratory model, which was built at a scale of 1:40. An acoustic Doppler velocity meter was used to measure the velocity field and scour outlines. The bridge piers were fitted with four fathometers in the field, which gave continuous readings of the channel bottom elevation at the central pier bend. A side-looking acoustic Doppler velocity meter was also connected to the upstream pier for measuring the velocity component across the cross section.

Chase and Holnbeck (2004) evaluate five pier scour equations for coarse-bed streams in collaboration with the Montana Department of Transportation. The Bridge Scour Data Management System was utilized to select pier scour and associated bridge geometry, bed material, and streamflow measurement data from bridges across coarse-bed streams in Montana, Alaska, Maryland, Ohio, and Virginia. For flood events with approximate recurrence intervals of less than 2 to 100 years, pier scour calculated using the Simplified Chinese equation, the Froehlich equation, the Froehlich design equation, the HEC-18/Jones equation, and the HEC-18/Mueller equation were compared to 42 pier scour measurements.

Briaud (2004) proposes the SRICOS-EFA approach, which is used to forecast the scour depth versus time curve for complex pier and contraction scour in soils such as sand, silt, clay, and soft rock. The approach entails collecting soil samples on-site, testing them in the EFA, and feeding the results into the SRICOS computer program. The method is described, and comparisons between forecasts and full-scale measurements are provided. A novel approach to forecasting future hydrographs and risk assessment is included. By comparing with the 1999 version of SRICOS, the SRICOS-EFA deepens the scour prediction analysis by extending the applicability range, being able to handle complex piers, contraction scour and both phenomena combined (Wang, 2004). Regarding contraction scour, the method proposes equations (maximum contraction scour and initial maximum shear stress equation) that consider the reduction in channel

width approaching the channel, the length of contraction, and the transition angle of the channel contraction.

Muller and Wagner (2005), in collaboration with the Federal Highway Administration and other state highway agencies, gathers and documents field data on scour at bridges at 79 sites in 17 states. These data were evaluated in order to identify pier scour, contraction scour, and abutment scour. In the study, they used 493 local pier scour measures, 18 contraction scour observations, and 12 abutment scour measurements in the national database.

Hong et al. (2006) researches contraction scour at a bridge in Macon, Georgia, located across the Ocmulgee River. In 2005, the Georgia Institute of Technology's Hydraulics Laboratory built a 1:45 scale model of the bridge, its embankments, and the approach and exit river bathymetry. The 50-year peak flood discharge, the 100-year peak flood discharge, and a 1998 historical flood discharge, for which the US Geological Survey collected field data, were all modeled. Contraction scour data from the lab and the field are compared, and a strategy for hydraulic modeling of contraction scour is proposed.

Lombard and Hodgkins (2008) predicted the maximum abutment-scour depths using five different approaches. They were compared to the maximum abutment-scour depths found at 100 abutments at 50 bridge sites in Maine with a median bridge age of 66 years, according to the Froehlich/Hire approach, the Sturm method, and the Maryland method, all of which were published in Federal Highway Administration Hydraulic Engineering Circular 18 (HEC-18).

Briaud et al. (2009) proposes a method for assessing a bridge scour. It consists of three levels of evaluation. Bridge Scour Assessment 1 is the first level (BSA 1). BSA 2 and BSA 3 refer to the second and third levels, respectively. By extrapolating current scour measurements to derive the scour depth corresponding to a particular future flood event, BSA 1 overcomes the qualitative nature of current initial evaluation methodologies. It utilizes computer-generated extrapolation charts based on a large number of fictitious bridges to relate the future scour depth-to-maximum observed scour depth ratio to the future flood velocity-to-maximum observed flood velocity ratio. If BSA 1 does not conclude with a specific plan of action for the bridge, BSA 2 must be implemented. The maximum scour depth is determined by BSA 2. BSA 2 was launched because of its simplicity, albeit being conservative. If BSA 2 does not conclude with a precise plan of action, BSA 3 must be implemented. Instead of just using the maximum scour depth, BSA 3 requires the calculation of time-dependent scour depth.

Calappi et al. (2010) points out two issues with then existing formulas for calculating scour on bridge crossings. Scaling effects hinder them, and they fail to account for the complex hydrodynamic forces at play throughout the scouring process. These flaws in the model might lead to an unreasonable overestimation of scour depths, resulting in extra construction costs. They developed a method utilizing field-scale data and nonlinear regression to construct a family of equations tailored to diverse non-cohesive soil conditions, thereby enhancing the forecasting capabilities of the HEC-18 scour model.

Schuring et al. (2010), with the support of the New Jersey Department of Transportation (NJDOT), conducts an assessment of existing scour practices among DOTs across the United States to improve scour design and evaluation methodologies. The ten-question poll asked about design standards, failure experiences, monitoring procedures, and countermeasure preferences, among other topics.

The fifth version of HEC-18, developed by Arneson et al. (2012), incorporates changes based on ongoing advances in scour-related research and the highway community's experience with the 2001 edition. Expanded discussion on the policy and regulatory basis for the FHWA Scour

Program, including risk-based approaches for evaluations, developing Plans of Action (POAs) for scour-critical bridges, and an expanded discussion on countermeasure design philosophy, are among the major changes in the fifth edition of HEC-18 (new vs. existing bridges). The HEC-18 fifth edition includes a new section on contraction scour in cohesive materials, an updated abutment scour section, alternative abutment design techniques, alternative methodologies for calculating pier scour, and new guidelines on pier scour with debris loading.

Schambeau (2012) develops a tool that examines five failure modes of timber piles and timber bents: bent kick-out due to zero or negligible embedment after scour; pile plunging due to soil failure; pile buckling failure in either the longitudinal or transverse direction; bent pushover failure due to the combined effects of superstructure gravity loading and lateral debris raft load; and beam-column failure of the upstream pile due to the combined latera. The automated screening tool was created using Visual Studio 2005 and 2010 software packages.

Zhang et al. (2013) evaluates the application of the HEC-18 technique to bridges in Louisiana, which are typically constructed on cohesive soils. They proposed a more accurate design method for estimating scour depth and rate. Factors that were considered in this study included : (1) the driving force of scour, i.e., the hydrologic and hydraulic characteristics of flood flows that cause scour; (2) the resistive force of scour, i.e., the geotechnical properties of streambed soils or sediments that are removed by stream flow; and (3) the geometry, size, and shape of the obstacles all contribute to the HEC-18 method's scour depth prediction errors (e.g., piers and pile caps).

Sheppard et al. (2014) uses combined laboratory and field information to analyze twenty-three of the more recent and commonly used equilibrium local scour equations for cohesionless sediments. This inquiry gathered data from 569 labs and 928 field locations. A method for evaluating data quality was created and applied to the data collection. The laboratory and field data were reduced to 441 and 791 values, respectively, using this approach.

Benedict and Caldwell (2014) conduct a literature review to identify sources of abutment-scour data, which was compiled into a database comprising 329 field and 514 laboratory scour measurements. The USGS collected all of the field data, which included: (1) measurements from the USGS National Bridge Scour Database; (2) from the South Carolina Piedmont (cohesive sediments) and Coastal Plain (non-cohesive sediments); and (3) from small, steep-gradient streams in Maine with coarse sediments.

Yorozuya and Ettema (2015) present the results of a large-scale, laboratory-based study of scour at compound channel bridge abutments. The study examined the impact of various characteristics of abutment architecture, including abutment and floodplain erodibility, on scour development. Its findings show that three types of scour can occur at abutments in compound channels: scour of the main-channel bed (Scour Condition A), scour of the floodplain around an abutment (Scour Condition B), and scour at an abutment column exposed once an abutment is breached (Scour Condition C). Depending on the location of the abutment and the site's circumstances, several variables may coexist.

Saha (2017) presented a comprehensive method of predicting maximum scour depth that is proposed based on laboratory findings combined with widely used empirical scour estimation methods, such as the Colorado State University (CSU) pier scour equation, Melville Sheppard equation, and the Ambient pier scour method, which overcomes the problem of separate estimation of different scour depths.

Schuring et al. (2017) developed a method for assessing bridge scour on non-tidal streams in New Jersey. A web-based survey of scour practices in the United States and a literature review

of predictive scour models initiated the research. The main project outcome is a new Scour Evaluation Model (SEM), a tiered, parametric, risk-based decision tool. To generate risk assessments for a specific bridge, a variety of geotechnical, hydrologic, and hydraulic data are reviewed. These ratings are then entered into a Risk Decision Matrix, which produces a scour priority level and suggests actions, ranging from expedited countermeasure installation to removal from scour critical status.

Briaud and Chedid (2019) propose a critical tool for making risk-informed decisions that ensure public safety at the lowest feasible cost. They provided recommendations on the maximum permissible scour depth, which has become a critical tool for making risk-informed decisions that ensure public safety at the lowest feasible cost. Such guidelines produce site-specific scour limits that are compared with the observed or calculated scour at an existing bridge in order to make a preliminary judgment of scour criticality at that bridge and assess the necessity for additional structural and geotechnical evaluations. The study proposed criteria for determining the maximum permissible scour depth at or near spill-through abutments, where the failure scour depth is governed by the slope stability of the abutment embankment.

Shahriar et al. (2021) presents an evaluation of the current state of knowledge on the geotechnical elements of erodibility, factors impacting pier scour, issues complicating pier scour assessment, and databases on erodibility and pier scour. In light of the parameters impacting scour rate and equilibrium magnitude, a synopsis of deterministic pier scour models published since 1990 is presented. According to the study, the paper's predictive methodologies have limitations. Advances in probabilistic pier scour models and observation-based models were also discussed.

3. Methodology for Scour Evaluation using HEC18 and OMS

To perform scour estimate calculations using OMS and HEC-18, preliminary steps are necessary to compute the flow characteristics associated with flooding conditions. Hydrological computations are needed to obtain peak flow estimates associated with a recurrence interval, which in this report was assumed to be 100 years. Such peak flow values are, in turn, introduced into hydraulic modeling tools along with additional geometric information on the bridge and stream cross-section to obtain the local flow depth and velocities in the vicinity of each bridge pier.

Since the research aimed to compare these two approaches for quantifying bridge scour, it was decided to perform this comparison while considering alternatives for hydrological and hydraulic modeling. This chapter presents the methodology employed in the various alternative modeling efforts and provides the results from these calculations. The chapter also presents the methodology used to compute the scour estimates based on these results.

3.1. Methodology for Hydrological Calculations

Three separate methods were used for peak flow calculations.

1. For all bridges, peak flows were estimated using regional regression equations (RRE), taking into account the location of each bridge, as illustrated in Section 2.1, and considering the corresponding watershed characteristics. The data can be obtained using the USGS StreamStats tool (https://streamstats.usgs.gov/ss/, Ries III et al., 2004).
2. For BIN 015002, a USGS gaging station enabled the development of Flood Frequency Analysis (FFA) using the statistics of peak flows
3. Finally, for all bridges considered in this study, hydrological models were developed using HEC-HMS 4.9 software and HEC-GeoHMS for ArcGIS Desktop 10.x.

The methodological steps for creating the HEC-HMS hydrological models were:

i. Delineate each watershed using StreamStats and download the area's shapefile (*.shp).
ii. Download the DEM from USGS National Maps (Carswell Jr., & William J., 2013). To this end, it is necessary to visit the website (https://apps.nationalmap.gov/downloader/#/), select the area of interest, review the available information, and then download it. It may be necessary to create a mosaic of several digital elevation models (DEM) to complete the required information for each watershed.
iii. Process the DEM using HEC-GeoHMS using the recommendations by Fleming and Doan (2009). This process is associated with the catchment and stream definition based on flow direction and accumulation. Also, this process defines a slope map for the watersheds.
iv. Define the watershed characteristics using the post-processed DEM with HEC-GeoHMS, following the guidelines proposed by Fleming and Doan (2009). Those characteristics are related to river length, river and basin slope, and definition of the longest flow path.
v. Define the hydrological methods to be simulated in HEC-HMS in terms of losses, transformations, base flow, and routing methods. Additionally, it is necessary to specify the required parameters for each method, depending on the one chosen. Typically, these methods have different parameters and necessary information. In this specific case, the Natural Resources Conservation Service curve number was used as a method for determining loss. A fully composite CNII is determined using geoprocessing analysis in ArcGIS 10.x, which integrates data from the National Land Cover Dataset (NLCD) (Dewitz, J., and U.S. Geological Survey, 2021) and the Soil Survey Geographic Database (Soil Survey Staff,

NRCS, USDA, 2015) as reference tables. In addition, values for other initial moisture contents, CNI and CNIII, are also obtained.

vi. Extract the rainfall data from Atlas 14 (Perica et al., 2013) and configure the other necessary methods to run HEC-HMS. In these specific simulations, a rainfall transformation method, the SCS dimensionless synthetic hydrograph (Mockus, 1972), was employed for each of the sub-basins. The base flow value was not taken into account in the analysis. Other processes, such as evaporation or recharge, were considered negligible because the simulations were event-based and, thus, not continuous.

vii. Export the model to HEC-HMS from HEC-GeoHMS following the recommendations by Fleming and Doan (2009). Figure 23 shows the models created in HEC-HMS.

viii. Run the models and obtain the output hydrographs. These hydrographs correspond to CNII or normal antecedent moisture conditions.

Create models for dry antecedent moisture conditions CNI and wet antecedent moisture conditions CNIII, taking as a reference the models constructed for CNII and using the equations from

Table *1* for each of the sub-basins belonging to each HEC-HMS model.

ix. Run the models for CNI and CNIII and obtain the additional output hydrographs for each watershed.

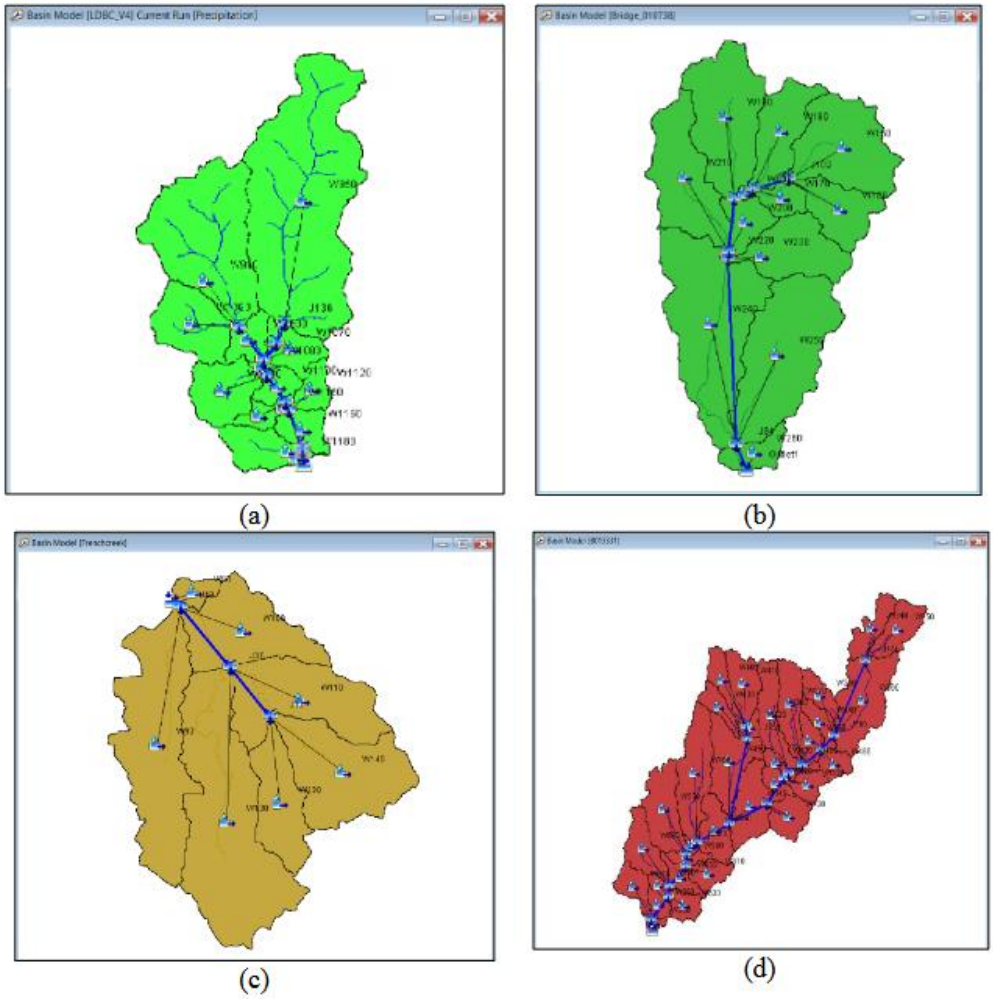

Figure 23. Models created in HEC-HMS for the watersheds associated with the bridges (a)

BIN 015002 (b) BIN 010738 (c) BIN 007070 (d) BIN 013310

3.2. Hydrological Modeling Results

The information provided below presents the results of the different hydrological alternatives used to calculate peak flow in the selected bridges. These alternatives include RRE, FFA, and hydrological models. RRE values for a 100-year event were calculated for the sites where the bridges are located, using the bridge as the watershed outlet. The values were computed according to the guidelines provided by Hedgecock and Lee (2010) and Anderson (2020). The results of the values obtained using RRE are presented in Table 4**.**

Table 4. Peak using RRE for 100-yr return period values for the four analyzed bridges

BIN	**River**	**Drainage Area (mi^2)**	**Peak Flow (CFS)**
015002	Little Double Bridges Creek	21.6	7,682
010738	Blue Creek	4.5	3,221
007070	French Creek	12.5	7,616
013310	Conecuh River	373.3	38,017

3.2.1. BIN 015002. Little Double Bridges Creek and County Road 606

For BIN 015002, which is equipped with a USGS streamflow gauge station, an FFA analysis was conducted. Analyzing 37 years of peak streamflow data from 1986 to 2022 and utilizing the USGS software PeakFQ 7.4, a 100-year streamflow event was calculated, obtaining a value of 14,570 cfs. This result is 89% longer than the corresponding RRE results. The cause of this difference was one extreme event, Tropical Storm Alberto, which hit the area around Enterprise, Alabama, and BIN 015002 on July 7, 1994. This event indicates that the very high flow value recorded at USGS Station No. 02362240 is realistic and illustrates that, in some cases, values calculated using RRE may not represent the worst scenario for peak flow calculation.

Using data collected from a rain gauge installed at Bridge No. 015002 and stream flow data recorded at USGS Station No. 02362240, parameter calibration was performed for the Little Double Bridges Creek watershed. The calibration process was carried out in HEC-HMS 4.9, aiming to minimize percent error in peak discharge (Equation (4)) for a significant event that occurred on March 18, 2022. The optimization results for minimizing the percent error in peak discharge for Little Double Bridges is shown in Figure 24 and the comparison between the two resultant outflow hydrographs is illustrated in Figure 25. In the calibration process, the values of the composite CN remained constant. In contrast, the roughness coefficients for overland flow planes and channels varied for a simplex optimization in each sub-basin of the watershed. After the calibration process, a difference in the peak flow discharge was found between the observed and calibrated data, corresponding to 10 cfs, which is equivalent to a 0.5% error in peak discharge. The roughness parameters adjusted during the calibration process were used in models representing different antecedent soil moisture conditions for the watershed associated with the mentioned bridge. Considering that the other bridge watersheds share similar land use characteristics, urbanization percentages, and rural predominance, these parameters served as references for developing the other watershed models.

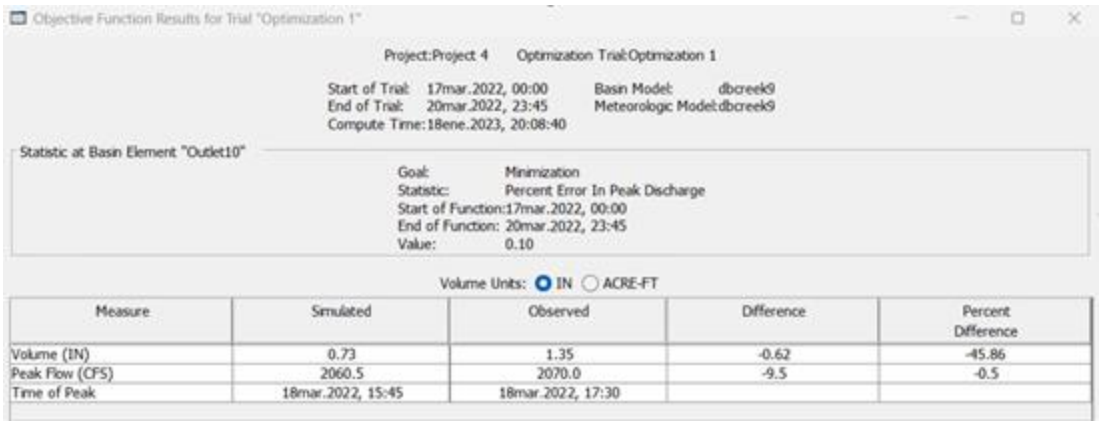

Measure	Simulated	Observed	Difference	Percent Difference
Volume (IN)	0.73	1.35	-0.62	-45.86
Peak Flow (CFS)	2060.5	2070.0	-9.5	-0.5
Time of Peak	18mar.2022, 15:45	18mar.2022, 17:30		

Figure 24. Calibration results for minimizing the percent error in peak discharge in Little Double Bridges Creek (BIN 015002)

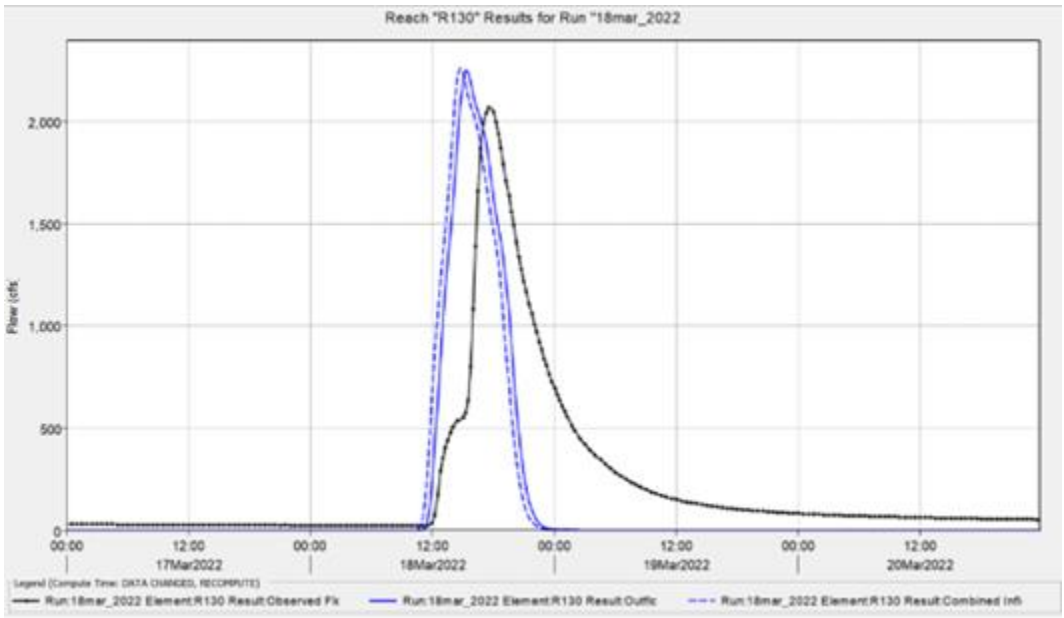

Figure 25. Comparison between the two resultant outflow hydrographs. Observed discharge (Black line) and Calibrated discharge (Blue line)

The hydrological model was used, considering a 100-year rainfall scenario, with varying antecedent moisture conditions (AMC) between dry conditions (CN_I), normal conditions (CN_{II}), and wet conditions (CN_{III}). The results of the outflow hydrographs by watershed for each of the antecedent soil moisture conditions CN_I, CN_{II}, and CN_{III} are presented in Figure 26 and Table 5. The results indicate significant changes in the peak flow between the AMC. Results reveal a difference of 3,789 cfs (or 64%) between the values of CN_{II} and CN_{III}. The peak flow values associated with the average moisture condition CN_{II} do not represent the worst-case scenario in the calculation of peak flows that were modeled and was under the peak flow rate estimates yielded by RRE.

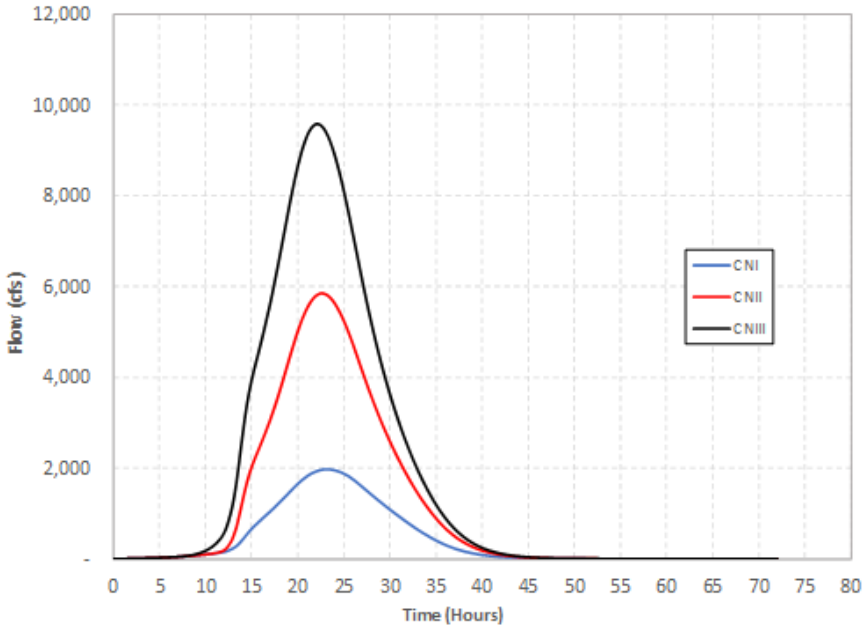

Figure 26. Outflow hydrographs for the watershed associated with BIN 015002 and different antecedent soil moisture conditions, CNI, CNII, and CN_{III}.

Table 5. Peak flow for different antecedent moisture conditions. BIN 015002 watershed

BIN	River	Peak flow AMC (CFS)		
		CN_I	CN_{II}	CN_{III}
015002	Little Double Bridges Creek	1,981	5,900	9,689

When comparing the peak flow of the RRE with CN_{II} and CN_{III}, the RRE is approximately 30% higher than CN_{II} and 26% lower than CN_{III}. Finally, when comparing RRE and CN_{III} with FFA, RRE is 89% and CN_{III} is 50% lower than FFA. In this specific case, due to the presence of the extreme event Tropical Storm Alberto in 1994, neither the values of RRE nor those of the models using CN_{II} or CN_{III} correspond to the worst-case scenario recorded for this bridge. However, the value from the model using CN_{III} (wet antecedent moisture conditions) could be the scenario to use in the absence of data.

3.2.2. BIN 010738. Blue Creek and Meriwether Trail

Similarly, scenarios using different antecedent soil moisture conditions were created and modeled for the Blue Creek watershed associated with BIN 010738. The outflow hydrographs for this watershed are presented in Figure 27 and the peak flows for the different antecedent moisture conditions are presented in Table 6.

Table 6. Peak flow for BIN 010738 watershed using different antecedent moisture conditions.

BIN	River	Peak flow (CFS)		
		CN_I	CN_{II}	CN_{III}
010738	Blue Creek	1,849	2,756	3,202

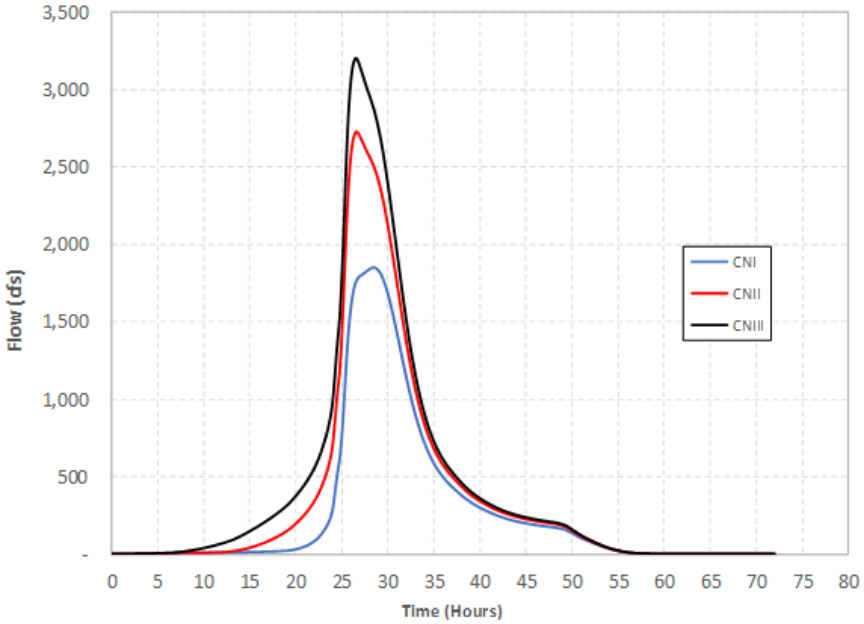

Figure 27. Outflow hydrographs for the watershed associated with BIN 0107038 and different antecedent soil moisture conditions, CNI, CNII, and CN_{III}.

The results provided in Figure 27 and Table 6 demonstrate a 16% difference in the values of the models employing CN_{II} and CN_{III}. Furthermore, when the peak flows modeled are compared to the RRE, it is found that the RRE value is greater by 0.6% and 16.9% than the models using CN_{III} and CN_{II}, respectively.

3.2.3. BIN 013310. Conecuh River and County Road 2243

Similarly, outflow hydrographs were generated for BIN 013310 over the Conecuh River, using the same previous soil moisture conditions. These hydrographs are presented in Figure 28 and the peak flows associated with those hydrographs are presented in Table 7.

Table 7. Peak flow for BIN 007070 watershed using different antecedent moisture conditions.

BIN	River	Peak flow AMC (CFS)		
		CN_I	CN_{II}	CN_{III}
13310	Conecuh River	13,072	38,926	64,934

For this bridge, Table 7 shows a difference of 66.8% between the peak flows calculated using CN_{II} and CNIII. When these values are compared with RRE, CNII is 2.39% greater than the RRE, and CN_{III} is 70.8% higher. In this case, it is observed that the RRE values are closer to CN_{II}.

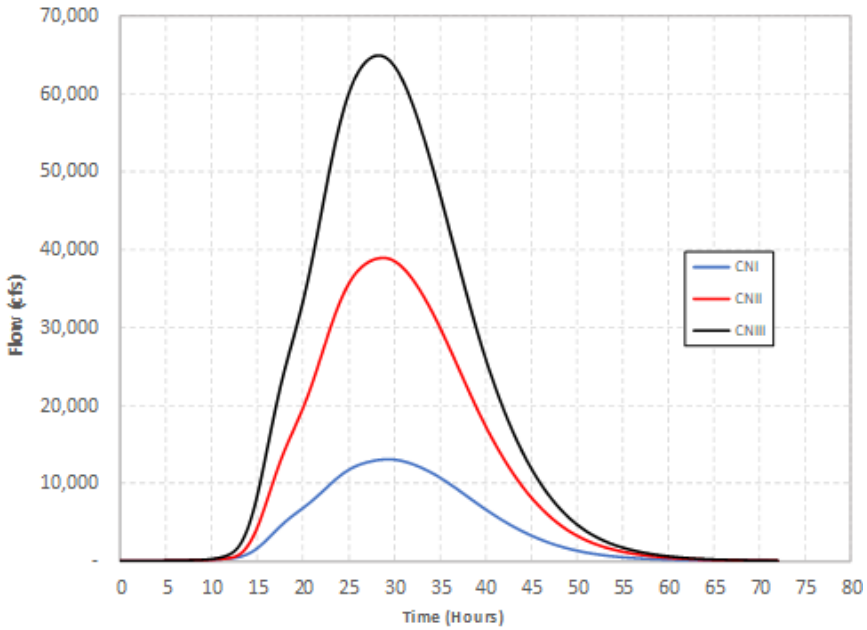

Figure 28. Outflow hydrographs for the watershed associated with BIN 013310 and different antecedent soil moisture conditions, CNI, CNII, and CN_{III}.

3.2.4. BIN 007070. French Creek and CO RT No 62

Finally, models were constructed for the watershed associated with BIN 007070 under different antecedent soil moisture conditions. These hydrographs are shown in Figure 29, and the peak flows related to those hydrographs are presented in Table 8.

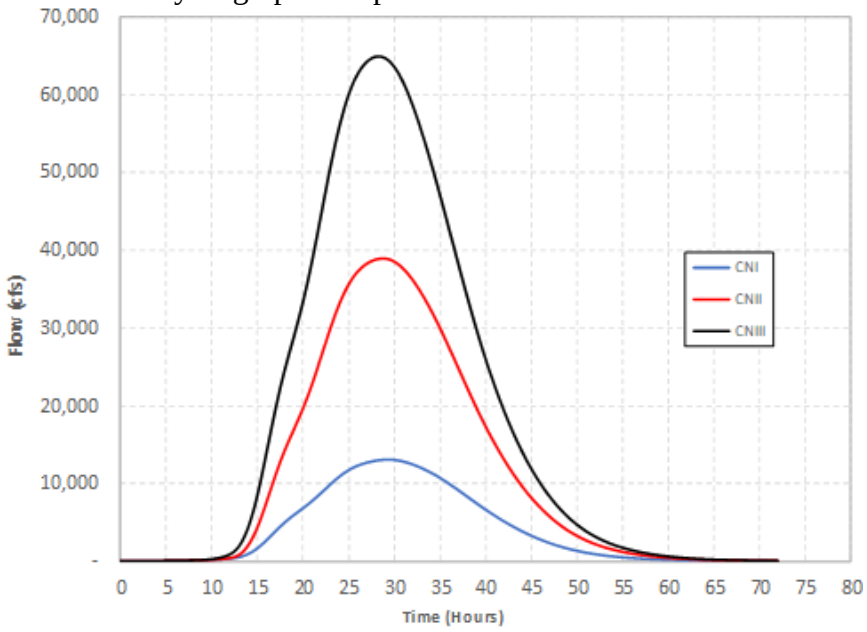

Figure 29. Outflow hydrographs for the watershed associated with BIN 007070 and different antecedent soil moisture conditions, CNI, CNII, and CN_{III}.

For this case, Table 8 shows a difference of 36.8% between the peak flows calculated using CN_{II} and CNIII. When these values are compared with RRE, CNII is 31% lower than RRE, and CN_{III} is 4.8% higher. In this case, it is observed that the RRE values are closer to CN_{III}.

Table 8. Peak flow for BIN 007070 watershed using different antecedent moisture conditions.

BIN	River	Peak flow AMC (CFS)		
		CN_I	CN_{II}	CN_{III}
007070	French Creek	2,867	5,811	7,986

3.2.5. Summary of the Hydrological Results

As a summary of the results described above, Table 9 presents the obtained peak flows for the hydrological methods used. It is notable that in two out of the four cases, the estimates from the RRE method were significantly lower (by as much as 41%) than the corresponding values obtained with HEC-HMS and AMC conditions corresponding to CN_{III}. This is a significant finding that should be taken into account in future bridge scour evaluations. Additionally, given the low peak flow values associated with AMC CNI, these conditions were not considered in the subsequent stages of this work.

Table 9. Peak flow using hydrological models for a 100-yr return period for the four analyzed bridges

BIN	River	Peak flow RRE (CFS)	HEC-HMS estimates Peak flow AMC (CFS)		
			CN_I	CN_{II}	CN_{III}
015002	Little Double Bridges Creek	7,682	1,981	5,900	9,689
010738	Blue Creek	3,221	1,849	2,756	3,202
007070	French Creek	7,616	2,867	5,811	7,986
013310	Conecuh River	38,017	13,072	38,926	64,934

3.3. Methodology for Hydraulic Calculations

The computation of scour estimates necessitates the calculation of flow depth at the locations of each bridge pier and over the same paths, ensuring consistency in the analysis. Four different hydraulic modeling approaches were employed to determine the velocity in the vicinity of the bridge, all of which used the HEC-RAS modeling tool.

1. HEC-RAS 1D modeling using WSPRO (Arneson & Shearman, 1998)
2. HEC-RAS 1D modeling using the Energy Equation (Brunner, 1995; Brunner & CEIWR-HEC, 2020). This approach employed the same geometry as the case above, with the only difference being the number of cross sections used to represent energy losses.
3. HEC-RAS 2D modeling using the approach referred to as Storage Area and 2D Flow Area Connections (SA/2D connection, Brunner et al., 2020). In this approach, the bridge structures are treated as breaklines that separate two consecutive 2D storage areas.
4. HEC-RAS 2D modeling with explicit DEM editing to create a terrain modification that leads to raised piers. In this approach, the mesh was discretized more finely in the areas

near the bridge approach and piers. Typically, cell values equal to or smaller than the pier size were considered to ensure variation in velocity between adjacent cells.

The strategy was to evaluate the linkage between the varying hydraulic modeling approaches and changes in the predicted flow characteristics created by bridge structures during peak flow conditions. The Courant number method, as described by Bruner (2021), was used in the implementation of the 2D models to ensure accurate and stable numerical simulations. The maximum Courant number used was 2.0, and the minimum was 0.5. This method accounts for the time step size and grid spacing to maintain stability and avoid numerical instabilities. Because HEC-RAS employs an implicit solution scheme, Courant numbers can exceed one and still yield a stable and accurate solution (Brunner et al., 2020). Given the degree of discretization associated with HEC-RAS 2D modeling with raised piers, this approach was considered the most accurate and served as the benchmark for comparison with other hydraulic modeling approaches.

3.4. Hydraulic Modeling Results

Considering the four bridges studied, three hydrological peak flow values (RRE, CN_{II}, and CN_{III}), and the four hydraulic modeling approaches, a total of 48 hydraulic models were constructed. The alternatives to estimate peak flows. To understand and visualize the differences that occur in various bridge modeling approaches, maps are presented as an example using a selected hydrological alternative, the antecedent soil moisture condition (CNII).

The results for each bridge are presented in two types of figures. The first type corresponds to velocity maps for the bridge modeling approaches, and the second type corresponds to water depth maps using the same approaches. For the first type of map, equal velocity ranges were created for comparing the velocity and depth results. The figures are labeled according to the hydraulic modeling approach: (a) 1D WSPRO, (b) 1D Energy Equation, (c) 2D/SA connection, and (d) 2D terrain modification with raised piers. The tables show the percentage differences for velocity and water depth between each approach against the benchmark modeling approach, i.e., the 2D terrain modification with raised piers model.

3.4.1. BIN 015002. Little Double Bridges Creek and County Road 606

Table 10 shows the velocity comparison between the benchmark and the other methods, finding percentage velocity average differences below the benchmark ranging from 17.1% to 24.1% according to each method, implying similar flow regimen conditions and velocity magnitude upstream of the bridge entrance for the 1D models and the 2D SA connection model.

Table 10. Velocity comparison between the benchmark model and other approaches for different alternatives to calculate peak flow. BIN 015002

Method	**RRE**	**CN_{II}**	**CN_{III}**
1D WSPRO	24 %	17.1%	23.5%
1D Energy	24.1%	20.5%	23.5%
2D Connection	21.7%	20.9%	23.5%

Figure 30 shows the velocity map for the different bridge modeling approaches for BIN 015002, where the alternative method for calculating the peak flow is based on the antecedent moisture condition CN_{II}. In general terms, the approach models, 1D WSPRO (a) and 1D Energy

(b), appear very similar, in contrast to the 2D models, which exhibit higher velocities at the bridge entrance. When the 2D models are compared to each other, the 2D/SA connection model (c) exhibits lower velocities than the 2D terrain modification with raised piers model (d).

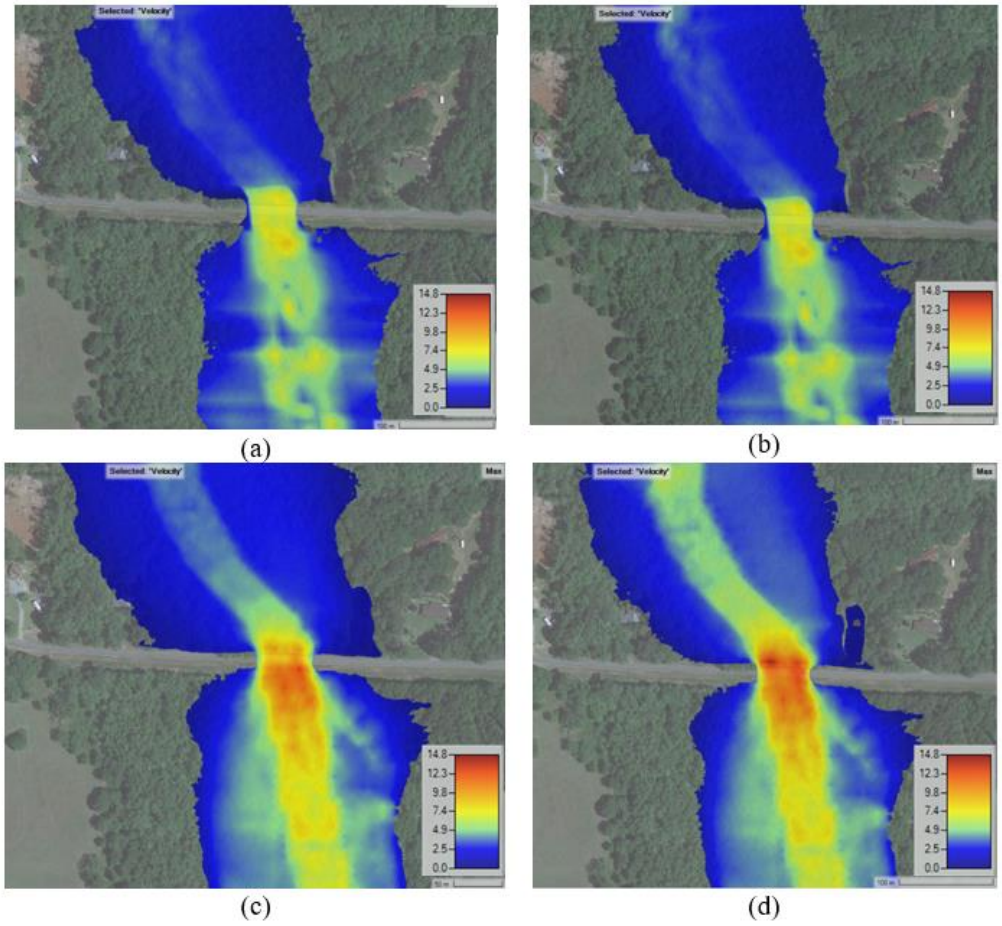

Figure 30. Velocities for different bridge modeling approaches, BIN 015002. (a) WSPRO (b) Energy (c) 2D/SA connection (d) 2D terrain modification with raised piers

Figure 31 shows the velocity differences in each pier according to each bridge modeling approach, indicating that the benchmark model (2D terrain modification with raised piers) exhibits the highest velocity, followed by the 2D-SA connection, WSPRO, and energy, respectively. The percentage velocity differences between the benchmark and the other approaches vary depending on each approach and the method used to calculate the peak flow.

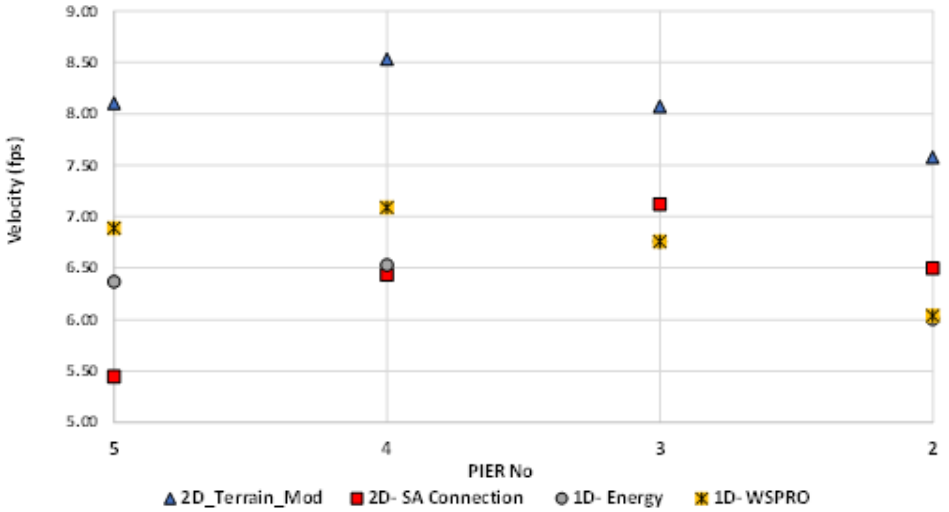

Figure 31. Velocities comparison for the bridge modeling approaches. BIN 015002

Similarly, Figure 32 shows that the water depth and floodplain results for the 1D models WSPRO (a) and 1D Energy (b) are very similar, contrary to the two-dimensional
Models (c) and (d) display a broader floodplain and deeper water depths compared to the one-dimensional models.

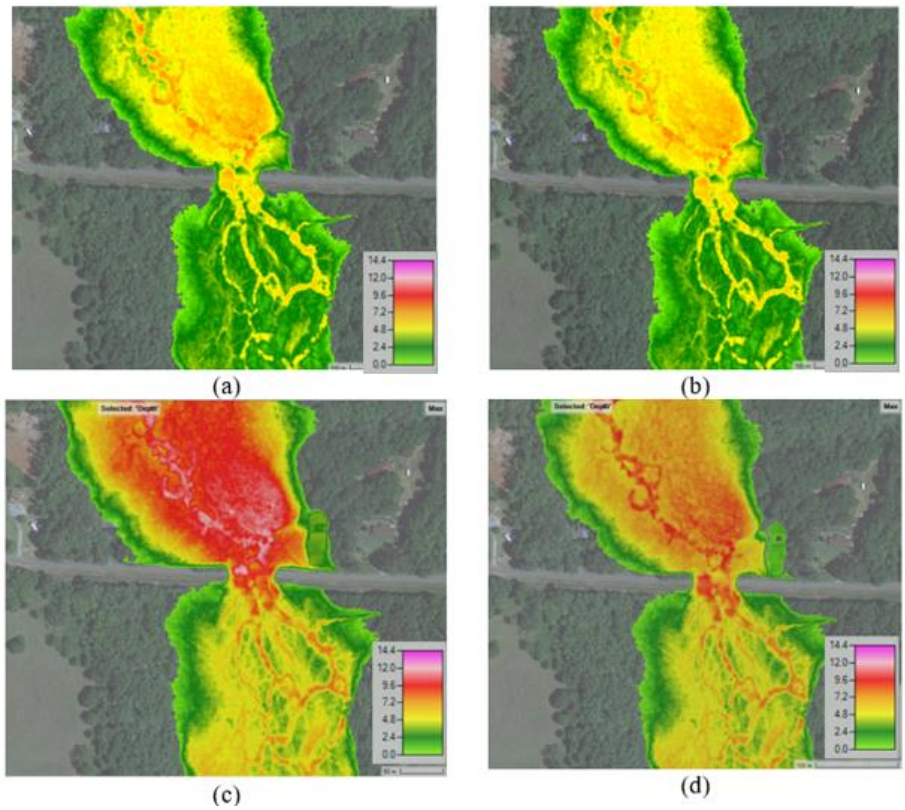

Figure 32. Water depth results for different bridge modeling approaches, BIN 015002. (a) WSPRO (b) Energy (c) 2D/SA connection (d) 2D terrain modification with raised piers

When the 2D models are compared, the 2D-SA connection (c) exhibits a deeper water depth upstream of the bridge than the 2D terrain modification with raised piers model (d), indicating lower velocities upstream of the bridge. It seems that the flow is pooled at the bridge entrance in the 2D-SA connection model (c), creating a control section. This condition may not be representative when compared to the benchmark model (2D terrain modification with raised piers), which does not represent this behavior in the results (d).

Figure 33 shows the results for the water depths. It shows that the water depths were high for the 2D-SA connection and low for the 2D terrain modification with raised piers. Table 11 shows the water depth comparison between modeling approaches, finding the percentage of water depth average differences above the benchmark, ranging from 11.6% to 55.5%, according to each method. In this specific case, the negative value indicates that the average water depth percentage is above the benchmark.

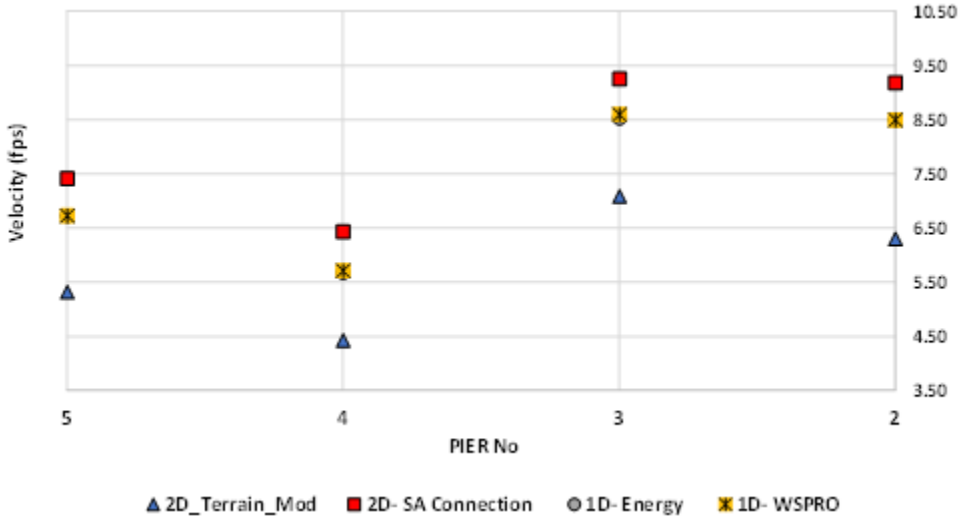

Figure 33. Water depth for the different bridge modeling approaches. BIN 015002

Table 11. Water depth comparison between the benchmark model and other bridge modeling approaches for different alternatives to calculate peak flow. BIN 015002

Method	RRE	CN_{II}	CN_{III}
1D WSPRO	-11.6%	-18.9%	-27.9%
1D Energy	-11.6%	-19.2%	-27.5%
2D Connection	-55.5%	-42%	-40.3%

3.4.2. BIN 010738. Blue Creek and Meriwether Trail

Figure 34 shows the results of velocities for the different bridge modeling approaches for BIN 010738 over Blue Creek. Once again, the 1D velocity results for 1D models, as shown in WSPRO (a) and energy (b), are almost identical to each other, unlike the 2D models that exhibit significant differences in velocity at the bridge entrance. Comparing the two 2D models, it was discovered that the 2D-SA connection model (c) has slower velocities upstream (bluer) than the 2D terrain modification model (d) (more yellow).

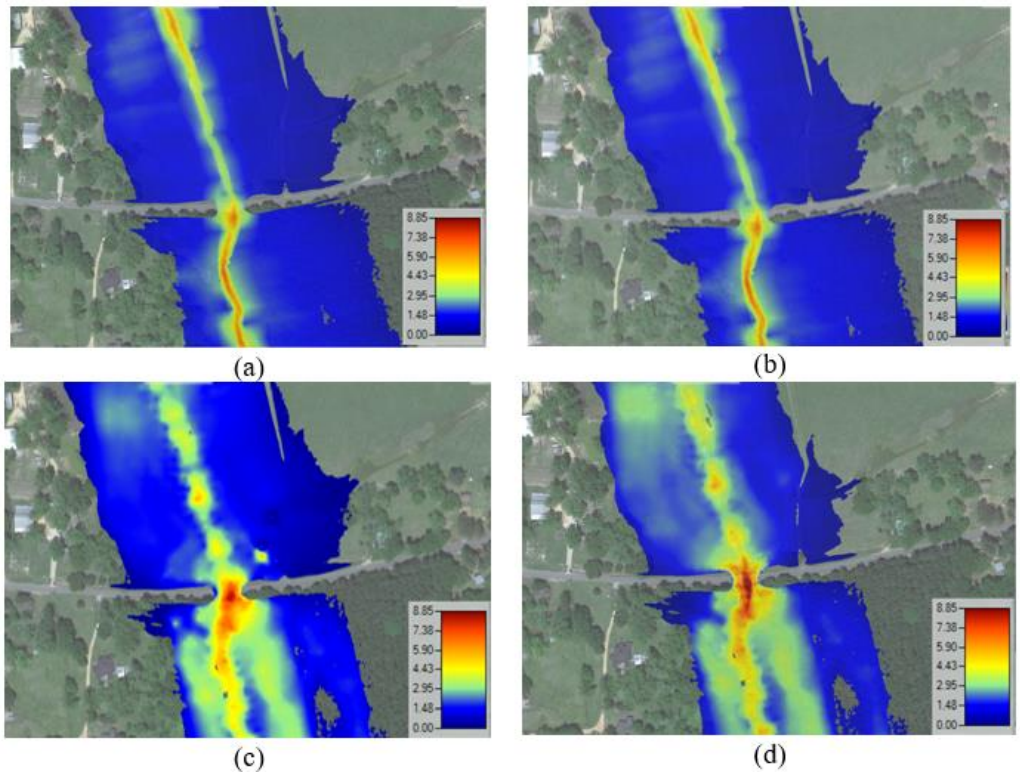

Figure 34. Velocities results for different bridge modeling approaches, BIN 010738. (a) WSPRO (b) Energy (c) 2D/SA connection (d) 2D terrain modification with raised piers

Figure 35 shows the velocity differences in each pier according to each bridge modeling approach, indicating that the benchmark model has the highest velocity, followed by the 2D-SA connection, WSPRO, and energy models, respectively. Table 12 shows the velocity comparison between the benchmark and the other methods, finding percentage velocity average differences from the benchmark to the other methods, which ranged between -1.8% below and 50% above the reference values according to each method. The negative sign indicates cases where the average velocity exceeds the benchmark.

Table 12. Velocity comparison between the benchmark model and other approaches for different alternatives to calculate peak flow. BIN 010738

Method	**RRE**	**CN_{II}**	**CN_{III}**
1D WSPRO	50%	43.3%	47%
1D Energy	50%	42.2%	47%
2D Connection	14.9%	-1.8%	6.7%

Figure 36 shows that the water depth in the 1D models, WSPRO (a) and Energy (b), appears notably alike. When contrasting these 1D models (a) and (b) with the 2D/SA connection (c) model, the floodplain exhibits similarity upstream of the bridge but reveals variations downstream, which are more extensive in the 1D models. Two-dimensional models were compared, and it was found that the 2D/SA connection (c) has a wider floodplain upstream of the bridge (with a yellower tone) than the 2D terrain modification with raised piers model (d), which has a greener tone. This model presents similar behavior to the previous model (BIN 015002) when the benchmark illustrates shallow water depths and higher velocity approaches.

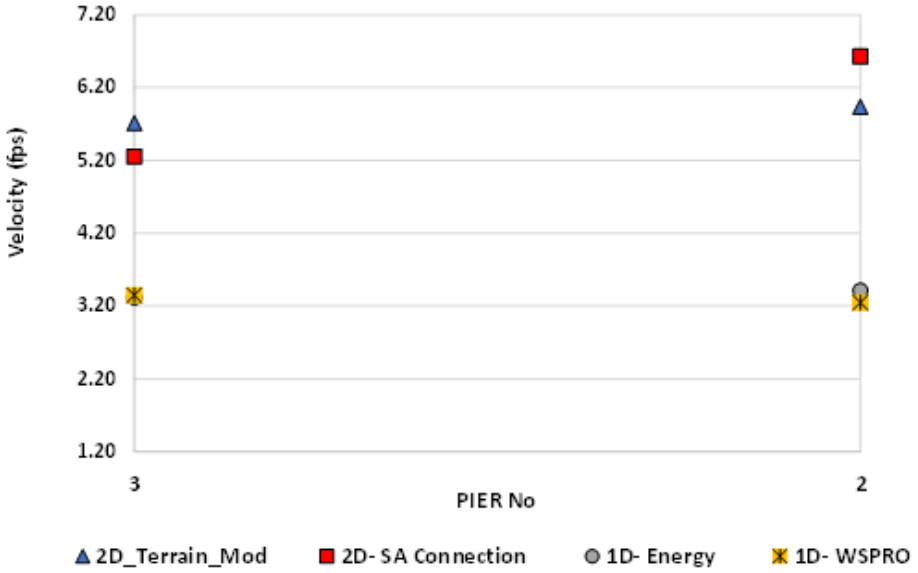

Figure 35. Velocities for the different bridge modeling approaches. BIN 010738

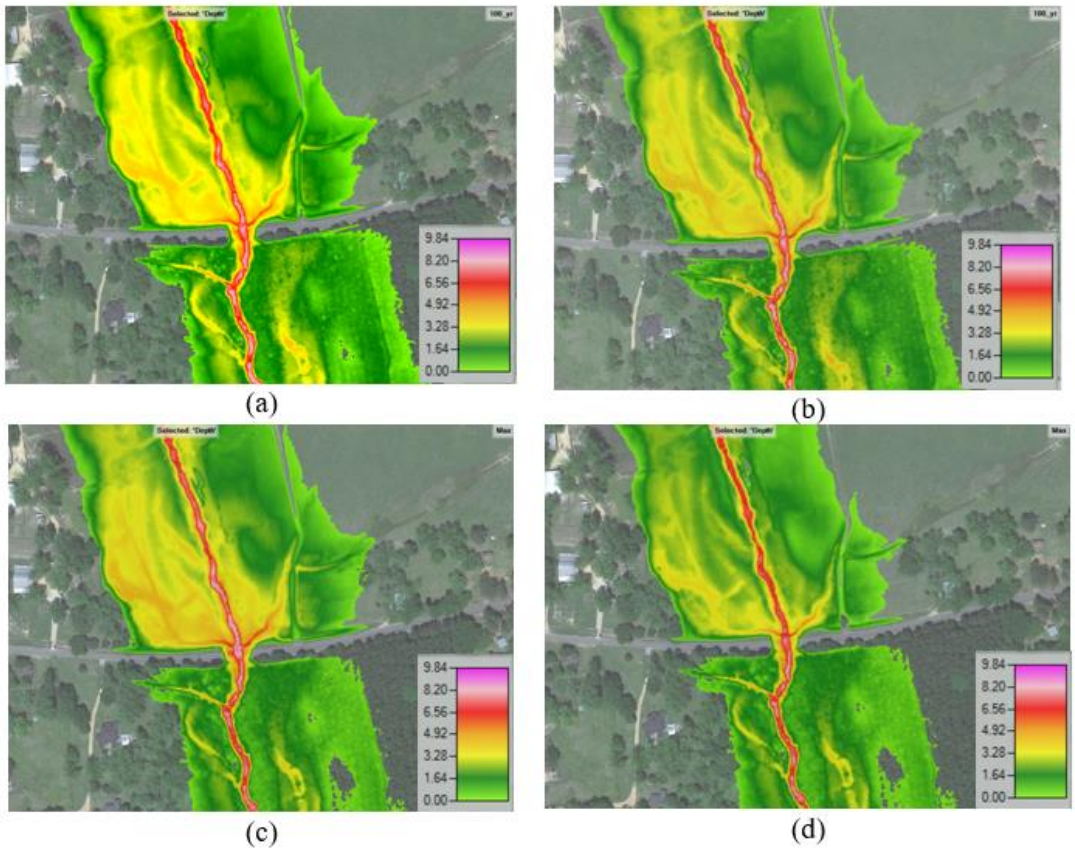

Figure 36. Water depth for different bridge modeling approaches, BIN 010738. (a) WSPRO (b) Energy (c) 2D/SA connection (d) 2D terrain modification with raised piers

Figure 37 displays the results for water depths, revealing variations in maximum values in water depth for the 2D-SA connection and minimum values for the benchmark. Once again, the values of the one-dimensional models behave very similarly, with water depths almost identical. Table 13 presents a comparison of water depths among different modeling approaches, indicating average differences in water depth percentages relative to the benchmark, which ranged from 9.6% to 33.8% depending on the specific method.

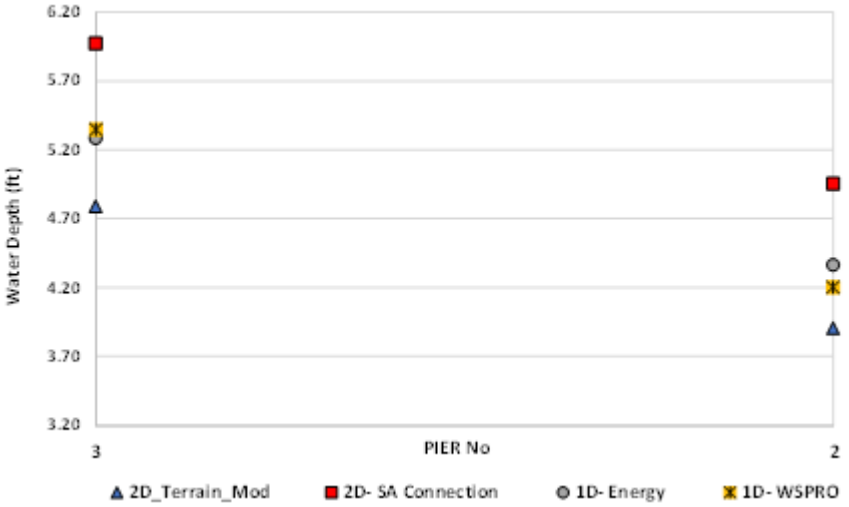

Figure 37. Water depth for the different bridge modeling approaches. BIN 010738

Table 13. Water depth comparison between the benchmark model and other bridge modeling approaches for different alternatives to calculate peak flow. BIN 015002

Method	RRE	CN_{II}	CN_{III}
1D WSPRO	14.9%	9.6%	11.9%
1D Energy	15.9%	11%	13.7%
2D Connection	33.8%	25.8%	32.7%

3.4.3. BIN 013310. Conecuh River and County Road 2243

Similar analyses were conducted for BIN 013310 over the Conecuh River. This river is unique due to its complex hydraulics, multiple openings and channels, and a wider floodplain. Figure 38 shows the results and differences between the 1D models. WSPRO (a) has lower velocity values at the bridge entrance (more yellow) than the energy (b) approach (redder), being the highest velocities among the four models. Comparing the 2D models, it can be observed that the 2D-SA connection (c) (greener) has higher velocities than the 2D terrain modification with raised piers (d) (green, yellow). Comparing the graphs of the 1D models to those of the 2D models, the latter display more realistic flow line characteristics.

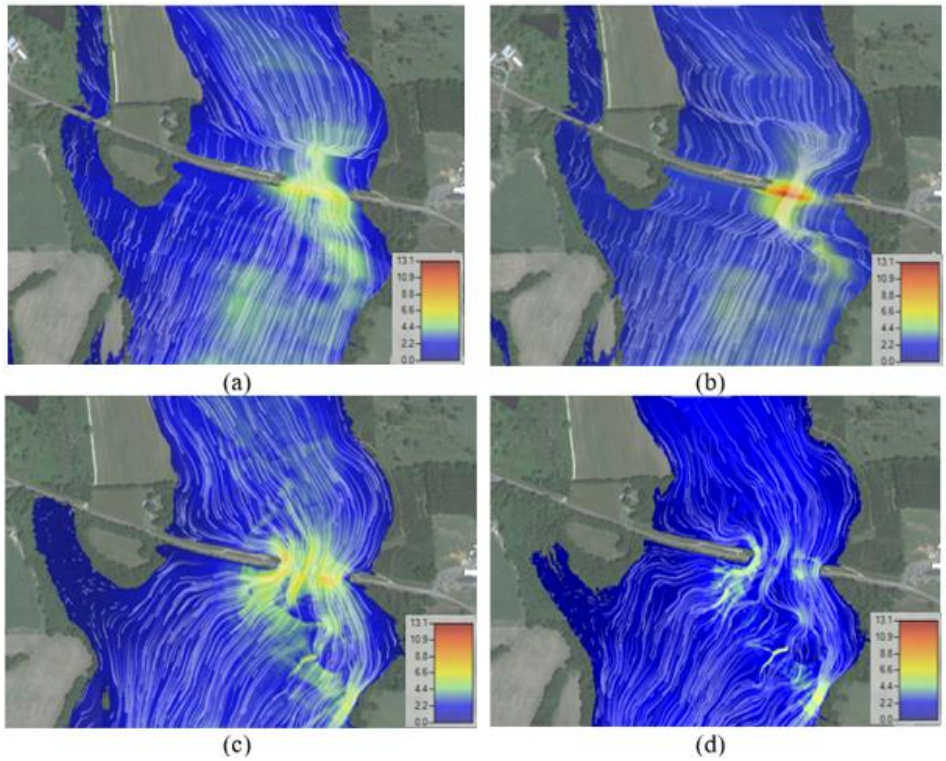

Figure 38. Velocities for different bridge modeling approaches, BIN 013310. (a) WSPRO (b) Energy (c) 2D/SA connection (d) 2D terrain modification with raised piers

Figure 39 shows the velocity differences in each pier according to each bridge modeling approach, showing a different behavior compared to the other two analyzed bridges. In this bridge, the 1D energy has a higher velocity compared to the other three approaches. Nevertheless, the results of this method are concentrated in the main channel, creating high velocities in this part of the cross-section, a condition that is considered unrealistic, given the assumptions underlying the 1D models and the benchmark approach's results. Moreover, Table 14 presents a comparison of velocities between the benchmark and alternative approaches, revealing that the percentage differences in average velocity vary between 1.6% and 119.6% above depending on the specific method employed. The negative sign indicates that the average water depth percentage is above the benchmark.

Table 14. Velocity comparison between the benchmark model and other approaches for different alternatives to calculate peak flow. BIN 013310

Method	**RRE**	**CN_{II}**	**CN_{III}**
1D WSPRO	-119.6%	-6.3%	-38.4%
1D Energy	-140.2%	-15.5%	-52.3%
2D Connection	-35.3%	-6.8%	-1.6%

Similarly, Figure 40 presents water depth values for the various bridge modeling approaches related to BIN 013310. The energy model (b) exhibits deeper water depths than the WSPRO model (a). Additionally, it can be observed that the 2D-SA connection model (c) displays a possible pooling effect upstream of the bridge section, acting as a flow control (red-magenta tones) due to the contraction. When this model is compared with the benchmark (d), both show significant differences, presenting the latter a smooth transition at the bridge entrance. Compared

to the other two bridges analyzed previously, this bridge exhibits distinct behavior, with maximum velocities registered for the 1D models and minimum velocities for the 2D models at the bridge entrance. This highlights the limitations of 1D models when applied to complex cross-sections, for which 2D models are more representative.

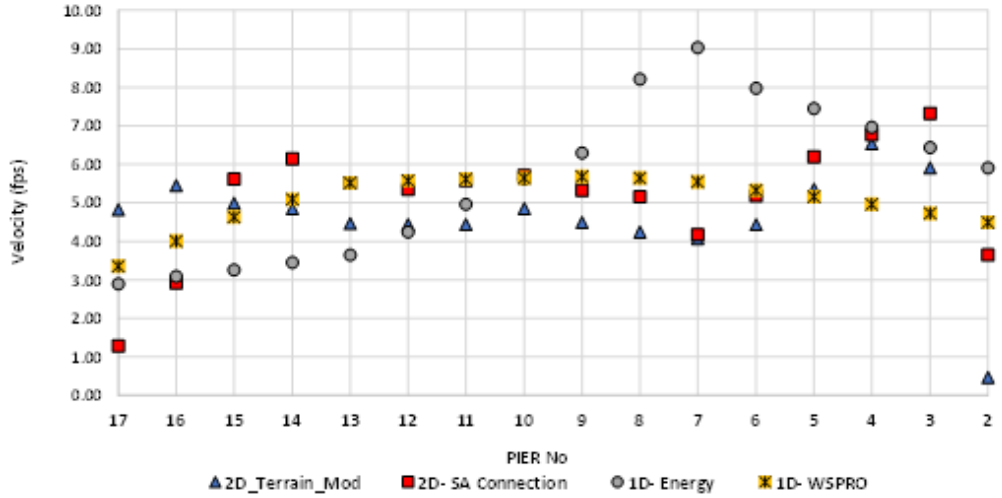

Figure 39. Velocities for the different bridge modeling approaches. BIN 013310

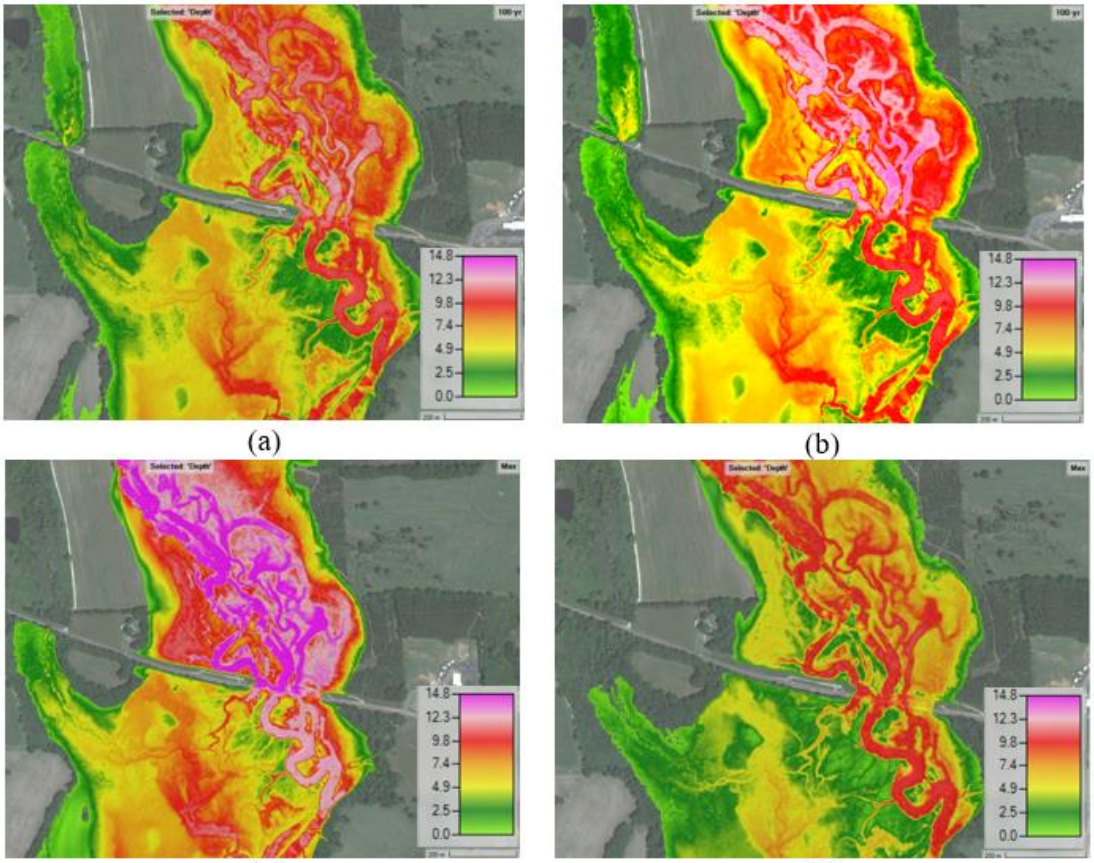

Figure 40. Water depth for different bridge modeling approaches, BIN 013310. (a) WSPRO (b) Energy (c) 2D/SA connection (d) 2D terrain modification with raised piers

Figure 41 shows the results for water depths, illustrating maximum values in water depth for the 2D-SA connection and minimum values for the WSPRO. Table 15 presents a comparison of water depth among different modeling approaches, indicating average differences in water depth percentages relative to the benchmark approach, which ranged from -31.4% to 10.6% depending on each specific method. The negative sign indicates that the average water depth percentage is above the benchmark.

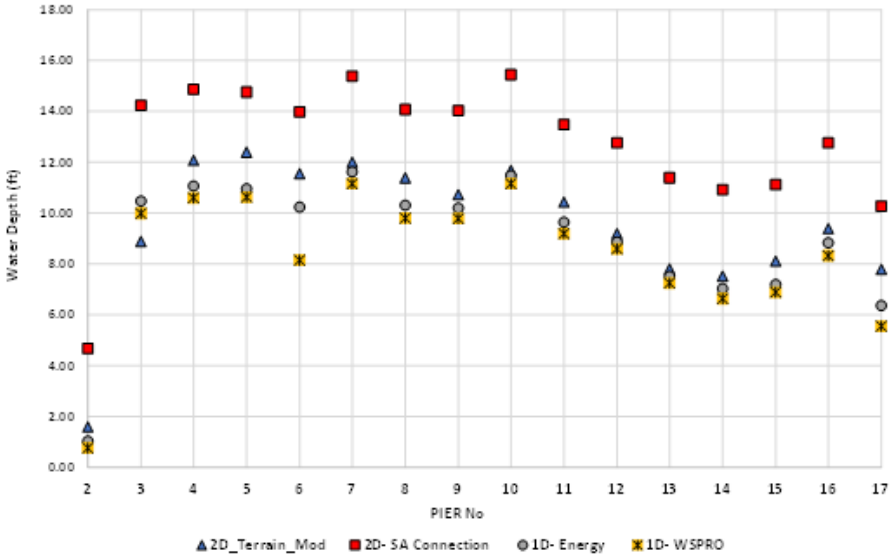

Figure 41. Water depth for the different bridge modeling approaches. BIN 013310

Table 15. Water depth comparison between the benchmark model and other approaches for different alternatives to calculate peak flow. BIN 013310

Method	RRE	CN_{II}	CN_{III}
1D WSPRO	-15.8 %	10.6 %	3.4 %
1D Energy	-22.1 %	5.6 %	0.8 %
2D Connection	-3.1 %	-31.4 %	24.3%

3.4.4. BIN 007070. French Creek and County Route 62

Lastly, comparable results for the velocities for French Creek BIN 07070 are shown in Figure 42. Again, the velocity findings obtained using the 1D energy (b) and 1D WSPRO (a) are almost identical. The two-dimensional models, on the other hand, depict significant variations in velocity near the bridge opening. When comparing the 2D models, the benchmark (d) showed higher upstream velocities (yellow, red) than the 2D-SA connection model (c).

Figure 43 illustrates the velocity differences in each pier according to the various bridge modeling approaches, showing the highest velocity in the benchmark model (2D terrain modification with raised piers), followed by the 2D-SA connection, WSPRO, and energy, respectively. The percentage velocity differences between the benchmark and the other approaches vary depending on each approach and the method used to calculate the peak flow. Table 16 presents a comparison of velocities between the benchmark and other methods, revealing percentage velocity average differences ranging from 16.9% above to 50.1% below the benchmark, according to each method. In this specific case, the negative sign indicates that, in some instances, the average velocity exceeds the benchmark.

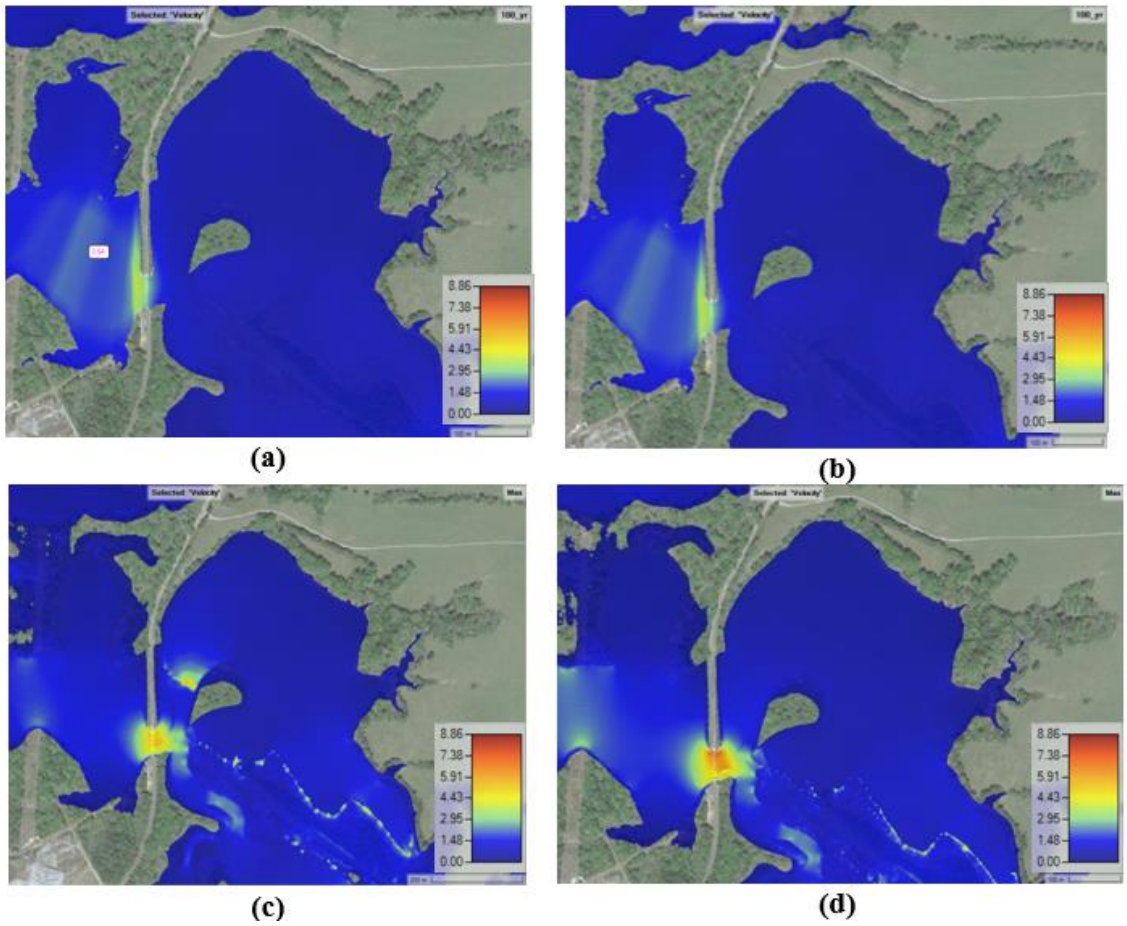

Figure 42. Velocities results for different bridge modeling approaches, BIN 007070. (a) WSPRO (b) Energy (c) 2D/SA connection (d) 2D terrain modification with raised piers

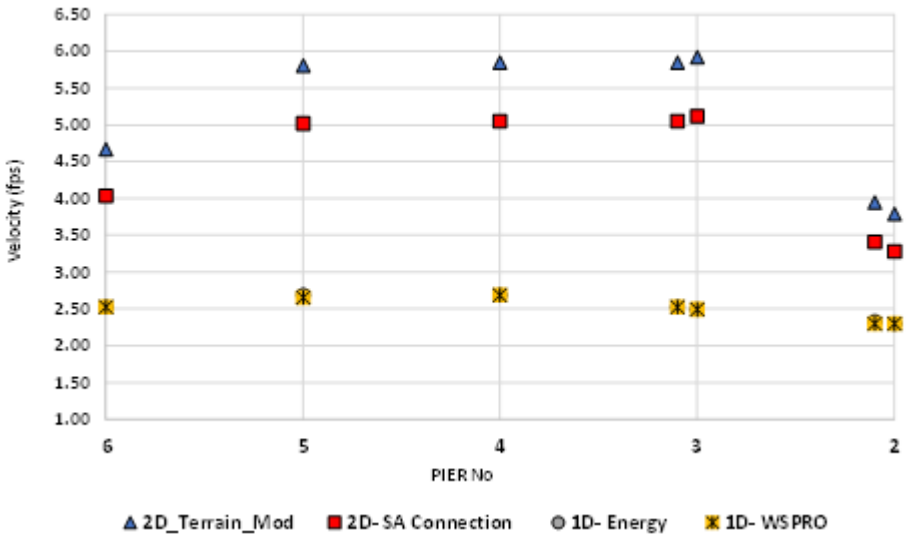

Figure 43. Velocity for the different bridge modeling approaches. BIN 007070

Table 16. Velocity comparison between the benchmark model and other approaches for different alternatives to calculate peak flow. BIN 007070

Method	RRE	CN_{II}	CN_{III}
1D WSPRO	35 %	50.1 %	46.4 %
1D Energy	35.2 %	49.9 %	46.4 %
2D Connection	-7.8 %	13.6 %	-16.9 %

In Figure 44 the water depth in the 1D models, WSPRO (a) and Energy (b), appears notably alike (same colors). When contrasting these 1D approaches (a) and (b) with the 2D approaches (c) and (d), there are notable differences downstream of the bridge where the 2D approaches present deep water depths and broader floodplains. Comparing the 2D models, it was found that the 2D/SA connection (c) has a wider floodplain upstream and downstream than the 2D terrain modification with raised piers model (d).

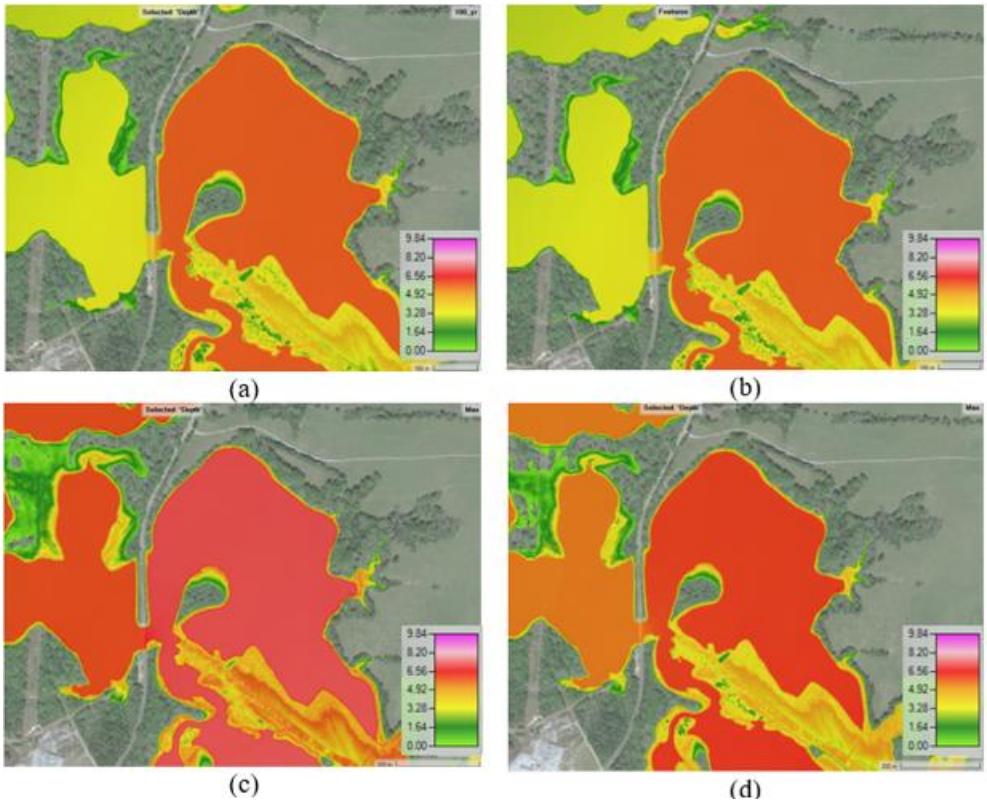

Figure 44. Water depth for different bridge modeling approaches, BIN 007070. (a) WSPRO (b) Energy (c) 2D/SA connection (d) 2D terrain modification with raised piers

Figure 45 displays the results for water depths, where the benchmark presents the maximum water depths and WSPRO and Energy the minimum values. Once again, the values of the 1D approaches behave very similarly, with water depths almost identical. Table 17 presents a comparison of water depths among different modeling approaches, indicating average differences in water depth percentages relative above the benchmark, which ranged from 9.2% to 32.1% depending on the specific method. In this case, the negative value indicates that the average water depth percentage is above the benchmark.

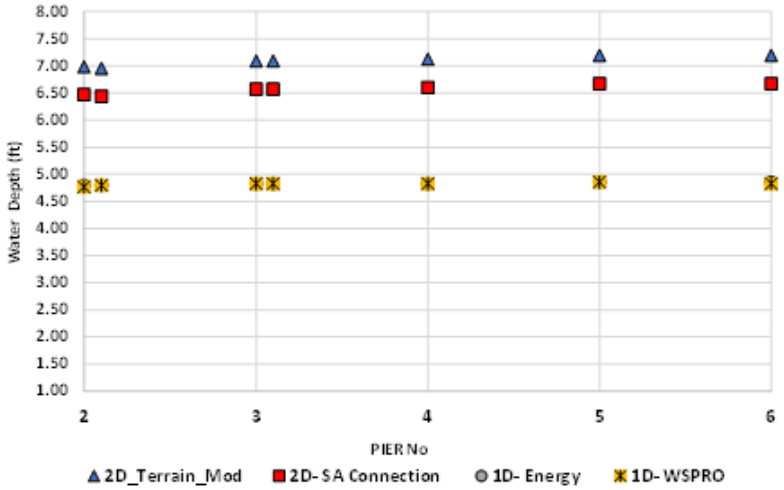

Figure 45. Water depth for the different bridge modeling approaches. BIN 007070

Table 17. Water depth comparison between the benchmark model and other approaches for different alternatives to calculate peak flow. BIN 007070

Method	RRE	CN_{II}	CN_{III}
1D WSPRO	-1.1 %	32.1 %	22.6 %
1D Energy	-1.3 %	31.9 %	22.7 %
2D Connection	-9.2 %	7.4 %	-1.8 %

3.4.5. Peak to Average Velocity Analysis

A peak-to-average analysis was performed for velocity to facilitate a comparison between the maximum predicted water velocity near a pier and the average velocity. This method involves dividing the maximum calculated velocity by the average velocity for each bridge modeling approach. This process helps standardize the values across methods, enabling the determination of which methods exhibit the highest skewness in velocity predictions. The results of this analysis for the four bridges are presented in Figure 46.

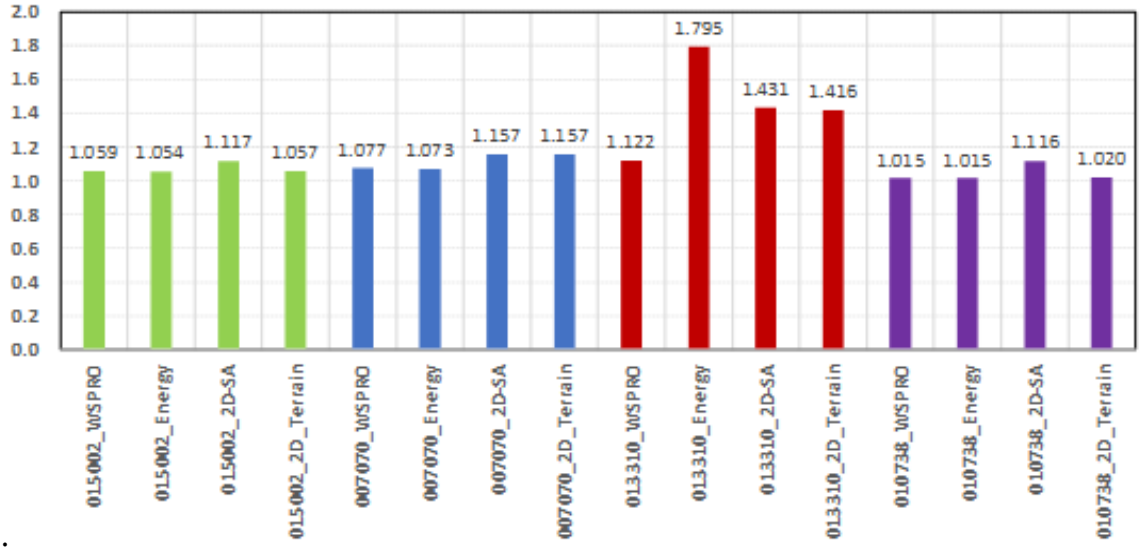

.

Figure 46. Peak to average velocities by bridge for the different bridge modeling approaches

The following observations can be drawn from the results shown in Figure 46:

- For BIN 015002 (in green) and BIN 010738 (purple), the bridge modeling approach with the highest peak-to-average value corresponds to the 2D SA connection with a value of 1.117, and the lowest value is for the 1D energy approach. In general, the differences between all hydraulic results are small, but the 2D raised pier results are similar to the 1D results. Both of these bridges have relatively simple cross-sections with very limited floodplains, which are conditions in which the 1D model can be applied more successfully.
- For Bridge 007070 (blue), the two hydraulic modeling approaches involving 2D simulations yielded the same peak-to-average ratios, both of which were higher than those of the 1D simulations. It is speculated that in this case, the stream cross-section had a greater impact on the differences in predicted flow velocities than in the previous two cases.
- BIN 013310 (red) exhibited the greatest disparity in peak-to-average values among the methods. The maximum peak-to-average value was recorded for the 1D energy approach, with a value of 1.795, and the minimum for 1D WSPRO, with a value of 1.122. This reflects the limitation of 1D models to represent the flow in such a complex river cross-section with multiple openings and channels. In this bridge, it was found that the peak-to-average values for the two-dimensional models are quite similar, with 1.413 for 2D SA connection and 1.416 for the benchmark, indicating more consistent hydraulic modeling performance for the 2D applications.

Summarizing all the hydraulic modeling efforts and results, it is crucial to employ the most effective modeling tool and make the most informed assumptions for any given bridge scour analysis. In simple cross-sections, there was a limited difference in the results between the 1D and 2D approaches, but the latter resulted in slightly higher flow velocities, which is critical to scour computations. On the other hand, rivers with complex cross-sections will not be properly represented if one-dimensional (1D) modeling tools are used. As shown, some velocity values in the same cross sections may be underestimated, while others may be overestimated. Even though 2D models are more complex to set up, they rely on fewer assumptions and, as a result, reduce the likelihood of incorrect assumptions regarding flow contraction and flow directions that must be made in 1D models. Especially in the case of bridge scour analysis, the fact that these models also predict the velocity vector direction, in addition to its magnitude, will improve the accuracy of scour computations when compared to 1D models. All these should be considered in the development of new bridge studies.

3.5. Methodology for Scour Calculations

This section provides an overview of the methodology used for pier scour calculations of the four analyzed bridges. These calculations were divided into two parts: scour calculation using the HEC-18 method and scour calculation using the OMS method. The methodological steps for both methods are described below. The results from applying these two methods are presented in Chapter 6 of this report.

3.5.1. Pier scour calculations using HEC-18 method.

The methodological steps used to perform scour calculations using the HEC-18 equation, based on CSU (Anerson et al., 2012), are outlined as follows:

1) Extract the depth and velocity values from HEC-RAS (Brunner et al., 2020) for each column comprising the bridges, using each of the analyzed approximation methods (WSPRO, Energy, 2D SA connection, and 2D terrain modification with raised piers).
2) Extract the directions of the velocity vectors in RAS-Mapper (Brunner et al., 2020) for each approximation method and determine the flow approach angle to the columns.
3) Define values for the K1, K2, and K3 factors, corresponding to pier nose shape, angle of flow attack, and bed condition, respectively (Anerson et al., 2012).
4) Estimate the particle distribution size of the soil for each bridge. It is necessary to collect samples from the riverbed of the bridge and conduct this type of analysis in the laboratory to obtain the D_{50}.
5) Perform calculations for each of the bridge piers using Equation (14) (See subsection 2.2.5) (Anerson et al., 2012). Use Hydraulic Toolbox 5.3 to solve hydraulic calculations (Bergendahl & Arneson, 2014; Ghelardi, 2021). Hydraulic Toolbox was used instead of HEC-RAS because the bridge scour calculations in HEC-RAS are based on the fourth edition of HEC-18 (Richardson & Davis, 2001). Brunner (2020) notes that the scour calculations in HEC-RAS have not been updated to incorporate the changes introduced in the fifth edition of HEC-18 (Anerson et al., 2020).

3.5.2. Pier scour calculations using OMS.

The methodology used to perform scour calculations using OMS (Govidasamy et al., 2013; Briaud et al., 2011) is described below:

i. Determine the maximum observed scour $Z_{mo.}$ This value is determined by considering the inspections recorded in BIN, where Zmo represents the value of the original profile compared to the current profile. Additionally, the pile with the greatest scour is identified, and its value is recorded.
ii. Calculate the recurrence interval using the TAMU Flood model (Briaud et al., 2011), based on nearby stream gauges and rain gauges.
iii. Obtain the ratio Q_{mo}/Q_{fut} as a function of the recurrence interval. Calculate the values of Q_{mo} and $Q_{fut} = Q_{100}$ using RRE (or using available FFA/Hydrological analysis results).
iv. Estimate the ratio between the maximum future velocity V_{max} and the maximum observed velocity V_{mo} through the local recurrence interval. Convert Q_{mo} to V_{mo} and Q_{fut} to V_{fut} using the Manning equation in HEC-RAS (1D or 2D)
Estimate future scour as a ratio between the maximum future scour Z_{max} and the maximum observed scour $Z_{mo.}$

3.5.3. Approach for Comparison Between OMS and HEC-18 Scour Predictions

The approaches used to compare the different alternatives for calculating the peak flow used for scour calculations through various bridge approximation models are presented below:

i. Direct comparison between the results and the different alternatives to calculate peak flow and scour. It was considered that the approach using HEC-HMS and HEC-RAS 2D with raised piers was the reference for comparison.
ii. Calculation of peak-to-average ratio for scour. This value corresponds to the maximum calculated scour depth in one of the columns divided by the average scour depth of all columns in the cross-section of the bridge.

4. Development of Instrumentation Strategy for Monitoring of Pier Scour in Alabama

4.1. Introduction

This chapter discusses the development of the instrumentation strategy devised by the research team, which was later deployed on several selected bridges in the state of Alabama.

4.2. Methodology

The research team focused on three main types of measurements: water flow velocity, water flow depth, and scour depth. Additionally, visual observation was conducted using a motion-activated field camera on one of the bridges, and rain gauges were installed on some of the bridges.

Figure 47 shows an overview of the instrumentation strategy used in this research.

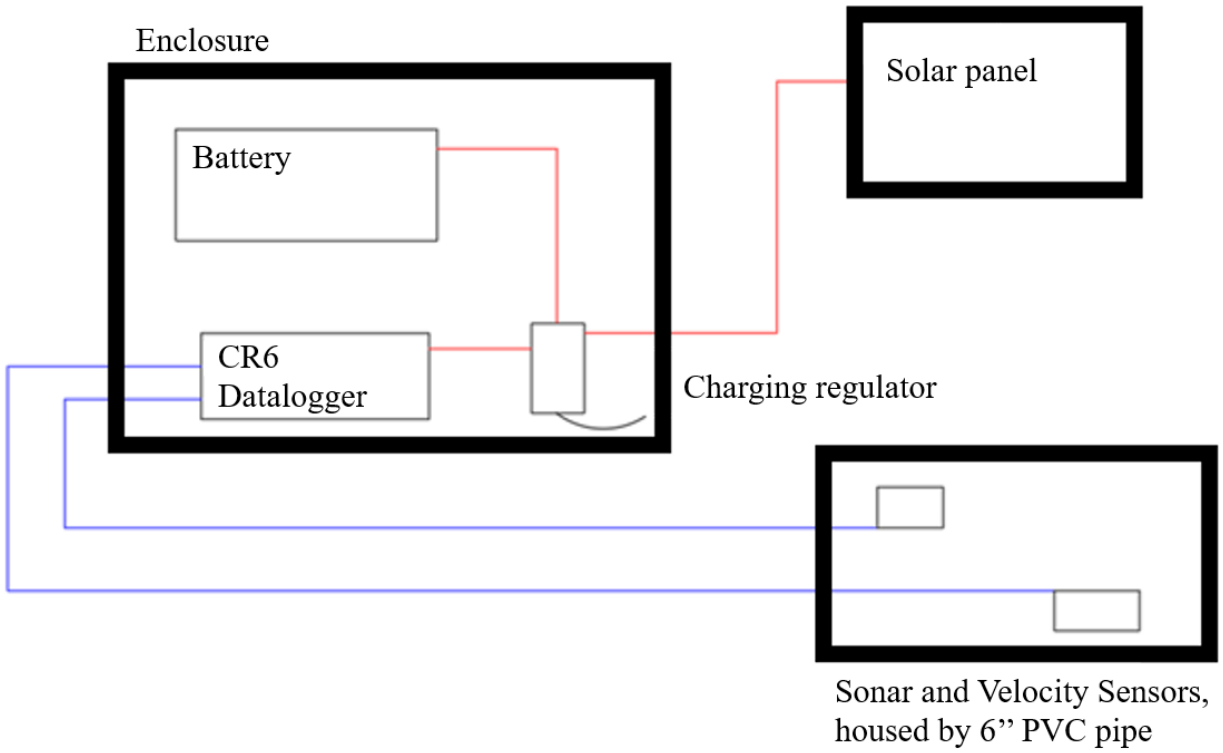

Figure 47. Overview of instrumentation strategy.

After conducting some research, the team decided that it would be beneficial to also measure the turbidity of the water at these locations. So, turbidity sensors were also purchased from Campbell Scientific and deployed. However, for the sole purpose of measuring scour, the AV sensor and the EchoRange sensor were enough.

The following subsections describe each component of the instrumentation strategy.

4.2.1. Blue Siren Area-Velocity (AV) sensor

This sensor is called a Dual-Wave Doppler Digital Area Velocity (AV) Flow, manufactured by Blue Siren (2019). This sensor is a fully submersible ultrasonic Doppler sensor

designed to measure velocity and depth in open channel flow applications. It integrates both a velocity sensor (Doppler-based) and a pressure-depth sensor, providing accurate flow data.

The sensor measures water velocity and depth in streams, pipes, and open channels using ultrasonic Doppler technology. The collected data can be utilized for flow monitoring, hydrological studies, and wastewater management applications. It outputs velocity as a digital signal and depth as an analog 0-5V signal.

The sensor works by emitting ultrasonic sound waves into the water. These waves bounce off small solid particles in the water and return to the sensor. The difference between the transmitted and received frequencies (Doppler effect) determines the velocity of the water. The pressure sensor determines the water depth by measuring changes in pressure.

The sensor uses different communication protocols. The velocity data can be manufactured by outputting serial TTL or RS485 communications (white wire). The depth data output uses an analog 0 to 5V signal (green wire). The red wire is the power input (6 to 16V DC), and the black wire is the common ground. The sensor has a current draw of 60 mA and a warm-up time of 2 seconds.

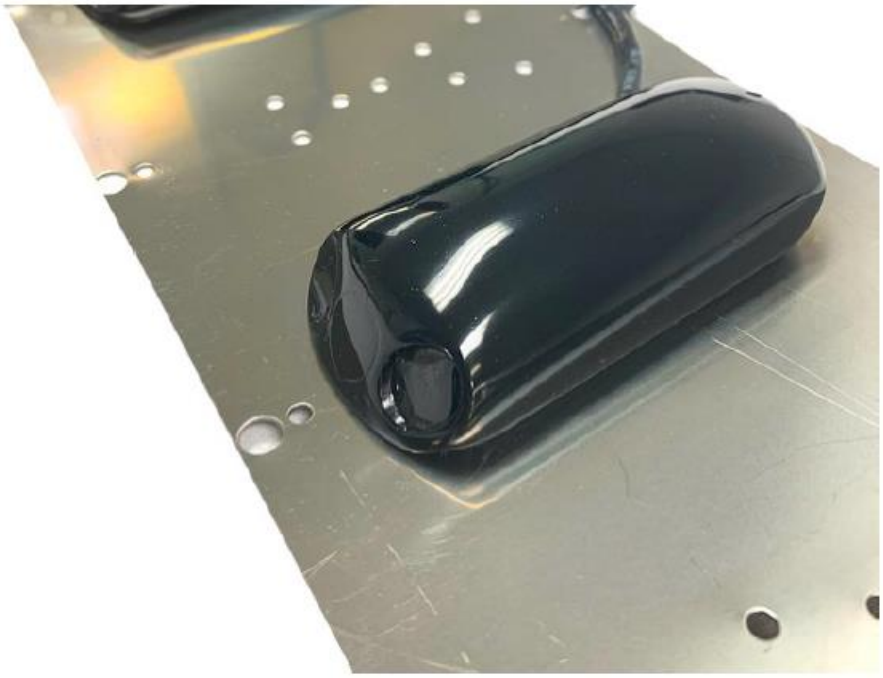

Figure 48. Dual-Wave Doppler Digital Area Velocity (AV) Flow Sensor (Blue Siren, 2019)

This sensor requires programming to work with the selected data logger. The programming details are provided in Appendix A. For deployment in the field, this sensor was housed in a 6-inch PVC pipe to provide some protection against possible debris.

4.2.2. Airmar, SS510 Single Frequency EchoRange

The Airmar EchoRange SS510 is a smart depth-sounding sensor designed for hydrographic surveying, dredging management, and mobile fieldwork. It is a portable single-frequency (200 kHz) transducer that features embedded signal processing for real-time depth measurement and data output. It can also be generically referred to as an echosounder, fathometer, or sonar.

It measures water depth by sending out sound waves and detecting their reflections from the seabed. It provides high-accuracy readings from 0.4 meters to 200 meters and transmits this data in real-time via the NMEA 0183 (National Marine Electronics Association Standard) protocol, using either RS-422 or RS-485 communication protocols. By default, the NMEA 0183 data stream includes the depth below the transducer ($DDPT) and the water temperature ($SDMTW).

The EchoRange SS510 single frequency connects via a multi-wire cable that provides both power and data transmission, as seen in Figure 49. The sensor requires an external power supply of 9 to 40 V (DC). During data transmission, the SS510 has an average current draw of 150 mA, with a peak current of 1 A during a ping (for 12 V batteries).

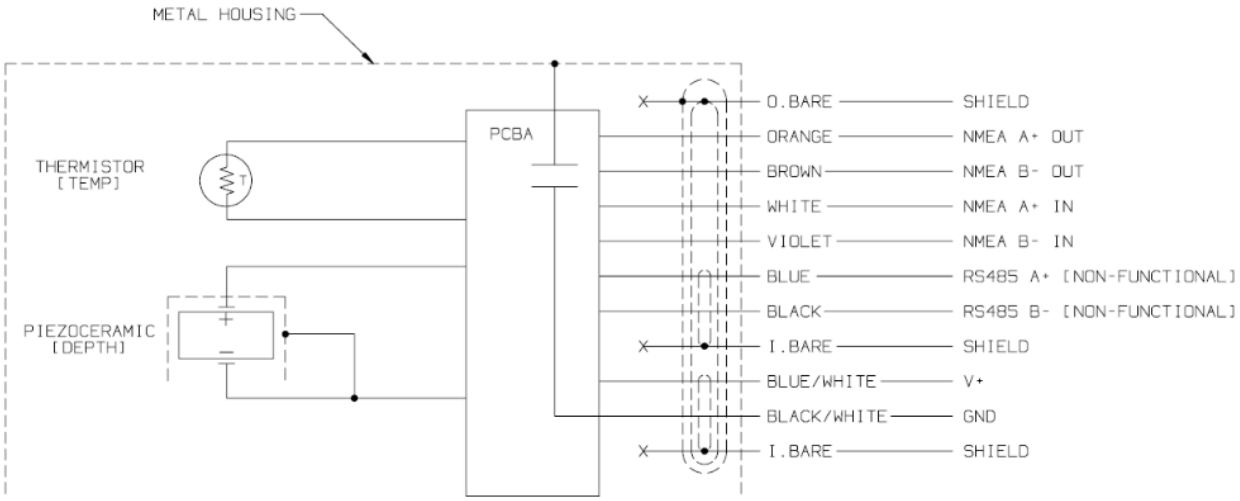

Figure 49. Wiring diagram for EchoRange SS510 Single Frequency Airmar sensor

Figure 50. EchoRange SS510 Single Frequency Airmar sensor

This sensor requires programming to work with the selected data logger. The programming details are provided in Appendix A.

Turbidity tests were conducted in the Advanced Structural Engineering Laboratory (ASEL) at Auburn University to investigate the behavior of the sonar sensor under varying turbidity

conditions. The results showed that the sonar sensor can show great noise measurements when turbidity rapidly increases, indicating the presence of coarse particles still in suspension. As the coarse particles start to wash away or settle, only the finer particles remain in suspension, and noise measurements become less frequent. However, for higher levels of turbidity, there is generally more noise compared to lower levels of turbidity. Additional details about the turbidity tests can be found in Appendix C.

These tests led to the inclusion of a few commands in the programming code for these sensors. These commands are sent to the sensor, changing its configuration (including the range of measurement, ping rate, and pulses per ping). These changes ensure that the EchoRange is better suited for making measurements in turbid and shallow waters.

For deployment in the field, this sensor was housed by a 6-inch PVC pipe to protect against possible debris.

4.2.3. Motion-Activated Camera

A motion-activated camera was used as a monitoring device in Lapine, AL. Normally designed for wildlife and outdoor surveillance, it features high-resolution image and video capture, night vision, motion detection, and waterproof durability. It is built to withstand various environmental conditions and has a long battery life, making it ideal for extended field monitoring. This camera, shown in Figure 51, was set to take pictures every six hours so that it would capture the progression of pier scour, if any.

Figure 51. DL001 Motion-activated camera (source: amazon.com)

4.2.4. Onset, HOBO sensors

HOBO Water Level Data Logger sensors from Onset were used for measuring air pressure and water pressure in some of the bridges in this study. Their sole purpose was to verify the water level measured by the AV sensor. Therefore, they were only used during specific periods and then removed. HOBO Rain Gauge data loggers were also used for measuring rainfall data at some of the bridges.

Figure 52. HOBO water level sensor and HOBO Rain gauge (source: onsetcomp.com)

These sensors are standalone devices with internal batteries. HOBOware software is used only to set the parameters of data measurement. No extra programming was required.

4.2.5. Campbell Scientific, Clarivue10 sensor

The Clarivue10 is a submersible side-scatter turbidity sensor that measures the concentration of suspended solids in water. It is ISO 7027 compliant and outputs data using the SDI-12 protocol. The sensor is designed to operate in both fresh and saline environments. The sensor measures turbidity in Formazin Nephelometric Units (FNU), with a range from 0 to 4000 FNU.

The sensor operates using side-scatter technology to measure the amount of light scattered by suspended particles in water. It has an infrared laser (VCSEL) emitter and a photodiode detector positioned at 90 degrees to measure side-scatter energy.

The sensor utilizes an SDI-12 communication protocol (white wire) and requires a 9-18 V DC power supply. The sensor has a current draw of 35mA.

Figure 53. Clarivue10 sensor (source: campbellsci.com)

This sensor requires programming to work with the selected data logger. The programming details are provided in Appendix A.

4.2.6. Datalogger and Power Supply

The Campbell Scientific CR6 is a data logger designed for a wide range of environmental, geotechnical, and structural monitoring applications. It features a multi-function interface that supports various sensor types, including analog, digital, and smart sensors, without requiring external modules. The integrated universal terminals simplify wiring and increase flexibility, making it a highly adaptable solution for field deployments. The CR6 is also equipped with a low-power design, making it suitable for remote applications.

One of the features of the CR6 is its high-speed processing and onboard data storage, which allows it to handle complex measurement and control tasks efficiently. It supports CRBasic programming, enabling users to customize their data collection and processing routines. The built-in web-based user interface provides easy remote access for configuration, diagnostics, and real-time data viewing. Additionally, the CR6 is designed for durability, with rugged, weather-resistant housing that ensures reliable operation in harsh environments.

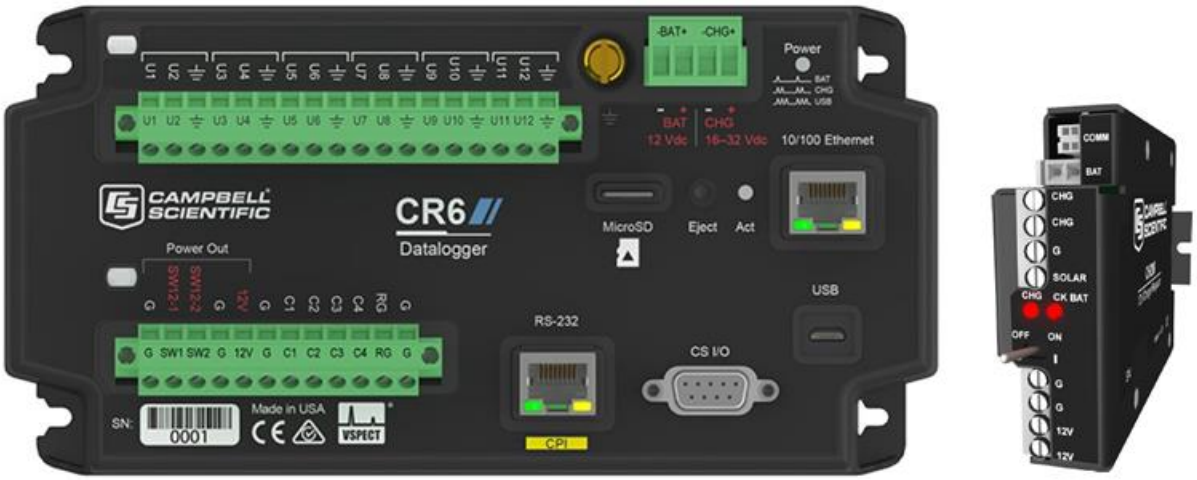

Figure 54. CR6 datalogger and CH200 charging regulator (source: campbellsci.com)

The data logger is connected to the sensors and a charging regulator (PH200), which, in turn, is powered by a 12V, 10Ah battery and a 10W solar panel.

The three main sensors combined (AV sensor, sonar, and Clarivue10) have a current draw of 0.245 A, which is only activated for 30 seconds every 15 minutes. Considering a very conservative 15% efficiency for the solar panel (providing charge for only 8 hours a day) and doubling the current draw to 0.500 A, it is possible to calculate that the battery capacity will never drop below 95% of its total capacity (10Ah).

In some of the deployed bridges, power consumption was also monitored to make sure battery capacity was holding as predicted. The results are presented in Appendix D.

5. Deployment of Scour Monitoring Instrumentation

5.1. Introduction

The instrumentation strategy developed by the research team was deployed to monitor scour occurrence in selected bridges in the state of Alabama. The selected bridges were:

- Bridge over Blue Creek, on Meriwether Trail, near Lapine, Montgomery Co. (BIN 010738).
- Bridge over Little Double Bridges Creek on County Road 606 near Enterprise, Coffee Co. (BIN 015002)
- Bridge over Conecuh River, on County Road 2243, near Goshen, Pike Co. (BIN 013310)
- Bridge over French Creek, on Arcola St, near Demopolis, Marengo Co. (BIN 007070)
- Bridge over Chewacla Creek, on I-85 Northbound Lane, near Tuskegee, Macon Co. (BIN 008598)

Each selected bridge in Chapter 1 was different. Therefore, although the instrumentation strategy was very similar, the deployment strategy had to be specifically planned for each location. Deployment decisions varied, including which pier the sensors would be installed on, how they would be attached to the pier, how the cables would run to reach the data logger enclosure, where the enclosure would be placed, and where the solar panel would be positioned, among others.

The basic setup is shown in Figure 55 and was used for all bridges where the AV sensor, Sonar sensor, and Turbidity sensor were installed.

Figure 55. Installation of sensors: Sonar and turbidity sensors are placed facing the streambed, and the AV sensor is facing the upstream flow.

The following subsections provide a detailed description of how each location was instrumented.

5.2. Bridge over Blue Creek, on Meriwether Trail (BIN 010738), near Lapine, Montgomery County, AL

On June 15, 2022, BIN 010738 over Blue Creek, Lapine, AL, was instrumented.

Figure 56. BIN 010738, Lapine, AL.

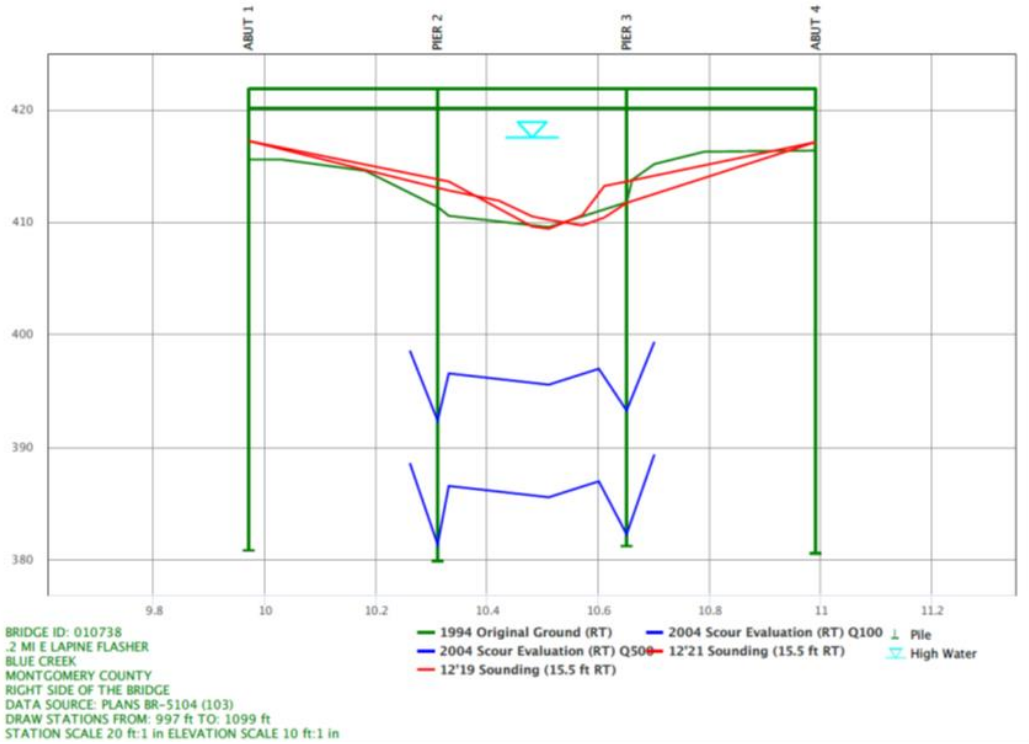

Figure 57. Cross-section of BIN 010738, Lapine, AL. Water flows in the direction into the page (source: AASHTOware Bridge Management System).

This bridge was instrumented with a motion-activated camera, an HOBO sensor for atmospheric pressure, an HOBO sensor for water level measurements, and a HOBO rain gauge. The shallow waters under this bridge did not allow for an AV sensor and Sonar to be placed. The camera was installed on pier #3, on the third pile of the pile bent, and was mounted facing the fourth pile of the pile bent, which was identified as having a potential scour occurrence.

Figure 58. BIN 010738, Lapine, AL, Pier #3. The Motion-activated camera was installed on pile #3 facing pile #4.


Figure 59. The field camera is installed on pile #3, facing pile #4.

Figure 60. BIN 010738, Lapine, AL. HOBO Water level sensor installed in the water stream, on the downstream side.

Figure 61. BIN 010738, Lapine, AL. Installation of HOBO atmospheric pressure sensor and HOBO Rain Gauge.

The instrumentation on this bridge was maintained until August 25, 2023. The research team, upon analyzing the data, determined that scour occurrence after flooding events was minor and insignificant, opting to dismantle the instrumentation on this bridge.

5.3. Bridge over Little Double Bridges Creek, on County Road 606, near Enterprise, Coffee Co. (BIN 015002)

In December 2022, BIN 015002 over Little Double Bridges Creek, located in Enterprise, AL, was instrumented. The sonar sensor and AV sensor were installed on pier #4, at the most upstream column, below water level. The turbidity sensor was not deployed at this bridge. Additionally, HOBO water level and HOBO atmospheric pressure sensors were installed. The Sonar and AV sensors were housed by a PVC pipe, which in turn was attached to the pile with multiple ratchet straps. The enclosure was attached to the bent cap on pier #5, also with multiple ratchet straps.

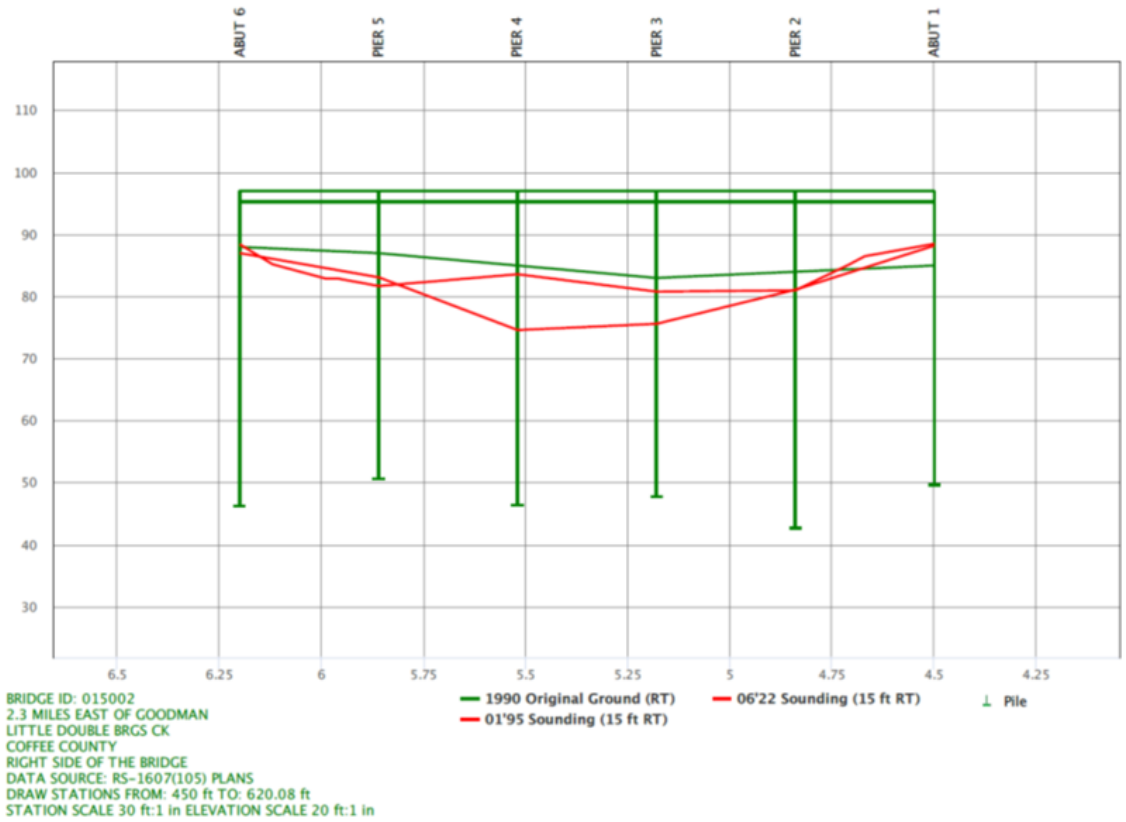

Figure 62. Cross-section of BIN 015002, Enterprise, AL. Water flows in the direction into the page (source: AASHTOware Bridge Management System).


Figure 63. BIN 015002, Enterprise, AL. Installation on Pier #4, upstream side.

Figure 64. BIN 015002, Enterprise, AL. Sensors cables installation.

Figure 65. BIN 015002, Enterprise, AL. Solar panel powering the system.

Figure 66. BIN 015002, Enterprise, AL. Enclosure housing the data logger and battery.

5.4. Bridge over Conecuh River, on County Road 2243, near Goshen, Pike Co. (BIN 013310)

In March 2023, BIN 013310 over Conecuh River in Goshen, AL, was instrumented. The apparatus was installed on Pier number 8 at the upstream column, below water level, as seen in Figure 68. The sensors installed at this pier were the Sonar sensor, AV sensor, and Turbidity sensor.

It is known that the column is supported by a footing, the edge of which is located 26 in away from the column face. Therefore, the pipe that houses the sensors (a 6-in-diameter PVC pipe) was designed to be long enough for the sensors to be placed at least 26 inches away from the column. The pipe is attached to the pier column by multiple ratchet straps for redundancy.

Figure 69 and Figure 70 show, additionally, the enclosure that houses the data acquisition system, battery, and solar panel. These figures also provide a general overview of the entire installation.

Additionally, this bridge was equipped with an HOBO water level sensor, an HOBO atmospheric pressure sensor, and a HOBO rain gauge.

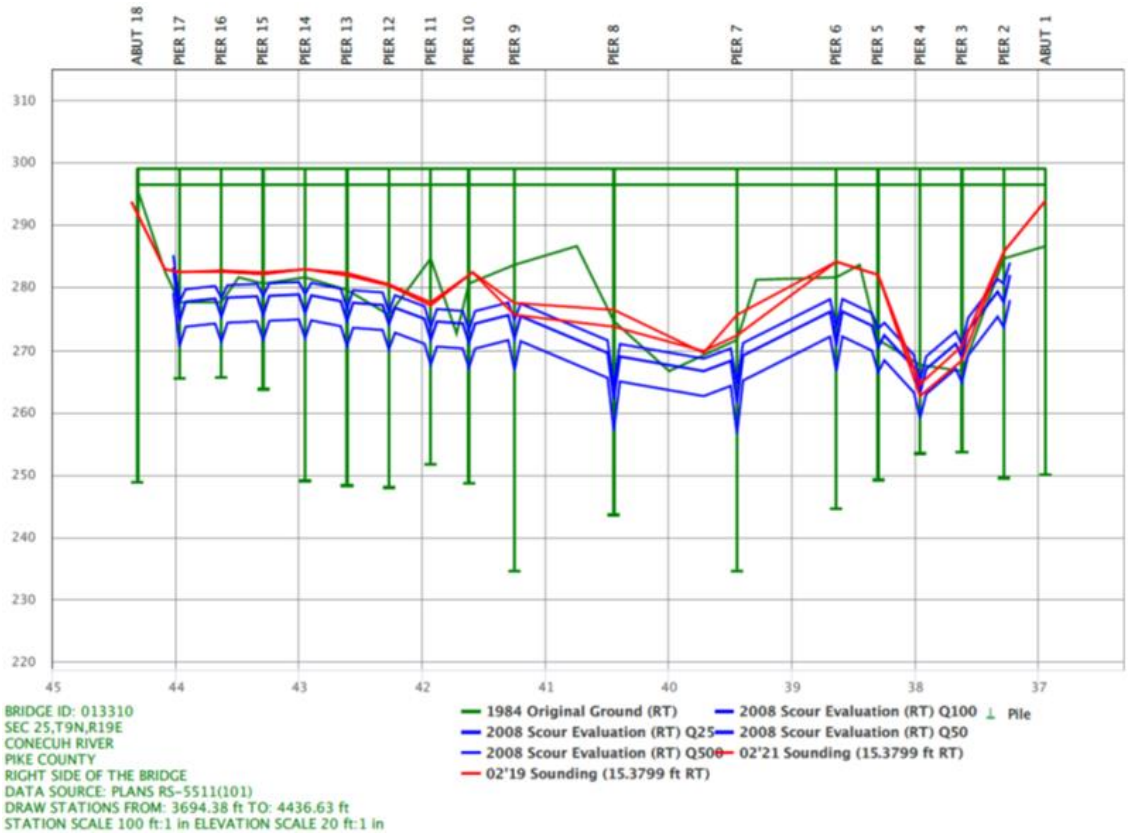

Figure 67. Cross-section of BIN 013310, Goshen, AL. Water flows in the direction into the page (source: AASHTOware Bridge Management System).

Figure 68. BIN 013310, Goshen, AL. Installation on pier #8.

Figure 69. BIN 013310, Goshen, AL. Enclosure containing the data acquisition system and battery.

Figure 70. BIN 013310, Goshen, AL. Enclosure and Solar panel attached to a wooden post, grouted to the ground.

5.5. Bridge over French Creek, on Arcola St, near Demopolis, Marengo Co. (BIN 007070)

The research team obtained permission from the Marengo County Road and Engineering Department to deploy sensors on the bridge over French Creek in Demopolis, AL. On August 10, 2023, the research team traveled to Demopolis for deployment. For this bridge, assistance from the ALDOT crew was requested, as a boat was necessary to expedite the deployment of sensors to bridge pier #4. However, any small boat (such as kayaks, canoes, or rowboats) would be sufficient for a single person to install the sensors on the bridge pier.

On this bridge, the sensors installed were an AV sensor, a Sonar sensor, and a Turbidity sensor. No HOBO sensors were installed.

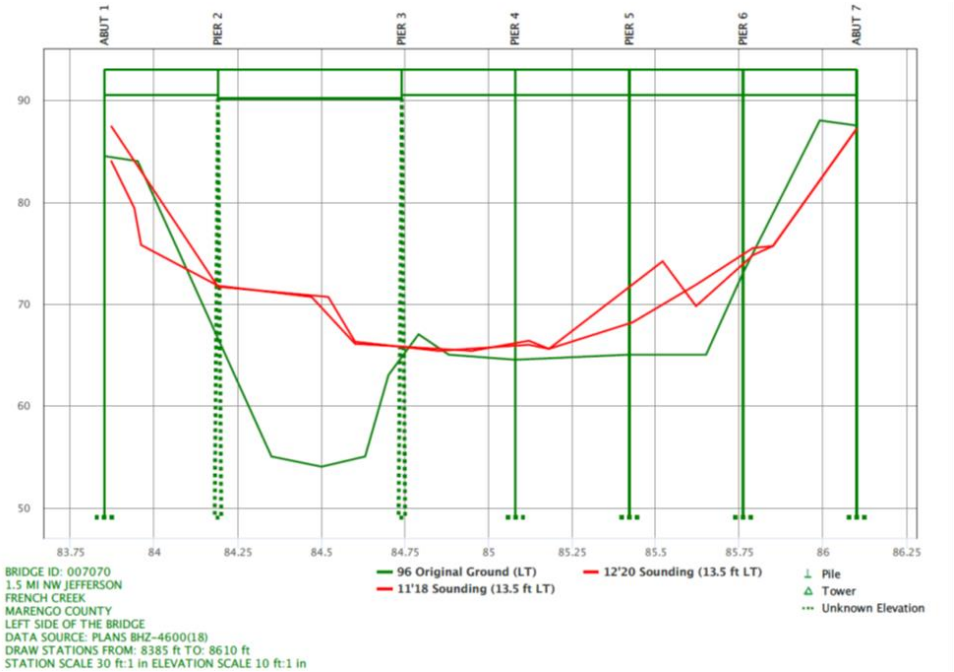

Figure 71. Cross-section of BIN 007070, Demopolis, AL. Water flows in the direction into the page (source: AASHTOware Bridge Management System).

Figure 72. BIN 007070, Demopolis, AL. Installation on pier 4.

As shown in Figure 72, the apparatus that houses the Sonar and AV sensors was bolted to pier #4, at the most upstream column. The PVC pipe has a diameter of 6 inches. Additionally, Figure 73 shows the enclosure that houses the battery and data logger. Right next to it, the solar panel was installed to supply power to the entire system.

Figure 73. BIN 007070, Demopolis, AL. Enclosure and Solar panel.

Figure 74. General view of deployment in bridge over French Creek, Demopolis, AL.

5.6. Bridge over Chewacla Creek, on I85 Northbound Lane, near Tuskegee, Macon Co. (BIN 008598)

The research team received permission to deploy the sensors on BIN 008598, spanning Chewacla Creek, on the northbound lane of I-85, near Tuskegee, AL. Figure 77 and Figure 78 show the data acquisition system, solar panel, and EchoRange, AV, and Turbidity sensors deployed at pier #6 of the bridge. The PVC pipe housing the sensors was attached to the pier using multiple ratchet straps, again for redundancy.

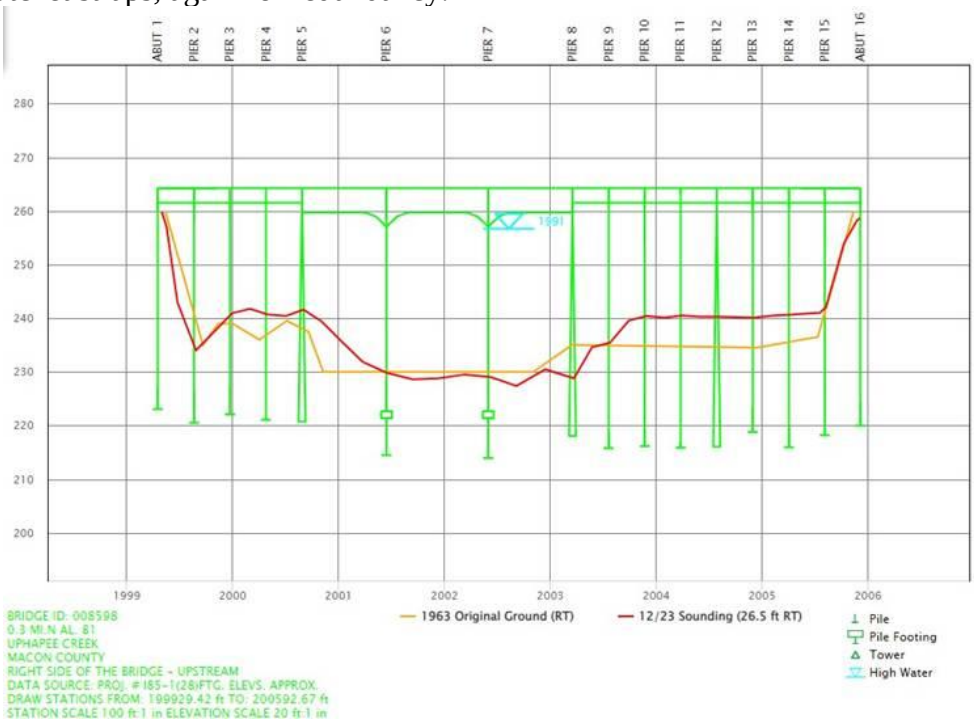

Figure 75. Cross-section of BIN 008598, Tuskegee, AL. Water flows in the direction into the page (source: AASHTOware Bridge Management System).

Figure 76. BIN 008598, Tuskegee, AL.

Figure 77. BIN 008598, Tuskegee, AL. Installation of sensors on Pier #6.

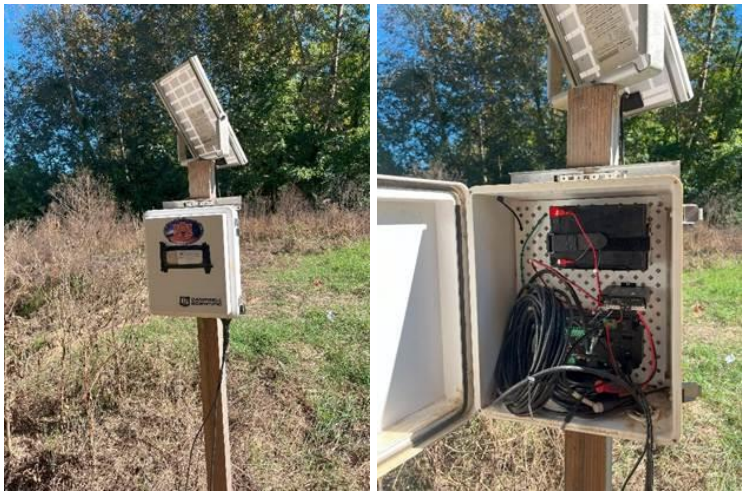

Figure 78. BIN 008598, Tuskegee, AL. Solar panel and enclosure containing data acquisition system.

6. Long-term Stream and Scour Depth Monitoring

6.1. Introduction

Following sensor deployment, data was collected from all sensors and bridge sites. Post-processing is necessary to remove noise from the dataset's measurements. The post-processing is described in detail for each sensor:

HOBO sensors

- Data from the HOBO atmospheric pressure sensor and the HOBO water pressure sensor are combined. The difference between both gives the actual water pressure above the sensor. After converting it, the result is the actual water level above the HOBO sensor.

AV sensors

- The raw data is averaged in order to obtain data values for each 15-minute time interval.
- Water level above the AV sensor is collected. Then, it must be verified and calibrated through manual measurements taken on field visits on different days. The result is the actual water level above the AV sensor.
- Velocity data: For each 15-minute data point, an average is calculated considering the previous data point, the current data point, and the following data point. A “buffer zone” is generated considering 10% above and below this average value. If the current datapoint falls outside this “buffer zone”, it is interpreted as “noise” and, therefore, eliminated from the dataset.

EchoRange (Sonar) sensors

- The raw data is averaged in order to obtain data values for each 15-minute time interval.
- The EchoRange, when reading “Depth below transducer”, often displays NAN data (“Not a Number”) that can be shown in the dataset as “NAN” or “#DIV/0!”. These must be eliminated from the data set.
- Also, the EchoRange has a minimum range of 0.40 meters. In noisy measurements, values lower than 0.40 m may be registered. These values, interpreted as “noise”, must be removed from the dataset.
- When the water level is too low, the EchoRange will make noisy measurements. Therefore, a minimum water level (0.30 m, for example) is established, and any measurement of “Depth below transducer” that corresponds to these low water levels is eliminated from the dataset.
- For each 15-minute data point, an average is calculated considering the previous data point, the current data point, and the following data point. A “buffer zone” is generated considering 10% above and below this average value. If the current datapoint falls outside this “buffer zone”, it is interpreted as “noise” and, therefore, eliminated from the dataset.

Turbidity sensors (Clarivue10)

- The raw data is averaged in order to obtain data values for each 15-minute time interval.
- When the water level is too low, the Clarivue10 will make meaningless measurements. Therefore, a minimum water level (0.30 m, for example) is established, and any measurement of “Turbidity” that corresponds to these low water levels is eliminated from the dataset.

6.2. Bridge over Blue Creek, on Meriwether Trail, (BIN 010738), near Lapine, Montgomery County, AL

The data from HOBO sensors deployed at the bridge over Blue Creek, Lapine, AL, was compiled, as seen in Figure 79.

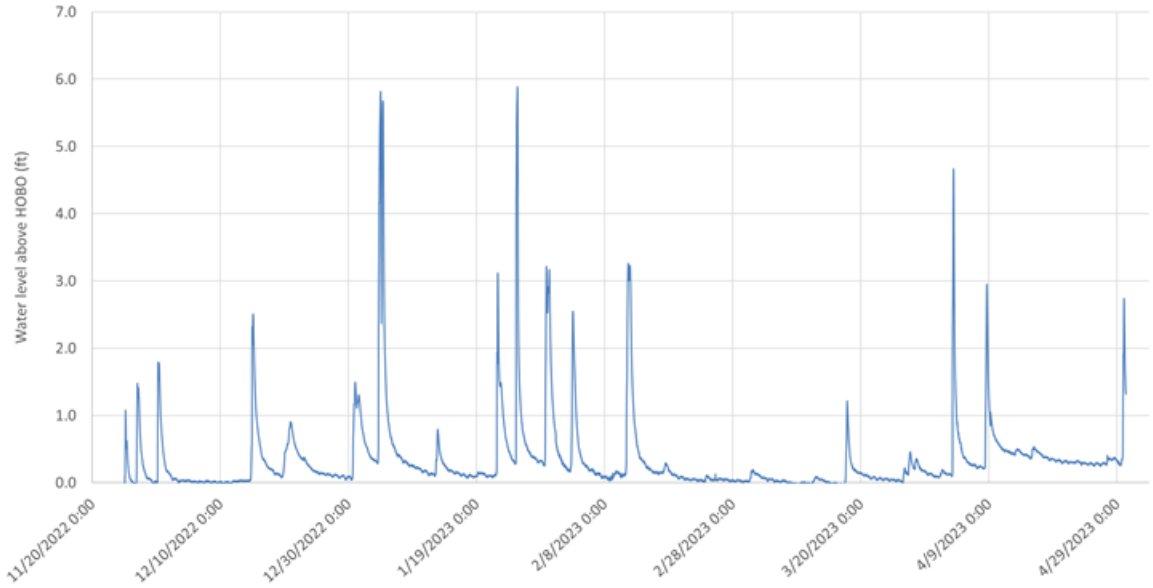

Figure 79. Water level measured by HOBO sensor in Blue Creek, Lapine, AL.

As observed, Blue Creek showed relatively few episodes of high water levels. Some spikes of water level rise can be seen in the plot, for example, on 1/25/2023, also seen in Figure 80. Three of these spikes were high enough for the water level to reach the pile of interest.

Figure 80. Pictures showing the Water level variation in Blue Creek, Lapine, AL.

As observed, there are some signs of scour after flooding events, but they are minor and unimportant in terms of observed scour. The maximum observed scour was around 6 inches. A time-lapse video containing the pictures taken with the motion-activated camera is available in Appendix B. All the collected sensor data is presented in the same appendix.

6.3. Bridge over Little Double Bridges Creek, on County Road 606, near Enterprise, Coffee Co. (BIN 015002)

The processed data is compiled and displayed as seen in Figure 81. The sensors are still deployed at this bridge and continue to measure data. The collected data covers an extensive period and is best visualized in a wide plot. Therefore, the data can be analyzed in greater detail in the download link provided in Appendix B.

Figure 81. BIN 015002, Enterprise, AL. Data from 11/15/2022 to 2/12/2025.

For this bridge, a few observations can be made:

- The water level above the AV sensor remained very shallow throughout the entire monitoring period. On a few occasions, the water level rose to beyond 50 cm (20 inches) above the AV sensor, for example. The sensors were also exposed above the water level for great periods. This means that even when submerged, the EchoRange data can be very noisy.
- The velocity data from the AV sensor aligns well with the water level data. In times when the water level rose, generally, so did water flow velocity.
- EchoRange data, specifically "Depth below transducer," barely registered any scour event at this bridge. After post-processing, the remaining data were scarce because the sonar was exposed above the water level for the most part, or the water level was too shallow. Besides, many "noisy" datapoints still were not eliminated by the filtering process.
- One observation that can be made is that the "Depth below transducer" data from around February 13, 2023, indicated a depth of approximately 45 cm to 50 cm. Months later, on August 12, 2023, the sensor measured depths of around 40 cm, indicating a minor backfilling of the scour hole.

6.4. Bridge over Conecuh River, on County Road 2243, near Goshen, Pike Co. (BIN 013310)

The processed data is compiled and displayed as seen in Figure 82. Regarding this bridge monitoring, the following observations can be made:

- The water level at this bridge varied significantly over time, with multiple high-flow events reaching over 3 meters. This is because the drainage area associated with this bridge is significantly larger than those considered in this event.
- Unlike the Enterprise bridge, the water level did not stay consistently low. Instead, it exhibited distinct peaks, indicating periodic flood events or changes in river discharge.
- There were also many periods of low water levels, during which the sensors were exposed above the surface and hence could not collect data.
- The velocity data closely follows the water level trends, confirming the expected relationship between increased discharge and higher flow velocities.
- Some extreme velocity spikes are present, particularly during peak water level events. During these peak events, the depth below the transducer also showed results of scour occurrence.
- Small levels of scour were observed during the flood events in March 2023, April 2023, and June 2023. Backfilling was also observed on these occasions, as well as in December 2024.
- A turbidity sensor was deployed at this bridge; however, as of the conclusion of this report, no data had been collected.

The sensors are still deployed at this bridge and continue to measure data. All the data covers a long period and is best observed in a very wide plot. Therefore, the data can be analyzed in greater detail in the weblink provided in Appendix B.

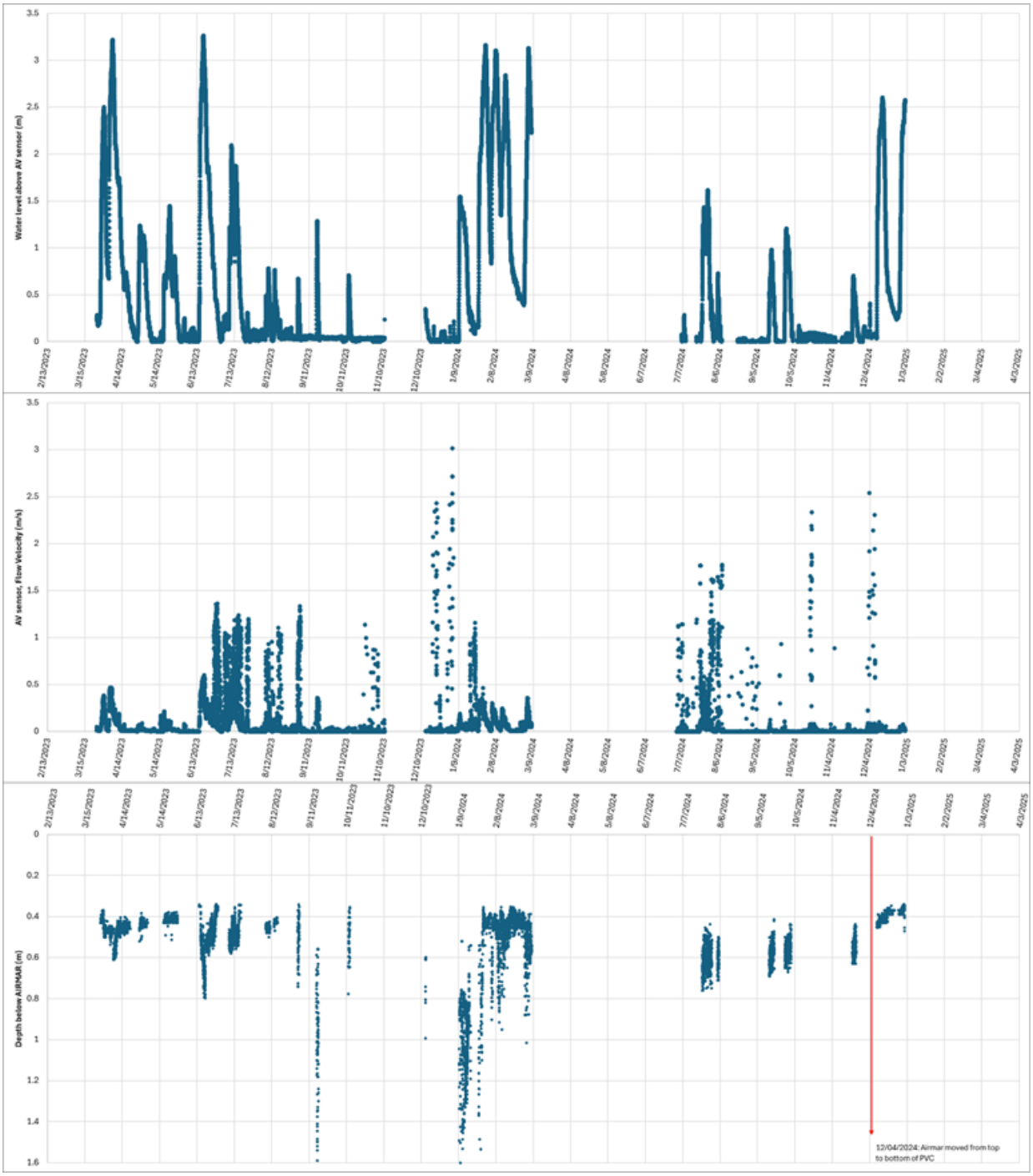

Figure 82. BIN 013310, Goshen, AL. Data from 3/15/2023 to 2/12/2025.

6.5. Bridge over French Creek, on Arcola St, near Demopolis, Marengo Co. (BIN 007070)

The processed data is compiled and displayed as seen in Figure 83.

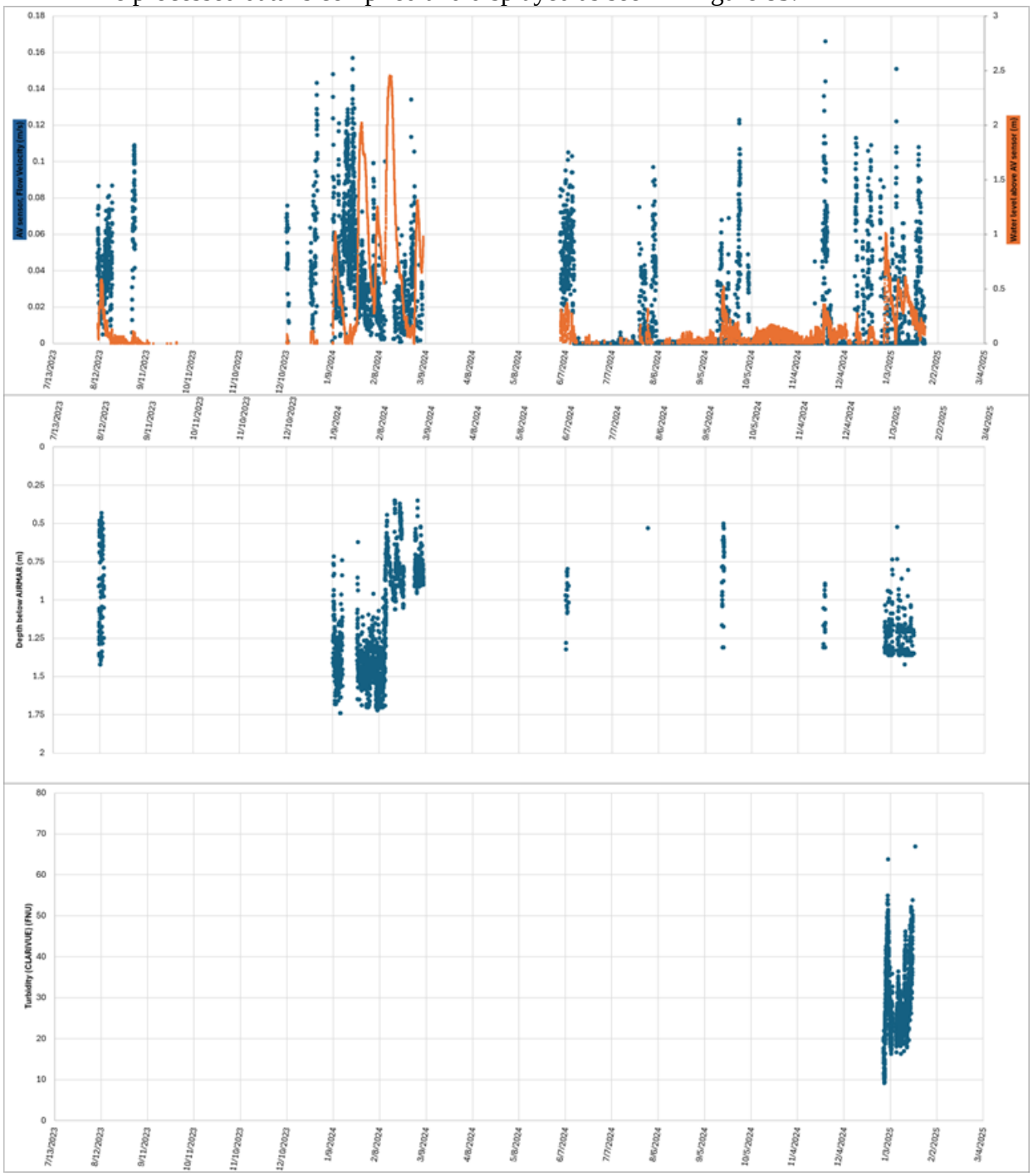

Figure 83. BIN 007070, Demopolis, AL. Data from 8/10/2023 to 2/12/2025.

For this bridge, the following observations can be made:

- The water level above the AV sensor varied greatly over this monitoring period. There were also many occasions when the sensors were exposed above the surface, resulting in numerous gaps in the data.
- Generally, the velocity data followed the trends of water level rise.
- Depth measurements below the transducer indicated a clear scour hole at a depth of approximately 1.50 m during January 2024 and February 2024. Some flood events occurred, indicating minor changes in scour hole depth, especially by the end of January 2024.
- A flood event occurred on 2/11/2024, resulting in a significant change in the scour depth measurement. The Depth below the transducer indicated backfilling, changing the measured depth from 1.50 m to approximately 0.75 m. Soon afterwards, the scour hole increased from 0.75m to 0.9 m~1.0 m. This could indicate that the flood event brought debris that filled the scour hole. Then, some of the debris was washed away.
- As time progressed, the measurements of depth below the transducer increased again, until stabilizing around 1.35 m. This can again be explained by debris being washed away with time.
- A turbidity sensor (Clarivue 10) was deployed at this bridge in December 2024. Changes in turbidity showed some correlations with changes in the water level. However, there is insufficient data to establish a behavioral relationship between raw depth below transducer measurements and turbidity.

The sensors are still deployed at this bridge and continue to measure data. All the data covers a long period and is best observed in a very wide plot. Therefore, the data can be analyzed in greater detail in the weblink provided in Appendix B.

6.6. Bridge over Chewacla Creek, on I85 Northbound Lane, near Tuskegee, Macon Co. (BIN 008598)

The processed data is compiled and displayed as seen in Figure 84. For this bridge, a few observations can be made:

- The water level remained very low for most of the monitoring period, with brief high-water events. This bridge saw extended periods of near-zero water levels.
- The few notable peaks in water level occurred in late 2024 and early 2025.
- The AV sensor only recorded water level, not velocity. This could indicate a malfunction in the specific wiring that transmits velocity data to the data logger or other power issues. As of the time of writing this report, the research team is still scheduling a site visit to address the issue.
- Recorded scour depths are scarce; very few valid measurements. The clusters of data (after the filtering process) indicate an average depth below the transducer of approximately 80 cm, which is consistent with the expected value. However, the sensor has still been unable to capture consistent scour events, even though flood events have occurred.
- Turbidity sensor (Clarivue10) was able to capture changes in turbidity during the flood events. As the flood increased, so did turbidity, and as the flood receded, so did turbidity. However, no significant changes in the EchoRange's ability to measure depth were detected compared to higher or lower levels of turbidity.

The sensors are still deployed at this bridge and continue to measure data. All the data covers an extensive period and is best observed in a very wide plot. Therefore, the data can be analyzed in greater detail in the weblink provided in Appendix B.

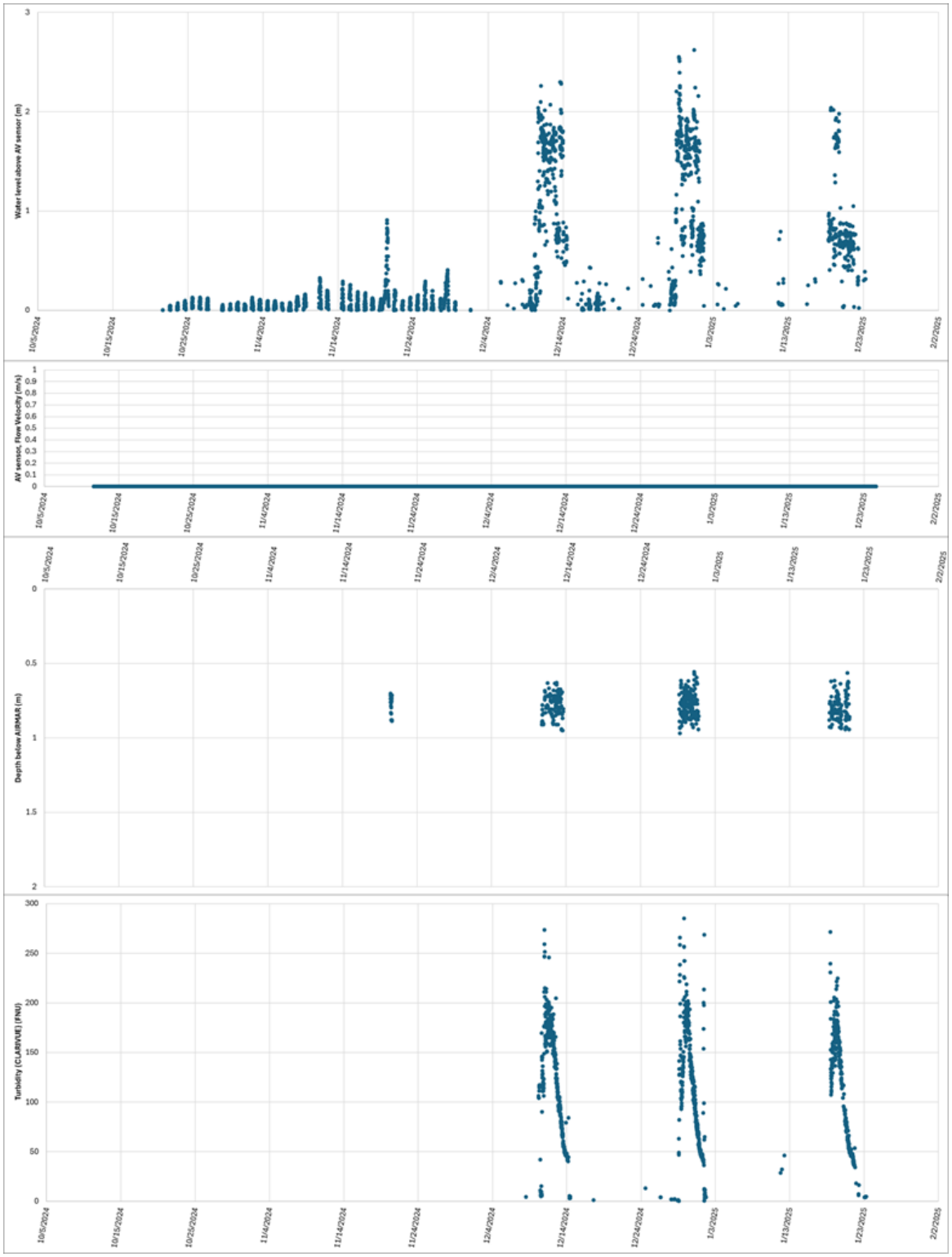

Figure 84. BIN 008598, Tuskegee, AL. Data from 10/11/2024 to 2/12/2025.

7. Incorporating Scour Observation into Design Procedures

This section presents the scour results for the evaluated methodologies HEC-18 and OMS. The values corresponding to HEC-18 calculations are depicted in graphs that compare the calculated values for each bridge modeling approach, identifying how the scour depth calculations behave across the different alternatives for calculating the peak flow.

A summary of the ranges for each bridge modeling approach and the analyzed alternatives for peak flow calculation corresponding to RRE, CN_{II}, and CN_{III} is provided, followed for the analysis the peak to average for scour depth when is possible recognize which method produce more peak to scour depth that indirectly relate the modeling approach with the scour depth production. Then, the HEC-18 scour values for each bridge modeling approach are compared against the benchmark, showing the percentage difference between each approach for each of the analyzed bridges. Finally, the HEC 18 calculations and corresponding OMS scour results are compared, using as a maximum observed scour the values consigned in BIN.

A summary of the ranges for each bridge modeling approach and the analyzed alternatives for peak flow calculations, corresponding to RRE, CNII, and CNIII, is provided, followed by an analysis of the peak-to-average ratio for scour depth. The latter analysis allows us to recognize indirectly which modeling approach is related to a greater scour depth.

7.1. HEC-18 Calculations

For the scour analysis using HEC-18, the methodology presented in subsection 3.4.1 of the present document was used. To develop the methodology, one of the necessary activities was determining the D_{50} of riverbed samples, as the methodologies require soil characterization or particle size distribution to assess critical velocity and scour depth. The particle size distribution for each bridge is presented in Figure F1 of Appendix F, and the D_{50} results are summarized in Table 18.

Table 18. D_{50} results for the analyzed bridges.

BIN	River name	D_{50} (mm)
015002	Little Double Bridges Creek	0.2
010738	Blue Creek	0.2
013310	Conecuh River	0.35
007070	French Creek	0.7

Using D_{50} information, Equation (14) and considering the considerations outlined in Section 2.2.5 of this document, pier scour calculations were performed using HEC-18 for the analyzed bridge. These calculations were conducted using various bridge modeling approaches, including 1D WSPRO, 1D energy, 2D SA-connection, and the benchmark 2D terrain modification with raised piers, for different alternatives to calculate the peak flow (RRE, CN_{II}, and CN_{III}).

The information below presents the results for each of the bridges, as described above. Table 19 shows the ranges for HEC-18 pier scour results for different analyzed methods in BIN 015002. This table shows minimum scour values for 1D WSPRO and 1D energy, which behave almost identically with values of 6.9 –7.3 ft, 6.7 – 7.1 ft, and 7.5-7.8 ft for RRE, CNII, and CN_{III}, respectively. The maximum scour values recorded corresponded to 2D Terrain modification with raised piers (benchmark), with values of 7.6-8.0 feet for the RRE, 7.1-7.5 feet for CNII, and 8.1–8.5 feet for CN_{III}. The detailed information of those calculations is presented from Figure F2 to Figure F4 and Table F1 to Table F3 of Appendix F.

Table 19. HEC-18 pier scour results for different alternatives to calculate the peak flow and bridge modeling approach. BIN 015002

Hydraulic method	RRE	CN_{II}	CN_{III}
1D WSPRO	6.9 - 7.3 ft	6.7 - 7.1 ft	7.5 - 7.8 ft
1D Energy	6.9 - 7.3 ft	6.5 - 7.0 ft	7.5 - 7.8 ft
2D SA connection	6.9 -7.9 ft	6.3 - 7.3 ft	7.2 - 8.2 ft
2D Terrain_mod	7.6 - 8.0 ft	7.1 - 7.5 ft	8.1 - 8.5 ft

Likewise, Table 20 displays the ranges of HEC-18 pier scour findings for different methods of analysis for BIN 010738. The minimum scour values were recorded for 1D energy, ranging from 4.4 to 4.5 feet for RRE, 4.2 feet for CN_{II}, and 4.3 feet for CN_{III}. The maximum scour values estimated corresponded to 2D Terrain modification with raised piers (benchmark) with values of 5.8 feet for the RRE, 5.2 - 5.3 feet for CN_{II}, and 5.6 feet for CN_{III}. Nevertheless, some high values are registered for 2D-SA connection using CN_{III}, corresponding to values ranging from 5.4 to 5.9 feet. The complete information of those calculations is presented from Figure F5 to Figure F7 and Table F4 to Table F6 of Appendix F. This bridge, similarly to the previous one, demonstrated that the maximum scour depths were related to the 2D Terrain modification with raised piers. In this case, the maximum scour did not correspond to the HEC-HMS CN_{III} peak flow because the RRE peak flow was slightly above the HEC-HMS CN_{III} peak flow.

Table 20. HEC-18 pier scour results for different alternatives to calculate the peak flow and bridge modeling approach. BIN 010738

Hydraulic method	RRE	CN_{II}	CN_{III}
1D WSPRO	4.4 – 4.5 ft	4.1 – 4.3 ft	4.3 ft
1D Energy	4.4- 4.5 ft	4.2 ft	4.3 ft
2D SA connection	5.5 ft	5.2 ft	5.4 – 5.9 ft
2D Terrain_mod	5.8 ft	5.2 – 5.3 ft	5.6 ft

Table 21 presents the HEC-18 pier scour calculation results for all tested methods evaluated for BIN 013310. The minimum obtained values for scour calculations were for 2D terrain modification with raised piers (benchmark), with values ranging from 0 to 4.5 feet for the RRE, 1.3 to 6.4 feet for CNII, and 1.1 to 6.1 feet for CN_{III}. The maximum obtained values for scour calculations were found for 1D energy, with values of 3.4 to 8.7 feet, 3.5 to 8.7 feet, and 4.0 to 9.2 feet. This model contrasts with the two previous ones, showing a greater scour depth for the 1D models than the D models. In this specific case, as mentioned earlier in the hydraulic results, the hydraulic complexity, with multiple openings and channels, suggests that the 1D models do not accurately represent the channel of approach. The complete information of those calculations is presented from Figure F8 to Figure F10 and Table F7 to Table F9 of Appendix F.

Table 21. HEC-18 pier scour results for different alternatives to calculate the peak flow and bridge modeling approach. BIN 013310

Hydraulic method	RRE	CN_{II}	CN_{III}
1D WSPRO	2.9 – 7.0 ft	3.2 – 7.0 ft	4.1 – 7.5 ft
1D Energy	3.4 -8.7 ft	3.5 – 8.7 ft	4.0 – 9.2 ft
2D SA connection	0 – 5.2 ft	2.6 – 7.1 ft	2.0 -6.1 ft
2D Terrain_mod	0 - 4.5 ft	1.3 – 6.4 ft	1.1 – 6.1 ft

Finally, Table 22 depicts HEC-18 pier scour calculation results for the various methods assessed for BIN 007070. This table shows minimum scour values for 1D energy of 3.9 - 4.2 ft, 3.4 - 3.9 ft, and 3.9 - 4.2 ft for RRE, CNII, and CN_{III}, respectively. The maximum scour values recorded corresponded to 2D Terrain modification with raised piers (benchmark) with values of 4.2 - 5.8 feet for the RRE, 4.8 - 5.8 feet for CN_{II}, and 4.8 - 6.1 feet for CN_{III}. Nonetheless, certain high values are registered for 2D-SA connection utilizing CN_{III}, corresponding to values ranging from 5.4 to 6.1 feet. The complete information of those calculations is presented from Figure F11 to Figure F13 and Table F10 to Table F12 of Appendix F.

Table 22. HEC-18 pier scour results for different alternatives to calculate the peak flow and bridge modeling approach. BIN 007070

Hydraulic method	**RRE**	**CN_{II}**	**CN_{III}**
1D WSPRO	3.6 – 3.9 ft	3.7 – 3.9 ft	4.0 – 4.2 ft
1D Energy	3.9 – 4.2 ft	3.4 – 3.9 ft	3.9 – 4.2 ft
2D SA connection	4.4 – 5.5 ft	4.5 – 5.4 ft	5.4 – 6.1 ft
2D Terrain_mod	4.2 – 5.8 ft	4.8 – 5.8 ft	4.8 - 6.1 ft

The results show a trend where the maximum scour calculations corresponded to the 2D Terrain modification with raised piers (benchmark), and the minimum values corresponded to 1D WSPRO. In some cases, as in BIN 013310, the maximum scour calculations correspond to 1D energy; however, as mentioned earlier, due to the complex hydraulics of that river, the 1D models do not accurately represent the channel approach.

Another type of analysis conducted was to determine the peak-to-average scour for the different alternatives, in order to calculate the peak flow and for the analyzed bridge modeling approaches. Figure 85 to Figure 86 show the peak-to-average ratio for scour for the different bridge modeling approaches when the alternative for calculating the peak flow is RRE and CN_{III}, respectively.

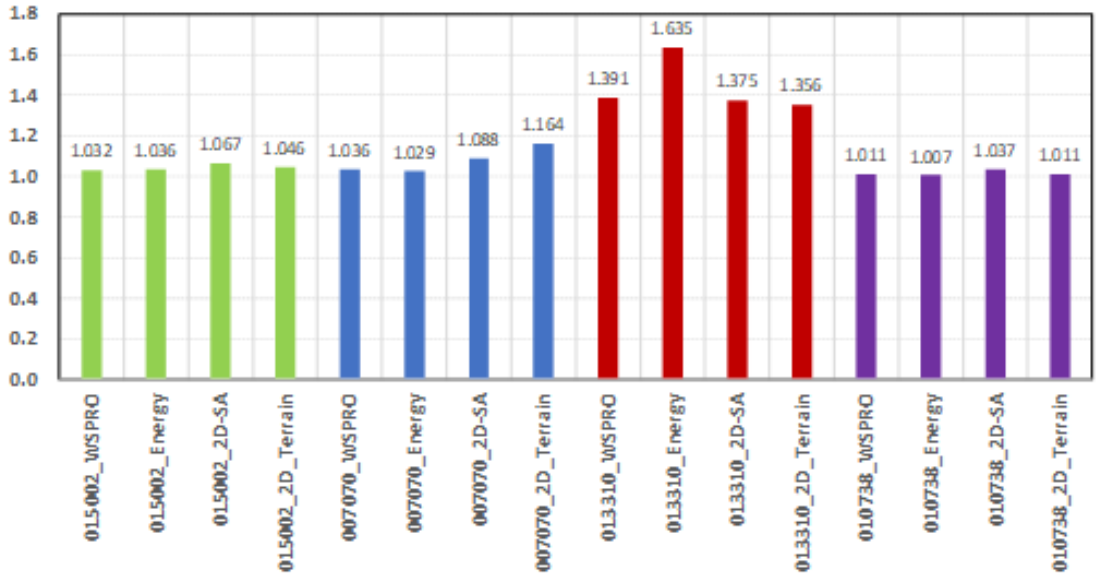

Figure 85. Peak to average for scour depth using RRE

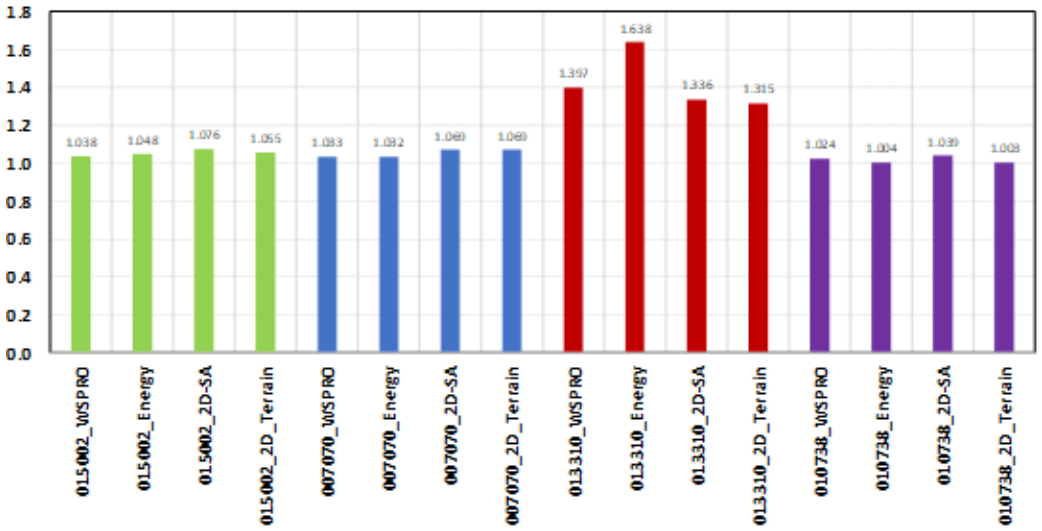

Figure 86. Peak to average for scour depth using CN_{III}

In these graphs, it can be observed that, for almost all cases, the 2D-dimensional models exhibit a higher peak to average for scour, which is associated with large velocities (Figure 46) and deeper scour depth. In the same scenarios, the models with a lower peak-to-average ratio for scour correspond to 1D models, which are associated with low velocities and shallow scour depths. The exception to the results mentioned earlier corresponds to BIN 013310, whose maximum scour values align with the 1D energy and exhibit the highest peak-to-average ratio for scour. Nevertheless, the obtained results were not considered appropriate because those types of models do not appropriately describe the complex hydraulics of the mentioned bridge.

Additionally, in the earlier analyses, a comparison was conducted using the 2D terrain modification with raised piers as the bridge modeling approach, while varying the alternative for calculating the peak flow. The pier scour values for each of the bridges were averaged to determine which peak flow alternative exhibited the highest average scour. Figure 87 and Table 23 present the results of this procedure for BIN 015002, showing that the worst-case scenario is represented by the alternative corresponding to CN_{III} with 8.28 ft, followed by RRE with 7.8 ft, and CN_{II} with 7.23 ft. The percentage variation between RRE, CN_{II}, and CN_{III} corresponded to -7.3% and 6.15%, respectively. The negative value indicates that the scour depth is below the corresponding one using the RRE.

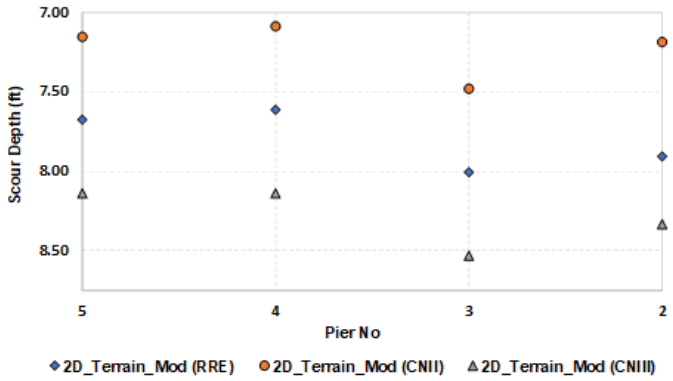

Figure 87. HEC-18 scour comparison values of the different alternatives to calculate the flow using the Bridge modeling approach (benchmark). BIN 015002

Table 23. HEC-18 scour comparison values of the different alternatives to calculate the flow using the Bridge modeling approach (benchmark). BIN 015002

PIER BIN	2D_Terrain_Mod (RRE)	2D_Terrain_Mod (CN_{II})	2D_Terrain_Mod (CN_{III})
2	7.91	7.19	8.33
3	8.01	7.48	8.53
4	7.61	7.09	8.14
5	7.68	7.15	8.14
Average	**7.80**	**7.23**	**8.28**

Figure 88 and Table 24 present the results of this process for BIN 010738, indicating that the alternative corresponding to RRE with 5.87 feet is the worst-case scenario for scour, followed by CNIII with 5.61 feet and CNII with 5.27 feet. The percentage variation between RRE, CN_{II}, and CN_{III} corresponded to -10.22% and -4.42%, respectively. The negative value indicates that the scour value depth is below the corresponding one computed RRE.

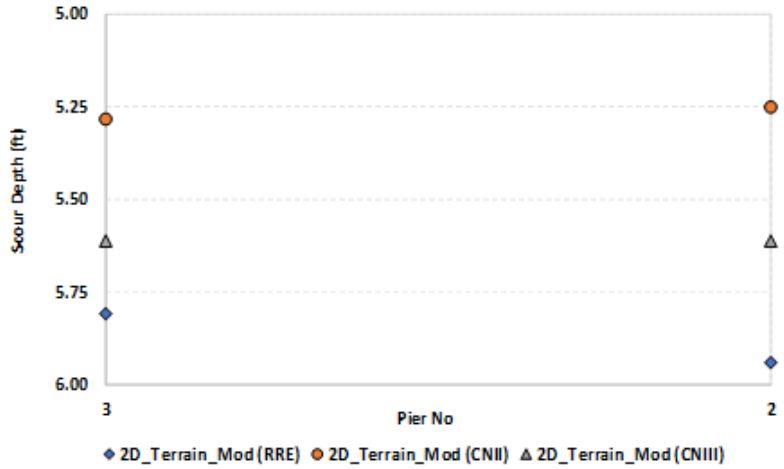

Figure 88. HEC-18 pier scour comparison of the different alternatives to calculate the flow using the Bridge modeling approach (benchmark). BIN 010738

Table 24. HEC-18 pier scour comparison values of the different alternatives to calculate the flow using the Bridge modeling approach (benchmark). BIN 010738

PIER BIN	2D_Terrain_Mod (RRE)	2D_Terrain_Mod (CN_{II})	2D_Terrain_Mod (CN_{III})
2	5.94	5.25	5.61
3	5.81	5.28	5.61
Average	**5.87**	**5.27**	**5.61**

Analogously, Figure 89 and Table 25 present the results of this procedure for BIN 013310, showing that the worst-case scenario is represented by the alternative corresponding to CN_{III} with 4.89 ft, followed by RRE 3.34 ft, and CN_{II} with 4.63 ft. The percentage variation between RRE,

CN_{II}, and CN_{III} corresponded to 27.86% and 31.69%, respectively. The positive value indicates that the scour value depth is larger than the corresponding one computed using the RRE.

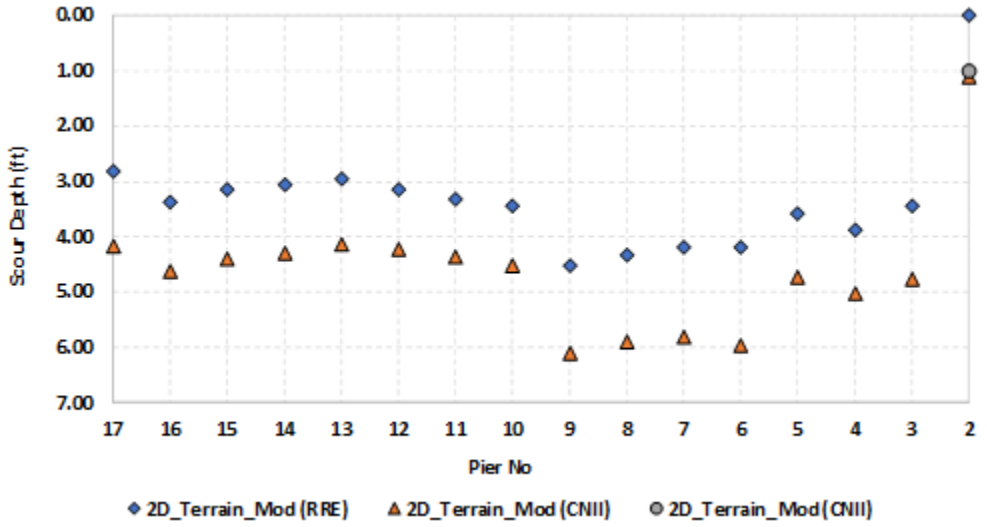

Figure 89. HEC-18 pier scour comparison of the different alternatives to calculate the flow using the Bridge modeling approach (benchmark). BIN 013310

Table 25. HEC-18 pier scour comparison values of the different alternatives to calculate the flow using the Bridge modeling approach (benchmark). BIN 013310

PIER BIN	2D_Terrain_Mod (RRE)	2D_Terrain_Mod (CN_{II})	2D_Terrain_Mod (CN_{III})
2	0.00	1.12	1.31
3	3.44	4.76	4.95
4	3.87	5.02	5.41
5	3.58	4.72	4.99
6	4.20	5.97	6.43
7	4.20	5.81	6.23
8	4.33	5.91	6.27
9	4.53	6.10	6.40
10	3.44	4.53	4.72
11	3.31	4.36	4.49
12	3.15	4.23	4.40
13	2.95	4.13	4.33
14	3.05	4.30	4.46
15	3.15	4.40	4.56
16	3.38	4.63	4.82
17	2.82	4.17	4.46
Average	**3.34**	**4.63**	**4.89**

Finally, Figure 90 and Table 26 present the results of this procedure for BIN 07070, depicting that the worst-case scenario is represented by the alternative corresponding to CN_{III} with 7.35 ft, followed by CN_{II} with 7.09 ft and RRE 5.47 ft, The percentage variation between RRE,

CN_{II}, and CN_{III} corresponded to 22.85 % and 25.58%, respectively. The positive value indicates that the scour value depth is larger than the corresponding one computed using the RRE.

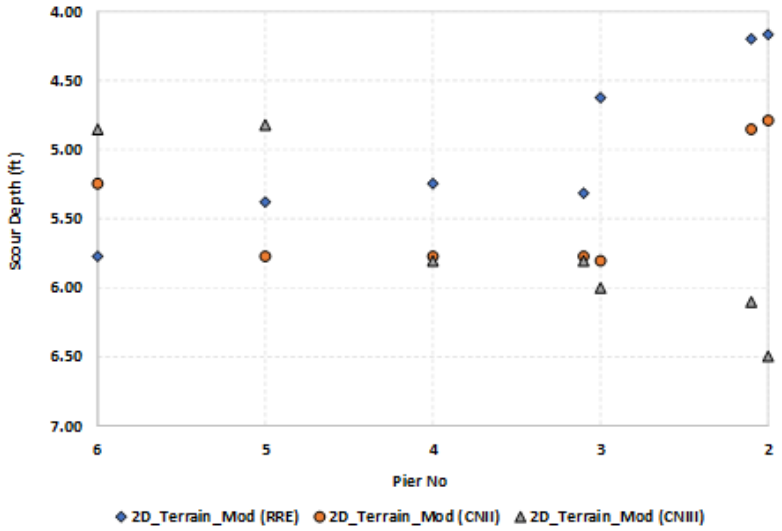

Figure 90. HEC-18 pier scour comparison of the different alternatives to calculate the flow using the Bridge modeling approach (benchmark). BIN 007070

Table 26. HEC-18 pier scour comparison values of the different alternatives to calculate the flow using the Bridge modeling approach (benchmark). BIN 007070

PIER BIN	2D_Terrain_Mod (RRE)	2D_Terrain_Mod (CN_{II})	2D_Terrain_Mod (CN_{III})
2	5.41	6.98	7.38
2.1	5.41	6.94	7.38
3	5.48	7.09	7.38
3.1	5.48	7.09	7.35
4	5.48	7.12	7.35
5	5.51	7.19	7.32
6	5.54	7.19	7.28
Average	**5.47**	**7.09**	**7.35**

7.2. OMS pier scour calculations

The following discussion presents the pier scour results using the OMS methodology (Govindasamy et al., 2013). Using TAMU-OMS software (Briaud et al., 2009), the future scour was calculated for the bridges analyzed. Following the methodological steps outlined in Chapter 3, the first step was to determine the maximum scour depth at the bridge, utilizing secondary information based on AASHTOWare Bridge Management BIN for bridges. The results of the OMS calculations are presented in Table 27. For BIN 007070, it was not possible to apply the methodology because it was found that, since its construction, this bridge has undergone an aggradation process.

Table 27. OMS pier scour calculations for the analyzed Bridges

BIN	Feature Intersected	OMS scour (ft)
015002	Little Double Bridges Creek	5.5 - 5.6
010738	Blue Creek	1.7 - 1.9
007070	French Creek	NA
013310	Conecuh River	5.4 - 5.7

Comparing the outcomes of the HEC-18 and OMS pier scours allowed for comparison. The results show the obtained ranges without considering the method used; they only display values within these ranges. For BIN 015002, the HEC-18 pier scour depth results showed differences that were 33.7% to 51.7% higher than those of OMS. For BIN 010738, the differences were 164.7 to 210.5% higher than OMS. For BIN 013310 and BIN 007070, the differences were 20% to 61.4% higher than OMS.

7.3. Summary of scour results

As a summary of scour the results described above, Table 28 presents the obtained scour depth using HEC-18 calculations for various hydrological and hydraulic approaches, as well as OMS calculations.

Table 28. Summary of pier scour results

BIN	METHOD	RRE	CN_{II}	CN_{III}	OMS
015002	1D WSPRO	6.9 - 7.3 ft	6.7 - 7.1 ft	7.5 - 7.8 ft	5.5-5.6 ft
	1D Energy	6.9 - 7.3 ft	6.5 - 7.0 ft	7.5 - 7.8 ft	
	2D SA connection	6.9 -7.9 ft	6.3 - 7.3 ft	7.2 - 8.2 ft	
	2D Terrain_mod	7.6 - 8.0 ft	7.1 - 7.5 ft	8.1 - 8.5 ft	
010738	1D WSPRO	4.4 – 4.5 ft	4.1 – 4.3 ft	4.3 ft	1.7-1.9 ft
	1D Energy	4.4- 4.5 ft	4.2 ft	4.3 ft	
	2D SA connection	5.5 ft	5.2 ft	5.4 – 5.9 ft	
	2D Terrain_mod	5.8 ft	5.2 – 5.3 ft	5.6 ft	
013310	1D WSPRO	2.9 – 7.0 ft	3.2 – 7.0 ft	4.1 – 7.5 ft	5.4-5.7 ft
	1D Energy	3.4 -8.7 ft	3.5 – 8.7 ft	4.0 – 9.2 ft	
	2D SA connection	0 – 5.2 ft	2.6 – 7.1 ft	2.0 -6.1 ft	
	2D Terrain_mod	0 - 4.5 ft	1.3 – 6.4 ft	1.1 – 6.1 ft	
007070	1D WSPRO	3.6 – 3.9 ft	3.7 – 3.9 ft	4.0 – 4.2 ft	NA
	1D Energy	3.9 – 4.2 ft	3.4 – 3.9 ft	3.9 – 4.2 ft	
	2D SA connection	4.4 – 5.5 ft	4.5 – 5.4 ft	5.4 – 6.1 ft	
	2D Terrain_mod	4.2 – 5.8 ft	4.8 – 5.8 ft	4.8 - 6.1 ft	

7.4. Comparison of Field Data with HEC-18 and OMS calculations

This section presents the results obtained from the Hydrological and Hydraulic modeling, as well as the HEC18 and OMS scour estimates, comparing them to the field data monitoring presented in Chapter 6 of this report. The comparisons are made for each bridge and for the specific pier where the instrumentation was deployed. Comparisons were made for the maximum velocity of the upstream water flow at the pier, the maximum water depth at the pier, and the measured scour at the pier. An important note about this comparison is that, in these tables, the maximum measured values of velocities, water depths, and scour depths did not occur simultaneously. They are simply the maximum measured values in the monitored period.

Table 29. Modeled and Observed Maximum velocity at the bridges of interest

Bridge	**Location**	**Pier**	**Modeled Velocity (ft/s) (Chapter 3)**	**Maximum Observed Velocity (ft/s) (Chapter 6)**
BIN 010738	Lapine, AL	#3	3.2 ~ 5.7	-
BIN 015002	Enterprise, AL	#4	6.4 ~ 8.5	~ 2.6
BIN 013310	Goshen, AL	#8	4.2 ~ 5.8	~ 4.5
BIN 007070	Demopolis, AL	#4	2.7 ~ 5.8	~ 0.55
BIN 008598	Tuskegee, AL	#6	-	-

Table 30. Modeled and Observed Maximum Water Depth at the bridges of interest

Bridge	**Location**	**Pier**	**Modeled Water Depth (ft) (Chapter 3)**	**Maximum Observed Water Depth (ft) (Chapter 6)**
BIN 010738	Lapine, AL	#3	4.8 ~ 5.95	~ 1.6
BIN 015002	Enterprise, AL	#4	4.4 ~ 6.5	~9.2
BIN 013310	Goshen, AL	#8	9.75 ~ 14	~11.5
BIN 007070	Demopolis, AL	#4	4.8 ~ 7.2	~ 12.9
BIN 008598	Tuskegee, AL	#6	-	~ 10.8

Table 31. Estimated and Observed Maximum Pier Scour at the bridges of interest

Bridge	**Location**	**Pier**	**Estimated Scour (ft) (Chapter 7)**		**Maximum Observed Scour (ft) (Chapter 6)**
			HEC-18	**OMS**	
BIN 010738	Lapine, AL	#3	5.3 ~ 5.8	1.7 ~ 1.9	~ 0.5
BIN 015002	Enterprise, AL	#4	7.1 ~ 8.2	5.5 ~ 5.6	~ 1.0
BIN 013310	Goshen, AL	#8	4.3 ~ 6.0	5.4 ~ 5.7	~ 1.3
BIN 007070	Demopolis, AL	#4	5.25 ~ 5.8	-	~ 0.2
BIN 008598	Tuskegee, AL	#6	-	-	-

8. Conclusions and Recommendations

This research systematically evaluated several computing methods used in bridge scour analysis, incorporating peak flow estimates and hydraulic modeling approaches. The goal was to assess how these different methods can alter the results of pier scour calculations in bridges that utilize HEC-18 and OMS. These combinations were implemented on four bridges in Alabama, which were identified using the same AASTHOWare BINentifier and pier nomenclature.

The evaluation considered various hydrological, hydraulic, and scour depth alternatives for hydrological events with a 100-year return period. The results presented in Chapter 3 indicate that, to compute peak flows, hydrological modeling using high initial soil moisture (i.e., HEC-HMS CNIII) may yield more conservative peak flow depths than the currently used approach based on regional regression equations. Likewise, an update on the hydraulic practices in ALDOT that introduce 2D stream flow computation based on HEC-RAS and raised piers approach will also increase the representativeness of depth and velocity estimates for scour calculations.

The project was also successful in devising, deploying, and monitoring scour depths in various bridges in the state. The sensors required programming work to make them compatible with the data loggers, battery, and solar charging system. This work involved practical issues such as power budgeting. The whole system needed to function independently in the selected remote locations. Additionally, due to noise issues, especially in measurements made by the EchoRange, the programming had to include commands to change the sensor's configurations, enabling it to measure in turbid and shallow waters. It was observed that the scour readings were affected by the water turbidity in the stream flow; therefore, the project also monitored this parameter to understand when it began to impact the results. Nevertheless, using sonar-based approaches is promising and should be considered in future evaluations of scour risk on bridges in Alabama. Based on the input from other researchers and DOTs that have been using sonar, the approach that was developed in this research is cost-effective, which should facilitate its adoption.

Upon the comparison between the field data collection and the scour estimate efforts, the following conclusions can be drawn:

- At the bridge in Lapine, AL, scour was not monitored using sonar but through visual observations from pictures taken by the motion-activated camera. As a result, when scour occurs, it is only possible to observe it before and after the flood event. If the scour was higher during the event, it would not be possible to report it. Additionally, water flow velocity was not measured.
- The observed scour in all bridges was much smaller than the values modeled through HEC-18 and OMS. The observed scour, reflected in OMS results, was based on episodical bridge inspections, which have some uncertainties and inaccuracies. However, this discrepancy may also reflect the conservatism inherent in the HEC-18 scour predictions.
- For bridges BIN 010738 and BIN 015002, the observed water depth is significantly smaller than the modeled values. It reflected the fact that heavy rain events did not impact these basins during this research period.
- For bridges BIN 013310 (Goshen), the water depth and flow velocities reached a range associated with large flooding. However, the observed maximum scour depth was not as large as predicted in either OMS or HEC-18, at least for the selected bridge pier. This could be an indication that the most critical pier is elsewhere in the structure.
- BIN 007070 (Demopolis) had very large observed water depths and much smaller associated flow velocities. This indicates that interactions with the nearby Black Warrior

River, which was not included in the HEC-RAS modeling, may be significant. Such interactions can also be common in other bridges across the state, posing difficulties in estimating hydrologic peak flows and hydraulic flow depths and velocities.

Regarding the comparisons between HEC-18 and OMS scour estimate approaches, HEC-18 results were consistently larger than the ones obtained by OMS:

- 33% to 51% greater than OMS for BIN 015002 in Enterprise,
- 164% to 210% greater than OMS BIN 010738 in Lapine, and
- 20% to 61% greater than OMS BIN 013310 in Goshen.

This comparison was not possible in Demopolis, as the bridge suffers from an aggradation issue, and thus, the OMS methodology does not apply to this bridge.

In summary, this research suggests that various design decisions can influence the accuracy of scour calculations, and therefore, the most conservative and accurate methods should be selected. Particularly in the case of complex bridge cross sections, such as BIN 013310, 2D hydraulic models should be the selected approach, as the assumptions used in 1D modeling tools may not yield representative velocity and depth values during peak flow conditions near these structures.

Regarding the practical implementation of the field monitoring, this research has various important recommendations:

- Deployment must be planned differently for each bridge. The points in which the instruments will be deployed must be predetermined, and the approach by which the equipment will be attached to the bridge pier needs to be defined. The chosen approach must ensure the equipment remains in place under harsh conditions.
- Despite the monitoring system being fully automated and independent, periodic site visits are still necessary. Sensors will become fouled over time due to the constant flow of water and sediments, which can cover them and interfere with the measurements. Therefore, the sensors should be cleared and wiped regularly. Additionally, occasional manual measurements will facilitate the calibration and validation of the sensor data.
- Other practical issues may arise and must be addressed, such as insects that can create nests and disrupt the equipment, the possibility of tampering and vandalism, and the accumulation of debris by the bridge pier, which, whenever possible, must be removed.

References

Ahamed, T. (2020). Fragility Analysis of Instream Bridges Subjected to Flood and Scour (Doctoral dissertation, The University of Arizona).

Anderson, J. B., Fang, X., Walker, M. E., Wright, W. H., & Chen, G. (2015). Evaluation of scour potential of cohesive soils-phase 2 (No. ALDOT 930-789-1). Auburn University. Highway Research Center.

Arneson, L.A., L.W. Zevenbergen, P.F. Lagasse, and P.E. Clopper. 2012. Evaluating Scour at Bridges. U.S. Department of Transportation, Federal Highway Administration, Washington, D.C. Hydraulic Engineering Circular No. 18, 5th ed., Publication No. FHWA-HIF-12-003. 340 pp.

Atkins, J. B., & Hedgecock, T. S. (1996). Scour at Selected Bridge Sites in Alabama, 1991-94 (Vol. 96, No. 4137). US Department of the Interior, US Geological Survey.

Beebee, R. A., Dworsky, K. L., & Knopp, S. J. (2017). Streambed scour evaluations and conditions at selected bridge sites in Alaska, 2013–15 (No. 2017-5149). US Geological Survey.

Benedict, S. T., & Caldwell, A. W. (2014). A pier scour database: 2,427 field and laboratory measurements of pier scour. US Geological Survey Data Series, 845

Blue Siren (2019). AV Flow Sensor, Dual Wave Ultrasonic Doppler Velocity. Blue siren web page accessed May 02, 2024, at https://www.blue-siren.com/products/copy-of-solosiren%C2%AE.

Boehmler, E. M., & Olimpio, J. R. (2000). Evaluation of pier scour measurement methods and pier scour predictions with observed scour measurements at selected bridge sites in New Hampshire, 1995-98 (No. FHWA-NH-RD-12323E,).

Boujia, N., Schmidt, F., Chevalier, C., Siegert, D., & Van Bang, D. P. (2018, April). Bridge scour monitoring technique using the vibratory response of rods embedded in the riverbed. In TRA 2018, Proceedings of 7th Transport Research Arena (pp. 10-p).

Briaud, J.-L., Govindasamy, A. V., Kim, D., Gardoni, P., Olivera, F., Chen, H., Mathewson, C. C. and Elsbury, K. (2009b). "Simplified method for estimating scour at bridges." Rep. 0 5505-1, Texas Department of Transportation, Austin, TX.

Briaud, J. L., Ting, F. C. K., Chen, H. C., Gudavalli, R., Peregu, S., and Wei, G. (1999). "SRICOS: prediction of scour rate in cohesive soils at bridge piers," Journal of Geotechnical and Geoenvironmental Engineering, 125 (4), April, pp. 237-246, American Society of Civil Engineers, Reston, VA.

Briaud, J.-L., Ting, F., Chen, H.C., Cao, Y., Han, S.-W., Kwak, K. (2001). "Erosion Function Apparatus for Scour Rate Predictions". Journal of Geotechnical and Geoenvironmental Engineering, ASCE, Vol. 127, No. 2, pp. 105–113, American Society of Civil Engineers, Reston, VA.

Briaud, J. L. (2004). The SRICOS-EFA Method. In Current Practices and Future Trends in Deep Foundations (pp. 348-360).

Briaud, J. L., & Chedid, M. (2019). Allowable Limit Contraction and Abutment Scour at Bridges: Technical Report (No. FHWA/TX-18/0-6935-R1). Texas A&M Transportation Institute.

Briaud, J. L., Govindasamy, A. V., Kim, D., Gardoni, P., & Olivera, F. (2009). Simplified method for estimating scour at bridges (No. FHWA/TX-09/0-5505-1). Texas. Dept. of Transportation. Research and Technology Implementation Office.

Briaud, J.L., H.C. Chen, K.A. Chang, S.J. Oh, S. Chen, J. Wang, Y. Li, K. Kwak, P. Nartjaho, R. Gudaralli, W. Wei, S. Pergu, Y.W. Cao, and F. Ting (2011), "The SRICOS – EFA Method" Summary Report, Texas A&M University

Briaud, J. L., Hurlebaus, S., Chang, K. A., Yao, C., Sharma, H., Yu, O. Y., Darby, C., Hunt, B.E. & Price, G. R. (2011). Realtime monitoring of bridge scour using remote monitoring technology (No. Report 0-6060-1). Texas Transportation Institute.

Briaud, J. L., & Chedid, M. (2019). Allowable Limit Contraction and Abutment Scour at Bridges: Technical Report (No. FHWA/TX-18/0-6935-R1). Texas A&M Transportation Institute.

Brown, S. A., Schall, J. D., Morris, J. L., Stein, S., & Warner, J. C. (2009). Urban Drainage Design Manual: Hydraulic Engineering Circular 22 (No. FHWA-NHI-10-009). National Highway Institute (US).

Calappi, T., Miller, C. J., & Carpenter, D. (2010). Revisiting the HEC-18 scour equation. In Scour and erosion (pp. 1102-1109).

Chase, K. J., & Holnbeck, S. R. (2004). Evaluation of pier scour equations for coarse-bed streams (Vol. 4, No. 4). US Department of the Interior, US Geological Survey.

Chedid, M. (2018). New In-situ Erosion Test and Maximum Allowable Scour Depth at Bridge Abutments (Doctoral dissertation).

Chen, H. L., Rao, A. R., Lyn, D. A., & Altschaeffl, A. G. (2000). Evaluation of scour and stream stability by using CAESAR.

Chen, Y.; Tang, F.; Li, Z.; Chen, G.; Tang, Y. (2018) "Bridge scour monitoring using smart rocks based on magnetic field interference". Smart Mater. Struct. 27, 085012.

Conaway, J. S. (2006). Comparison of Long-Term Streambed Scour Monitoring Data with Modeled Values at the Knik River, Alaska. In Proceedings 3rd International Conference on Scour and Erosion (ICSE-3). November 1-3, 2006, Amsterdam, The Netherlands (pp. 145-153).

Conaway, J. S., & Brabets, T. P. (2011). Streamflow and streambed scour in 2010 at bridge 339, Copper River, Alaska (No. 1784-C). US Geological Survey.

De Falco, F., & Mele, R. (2002). The monitoring of bridges for scour by sonar and sedimetri. NDT & E International, 35(2), 117-123.

Fisher, M., Chowdhury, M. N., Khan, A. A., and Atamturktur, S. (2013). "An evaluation of scour measurement devices". Flow Measurement and Instrumentation, 33, 55-67.

Fondriest Environmental. "Monitoring Scour at Bridges and Offshore Structures: a Guide to Understanding and Establishing Scour as a Real-Time Monitoring Solution". Online resource: https://www.fondriest.com/pdf/fondriest_scour_guide.pdf.

Forde, M. C., McCann, D. M., Clark, M. R., Broughton, K. J., Fenning, P. J., & Brown, A. (1999). Radar measurement of bridge scour. Ndt & E International, 32(8), 481-492.

Fosness, R. L., & Schauer, P. V. (2024). Real-time pier scour monitoring and observations at three scour-critical sites in Idaho, water years 2020–22 (No. 2024-5095). US Geological Survey.

Gee, K.W. (2008), "Action: National Bridge Inspection Standards—Scour Evaluations and Plans of Action for Scour Critical Bridges," Federal Highway Administration, Washington, D.C.

Govindasamy, A. V. (2009). "Simplified method for estimating future scour depth at existing bridges." Ph.D. dissertation, Texas A&M Univ., College Station, TX.

Govindasamy, A. V., Briaud, J. L., Kim, D., Olivera, F., Gardoni, P., & Delphia, J. (2010). Observational method for estimating future scour depth at existing bridges. In Scour and Erosion (pp. 41-65).

Govindasamy AV, Briaud J-L, Kim D, Olivera F, Gardoni P, Delphia J. Observation method for estimating future scour depth at existing bridges. J Geotech Geo-environmental Eng ASCE (2013) V. 139(7):1165–75.

Henneberg, M. F. (2018). *Real-time streambed scour monitoring at two bridges over the Gunnison River in western Colorado, 2016–17* (No. 2018-5123). US Geological Survey.

Hong, S. H., Gotvald, A., Sturm, T. W., & Landers, M. (2006). Laboratory and field measurements of bridge contraction scour. In Proceedings 3rd International Conference on Scour and Erosion (ICSE-3). November 1-3, 2006, Amsterdam, The Netherlands (pp. 316-321).

Hopkins, M. S., & Robinson, B. A. (1997). Data Base for Assessment of Streambed Scour and Channel Instability at Selected Bridges in Indiana, 1991-95. US Department of the Interior, US Geological Survey.

Hou, S., Jiao, D., Dong, B., Wang, H., & Wu, G. (2022). Underwater inspection of bridge substructures using sonar and deep convolutional network. Advanced Engineering Informatics, 52, 101545.

Hunt, B. E. (2009). "Monitoring of Scour Critical Bridges." NCHRP Synthesis of Highway Practice 396, Transportation Research Board, Washington, D.C.

Jackson, K. S. (1996). Evaluation of bridge-scour data at selected sites in Ohio (Vol. 97, No. 4182). US Department of the Interior, US Geological Survey.

Jones, J. S., & Richarson, E. V. (2003, April). Physical Modeling of Scour in Bridge Management. In 9th International Bridge Management Conference (p. 277).

Kazemian, A., Yee, T., Oguzmert, M., Amirgholy, M., Yang, J., & Goff, D. (2023). A review of bridge scour monitoring techniques and developments in vibration based scour monitoring for bridge foundations. Advances in Bridge Engineering, 4(1), 2.

Kariyawasam, K. D., Middleton, C. R., Madabhushi, G., Haigh, S. K., & Talbot, J. P. (2020). Assessment of bridge natural frequency as an indicator of scour using centrifuge modelling. Journal of Civil Structural Health Monitoring, 10, 861-881.

Ko YY, Lee WF, Chang WK, Mei HT, Chen CH (2010) Scour Evaluation of Bridge Foundations Using Vibration Measurement. In: Burns SE, Bhatia SK, Avila CMC, Hunt BE (eds) Proceedings 5th International Conference on Scour and Erosion [ICSE-5]. Reston, Va.: American Society of Civil Engineers. S, San Francisco, pp 884–893

Lagasse, P.F., Clopper, P.E., Pagan-Ortiz, J.E., Zeverbergen, L.W., Arneson, L.A., Schall, J.D. and Girard, L.G., 2009. *Bridge Scour and Stream Stability Countermeasures (Vols. 1 and 2)*, Hydraulic Engineering Circular 23. FHWA-NHI-09-111, Federal Highway Administration, US Department of Transportation, Washington, DC.

Landers, M. N., & Mueller, D. S. (1996). Evaluation of selected pier scour equations using field data. Transportation research record, 1523(1), 186-195.

Lee, K. G., & Hedgecock, T. S. (2008). Clear-water contraction scour at selected bridge sites in the Black Prairie Belt of the Coastal Plain in Alabama, 2006 (No. 2007-5260). Geological Survey (US).

Lee, S. O., Sturm, T. W., Gotvald, A., & Landers, M. (2004). Comparison of laboratory and field measurements of bridge pier scour. In Proceedings 2nd International Conference on Scour and Erosion (ICSE-2). November 14.–17., 2004, Singapore.

Lombard, P. J., & Hodgkins, G. A. (2008). Comparison of observed and predicted abutment scour at selected bridges in Maine (No. 42951). Maine. Dept. of Transportation.

Molinas, A. (2004). Bridge scour in nonuniform sediment mixtures and in cohesive materials: synthesis report (No. FHWA-RD-03-083). United States. Federal Highway Administration. Office of Infrastructure Research and Development.

Mueller, D. S., & Wagner, C. R. (2005). Field observations and evaluations of streambed scour at bridges (No. FHWA-RD-03-052). United States. Federal Highway Administration. Office of Research, Development, and Technology.

Mueller, D. S., & Landers, M. N. (1999). Portable instrumentation for real-time measurement of scour at bridges (No. FHWA-RD-99-085). United States. Federal Highway Administration.

National Cooperative Highway Research Program (2004). "Pier and Contraction Scour in Cohesive Soils," NCHRP Report 516, Transportation Research Board, National Academy of Science, Washington, D.C. (Briaud, J.L., H.C. Chen, Y. Li, P. Nurtjahyo, and J. Wang).

National Cooperative Highway Research Program (2009). "Monitoring Scour Critical Bridges, A Synthesis of Highway Practice" NCHRP Synthesis 396, Transportation Research Board, National Academy of Science, Washington, D.C.

National Cooperative Highway Research Program (2011). "Evaluation of Bridge Pier Scour Research: Scour Processes and Prediction," NCHRP Project 24-27(01), Transportation Research Board, National Academy of Science, Washington, D.C. (Ettema, R., Constantinescu, G., and B.W. Melville).

Olimpio, J. R. (2000). Use of a ground-penetrating radar system to detect pre-and post-flood scour at selected bridge sites in New Hampshire, 1996-98 (No. WRI Report 00-4035). US Department of the Interior, US Geological Survey.

Pokharel, S. (2017). Evaluating and Understanding of Bridge Scour Calculation. (Doctoral dissertation), Auburn University

Prendergast, L. J., and Gavin, K. (2014). "A Review of Bridge Scour Monitoring Techniques." Journal of Rock Mechanics and Geotechnical Engineering 6, February. Pp. 138-149, Institute of Rock and Soil Mechanics, Chinese Academy of Sciences.

Richardson, E. V., & Davis, S. R. (2003). Evaluating scour at bridges (No. FHWA-NHI-01-001). United States. Federal Highway Administration. Office of Bridge Technology.

Robinson, B. A., & Thompson Jr, R. E. (1995). An observed-streambed-scour index for selected bridges in southwestern Indiana, 1991. Water-Resources Investigations Report, 95, 4264.

Saha, R. (2017). Prediction of Maximum Scour Depth Using Scaled Down Bridge Model in a Laboratory. West Virginia University.

San Martin, C., Rifo, C., Guerra, M., Ettmer, B., & Link, O. (2023). Monitoring scour at bridge piers in rivers with supercritical flows. Hydrology, 10(7), 147.

Schambeau, M. (2012). Stability of Timber Bridges Subject to Scour (Doctoral dissertation).

Schuring, J. R., Dresnack, R., & Golub, E. (2017). Design and Evaluation of Scour for Bridges using HEC-18.

Schuring, J. R., Dresnack, R., Golub, E., Khan, M. A., Young, M. R., Dunne, R., & Aboobaker, N. (2010). Review of bridge scour practice in the US. In Scour and Erosion (pp. 1110-1119).

Shahriar, A. R., Ortiz, A. C., Montoya, B. M., & Gabr, M. A. (2021). Bridge Pier Scour: An overview of factors affecting the phenomenon and comparative evaluation of selected models. Transportation Geotechnics, 28, 100549

Shen, J., Forsyth, R., & Kilgore, R. (2018). Underwater Inspection of Bridge Substructures Using Imaging Technology (No. FHWA-HIF-18-049). Federal Highway Administration (US).

Sheppard, D. M., Melville, B., & Demir, H. (2014). Evaluation of existing equations for local scour at bridge piers. Journal of Hydraulic Engineering, 140(1), 14-23.

Sreedhara, B. M., & Manu, P. U. (2015). Comparative study on different bridge scour monitoring techniques: a review. In HYDRO 2015 International Conference, DOI (Vol. 10).

Shinoda M, Haya H, Murata S (2008). Nondestructive evaluation of railway bridge substructures by percussion test. In: Fourth international conference on scour and Erosion. The Japanese Geotechnical Society, Tokyo

South Carolina Department of Transportation (SCDOT) (2024) "Bridge Scour, South Carolina". https://sc.water.usgs.gov/bridgescour/index.php

Straub, T. D., & Over, T. M. (2010). Pier and contraction scour prediction in cohesive soils at selected bridges in Illinois.

Straub, T. D., Over, T. M., & Domanski, M. M. (2013). Ultimate Pier and Contraction Scour Prediction in Cohesive Soils at Selected Bridges in Illinois.

Tola, S., Tinoco, J., Matos, J. C., & Obrien, E. (2023). Scour detection with monitoring methods and machine learning algorithms—a critical review. Applied Sciences, 13(3), 1661.

Topczewski, Ł., Cieśla, J., Mikołajewski, P., Adamski, P., & Markowski, Z. (2016). Monitoring of scour around bridge piers and abutments. Transportation Research Procedia, 14, 3963-3971.

Vasconcelos, J. G., Fang, X., Anderson, J. B., Tamang, S., & Song, W. (2018). Analysis and Potential Solutions to Sediment Deposition in Dean Road Bridge Watershed, Midland City, AL (No. ALDOT 930-925-1). Auburn University. Highway Research Center.

Walker, M. (2013). Scour potential of cohesive soils (M.Sc. dissertation).

Walker, J. F., & Hughes, P. E. (2005). Bridge scour monitoring methods at three sites in Wisconsin. US Geological Survey.

Wilson Jr, K. V. (1995). Scour at selected bridge sites in Mississippi (No. 94-4241). US Geological Survey; Earth Science Information Center, Open-File Reports Section [distributor]

Wang, Jun. "The SRICOS -EFA Method for Complex Pier and Contraction Scour." Order No. 3132140 Texas A&M University, 2004. Ann Arbor: ProQuest. Web. 23 Jan. 2022.

Webb, D. J., Anderson, N. L., Newton, T., & Cardimona, S. (2000). Bridge scour: Application of ground penetrating radar. In Proceedings of the First International Conference on the Application of Geophysical Methodologies and NDT to Transportation Facilities and Infrastructure. Federal Highway Commission and Missouri Department of Transportation.

Wright, W. (2014). Laboratory Scour Testing of Hard Cohesive Soils in Alabama (M.Sc. dissertation).

Yao C, Darby C, Yu O-Y, Hurlebaus S, Chang K-A, Price J, Hunt B, Briaud J-L (2010). Motion sensors for scour monitoring: laboratory experiment with a shallow foundation. GeoFlorida 2010: Advances in analysis, Modeling & Design. GeoFlorida, West Palm Beach

Yorozuya, A., & Ettema, R. (2015). Three abutment scour conditions at bridge waterways. Journal of Hydraulic Engineering, 141(12), 04015028.

Zhang, G., Hsu, S. A., Guo, T., Zhao, X., Augustine, A. D., & Zhang, L. (2013). Evaluation of design methods to determine scour depths for bridge structures (No. FHWA/LA. 11/491). Louisiana. Dept. of Transportation and Development.

Zhang, H.; Li, Z.; Reven, A.; Scharfenberg, B.; Chen, G.; Ou, J. (2019) UAV-Based Smart Rock Positioning for Determination of Bridge Scour Depth. In Proceedings of the 9th International Conference on Structural Health Monitoring of Intelligent Infrastructure (SHMII-9), St. Louis, MO, USA, 4–7 August 2019.

Zheng, S., Xu, Y. J., Cheng, H., Wang, B., & Lu, X. (2018). Assessment of bridge scour in the lower, middle, and upper Yangtze River estuary with riverbed sonar profiling techniques. Environmental monitoring and assessment, 190, 1-13.

Appendix A – Programming Code

The programming was done in CRBasic. This language is a proprietary programming language used for Campbell Scientific data loggers. It is a structured, BASIC-like language designed for environmental monitoring, geotechnical instrumentation, and other data acquisition applications.

CRBasic is similar to traditional BASIC but incorporates structured programming concepts. It supports variables, loops, conditional statements, and functions, allowing users to create efficient and readable programs. The language is optimized for working with sensor measurements, data storage, and control logic, making it particularly useful for applications that require real-time data acquisition and processing.

Programs written in CRBasic are created using the CRBasic Editor, which is part of Campbell Scientific's LoggerNet or PC400 software. These programs operate in a continuous scan loop, meaning they continually collect, process, and store data according to the programmed logic. This execution method ensures that environmental data is logged at precise intervals, allowing for accurate long-term monitoring.

Structurally, every programming code in this language follows the same logic:

- Declare the variables that will be used
- Declare the Data Tables that will contain the data measured
- Write the main program

This appendix describes the programming code used in this research. For better understanding, read the code line by line, including the comments (marked by apostrophe sign). Some parameters must change depending on the sensor being used.

```
'----------------------------------------
'Program author: Murilo Tarozzo/J. Brian Anderson

'Wiring details for a Campbell Scientific CR6 Datalogger

'Wiring for AV SENSOR (TTL or RS-232 communication protocol)
'Black - Ground
'Red - +12V DC or  SW12_2
'White - connected to U4 (ComU3) -> Serial Output (Velocity/Temp)
'Green - connected to U1 -> Analog Output (Depth - Requires Coefficient/Offset For measurement)

'Wiring for AIRMAR / DEPTH SENSOR (RS485 full duplex)
'Black/White - Ground
'Blue/White - Voltage SW12-1 or 12V
'Orange - NMEA_A [NMEA_out(A)+ or Tx+] -- to C3 (Rx-)
'Brown - NMEA_B [NMEA_out(B)- or Tx-] -- to C4 (Rx+)
'White - NMEA_INA [NMEA_in(A)+ or Rx+] -- to C1 (Tx-)
'Violet - NMEA_INB [NMEA_in(B)- or Rx-] -- to C2 (Tx+)
'Blue - RS485_A [Non functional]
'Black - RS485_B [Non functional]
```

```
'Wiring for SDI12 (For battery measurements, if desired)
'(requires an SDI12 interface cable for the CH200 charging regulator)
'Green - U5
'Black - Ground
'Transparent - to the same ground as black wire

'Wiring for solar panel (connected to the CH200 charging regulator)
'Black - ground
'Red - solar

'Wiring for Clarivue10 (turbidity sensor)
'Red -> power, SW12-1, SW12-2 or 12V (must share the same port as one the other sensors).
'Black -> G
'Clear -> same G as black wire
'White -> U11

'Calibration instructions
'AV sensor must be calibrated for water level (parameters offset and ceof) in a barrel or bucket.
And for velocity (parameters k and offsetvel) in a flume. See manual.
'AIRMAR should be verified/calibrated for the depth below transducer (parameters coefairmar
and offsetairmar) in a barrel. See Manual.

'--------------------------------------------------------------------------
'Declare Public Variables Velocity sensor
Public Sentence As String * 100, 'Sentence will be the string where the AV sensor digital data will
be stored in
Dim NBReturned 'Auxiliary variable for storing number of bytes in serialinRecord command
Dim Array(2)'An array with 2 spots. First spot will store velocity and second spot will store
temperature
Public Level_mV
Public Level_mm
Public Level_m
Public offset=-1773 'CAlibration factor for AV sensor water level. Goshen = -2653; Enterprise =
-1345; Tuskegee I85 = +298.05 ; Demopolis = -1773
Public Coef=2495 'CAlibration factor for AV sensor water level. Goshen = 2841; Enterprise =
2537; Tuskegee I85 = 2853.8; Demopolis = 2495
Public k=1 'CAlibration factor for AV sensor velocity. Normally, k~1
Public offsetvel=0 'CAlibration factor for AV sensor velocity. Normally,offsetvel~0
Public Velocity_mm
Public Velocity_m
Public Water_TempC
Alias Array(1)= Raw_Velocity 'An array with 2 spots was declared: Array (2). The first spot will
be called Raw_velocity
Alias Array(2) = Raw_Temp 'An array with 2 spots was declared: Array (2). The second spot will
be called Raw_Temp
```

```
'Declare Public Variables Airmar sensor
Public RawString As String * 100 'RawString will be the string where the AIRAMR sensor digital data will be stored in
Dim SplitResult(6)
Alias SplitResult(2)= rawdepth_m
Alias SplitResult(3)= Offset_m
Alias SplitResult(5) = Temp_C
Public Depth_m
Public coefairmar = 1 'CAlibration factor for Airmar sensor depth below transducer. Normally, it's 1.
Public offsetairmar = 0 'CAlibration factor for Airmar sensor depth below transducer. Normally, it's 1.
Public Stringrange As String * 100 'string for setting airmar range
Public Stringsetping As String * 100 'string for setting airmar ping rate
Public Stringpulsespp As String * 100 'string for setting airmar pulses per ping

'DEclare Public variables for Clarivue10
Public ClariVUE6(7)
Alias ClariVUE6(1)=CV_Med_Turb6
Alias ClariVUE6(2)=CV_Mean_Turb6
Alias ClariVUE6(3)=CV_SD_Turb6
Alias ClariVUE6(4)=CV_Min_Turb6
Alias ClariVUE6(5)=CV_Max_Turb6
Alias ClariVUE6(6)=CV_Mean_Temp6
Alias ClariVUE6(7)=CV_Err_Code6
Units CV_Med_Turb6=FNU
Units CV_Mean_Turb6=FNU
Units CV_SD_Turb6=FNU
Units CV_Min_Turb6=FNU
Units CV_Max_Turb6=FNU
Units CV_Mean_Temp6=deg C
Units CV_Err_Code6=code

'Define Data Table Velocity sensor
DataTable (VelocitySensor,True,-1)
  DataInterval (0,1,sec,10) 'It will store the scanned data, every 1 second of the subscan.
  CardOut(0,1000000)'If you're using a SD card to increase datalogger capacity and store data, this command must be included! Otherwise, hide it as a comment.
  Sample (1,Level_m,IEEE4)
  Sample (1,Sentence,String)
  Sample (1,Array(1),IEEE4)
  Sample (1,Array(2),IEEE4)
  Sample (1,Velocity_m,IEEE4)
  Sample (1,Water_TempC,IEEE4)
EndTable
```

```
'Define Data Table Depth sensor
DataTable (DepthSensor,True,-1)
  DataInterval (0,1,sec,10) 'It will store the scanned data, every 1 second of the subscan.
  CardOut(0,1000000)'If you're using a SD card to increase datalogger capacity and store data, this command must be included! Otherwise, hide it as a comment.
  Sample (1,RawString,String)
  Sample (1,SplitResult(2),IEEE4)
  Sample (1,SplitResult(3),IEEE4)
  Sample (1,SplitResult(5),IEEE4)
  Sample (1,Depth_m,IEEE4)
EndTable

'Define Data Tables for clarivue sensors
DataTable(Sensor6,True,-1)
DataInterval(0,1,Sec,10) 'It will store the scanned data, every 1 second of the subscan.
  CardOut(0,1000000)'If you're using a SD card to increase datalogger capacity and store data, this command must be included! Otherwise, hide it as a comment.
    Sample(1,CV_Med_Turb6,FP2)
  Sample(1,CV_Mean_Turb6,FP2)
  Sample(1,CV_SD_Turb6,FP2)
  Sample(1,CV_Min_Turb6,FP2)
  Sample(1,CV_Max_Turb6,FP2)
  Sample(1,CV_Mean_Temp6,FP2)
  Sample(1,CV_Err_Code6,FP2)
EndTable

'Main Program ----- for AV sensor, AIRMAR sensor, and Clarivue
BeginProg

Scan (15,min,0,0)'Datalogger program will scan every 15 minutes
  SW12 (SW12_1,1) 'Turn on 12V power to Airmar sensor
  SW12 (SW12_2,1) 'Turn on 12V power to AV sensor and Clarivue10
  SerialOpen (ComC1,4800,0,0,1000,5) 'For airmar sensor: Set up communication with port ComC1, but using in a RS485/RS422 full duplex configuration. This means that all 4 C ports must be used. See wiring diagram above.
  SerialOpen (COMU3,4800,0,0,1000) 'For AV sensor: open U3/U4 port. If AV sensor is TTL, the third parameter (format) must be 0. If AV sensor is RS232, the third parameter (format) must be 16.

      Stringrange ="$PAMTC,OPTION,SET,RANGE,0*65" + CHR(13) + CHR(10) 'Assigning an AIRMAR proprietary command to a string. Setting the range to Short
      SerialOut(ComC1,Stringrange, "", 0, 0 ) 'send the stringrange string to the AIRMAR sensor

      Stringsetping = "$PAMTC,OPTION,SET,PINGSPS,1,1,1,1*66" + CHR(13) + CHR(10) 'Assigning an AIRMAR proprietary command to a string. Setting ping rate to: SHort 1, Medium 1, Long 1, very long 1
```

```
        SerialOut(ComC1,Stringsetping, "", 0, 0 ) 'send the stringrange string to the AIRMAR sensor

        Stringpulsespp = "$PAMTC,OPTION,SET,PULSESPP,2,2,2,2*2A" + CHR(13) + CHR(10) 'Assigning an AIRMAR proprietary command to a string. Setting pulses per ping to: SHort 2, Medium 2, Long 2, very long 2
        SerialOut(ComC1,Stringpulsespp, "", 0, 0 ) 'send the stringrange string to the AIRMAR sensor

  SubScan(1,sec,20)'when each scan runs, it will run a subscan every second for 20 seconds.
'------------------------------VELOCITY SENSOR-------------------------------------------------------
    VoltDiff (Level_mV,1,mV5000,U1,0,0,60,1.0,0) 'measure the voltage and store it in level_mV variable
    Level_mm = ((Level_mV / 1000) * Coef) + offset   'Convert Level_mV to Level in mm
    Level_m = Level_mm / 1000                        'Convert level from mm to m

    SerialInRecord (COMU3,Sentence,&H0A,0,&H0D,NBReturned,01) 'Read the incoming data in U3 port (ComU3) and Store in string Sentence.
    SplitStr (Array(),Sentence,CHR(09),2,5)

    If Raw_Velocity <> "NAN" Then
       Velocity_mm = (Raw_Velocity * k) + offsetvel
    EndIf

      Velocity_m = Velocity_mm / 1000 'Convert Velocity to m/s

    If Raw_Temp <> "NAN" Then
       Water_TempC = Raw_Temp / 100 'Convert temperature to Celsius
    EndIf

'------------------------------AIRMAR SENSOR---------------------------------------------------------
    SerialInBlock(ComC1,RawString,10000) 'Store the incoming serial data from AIRMAR and store it into the string RawString
    SplitStr (SplitResult(),RawString,CHR(44),6,5) 'Split sentence

    Depth_m = (rawdepth_m * coefairmar) + offsetairmar

'------------------------------CLARIVUE10 SENSOR ----------------------------------------
    SDI12Recorder(ClariVUE6(),U11,"0","C!",1,0,-1) 'Clarivue10 sensor, named sensor 6

'--------------------Now we simply call the OUTPUT tables

    CallTable VelocitySensor
    CallTable DepthSensor
    CallTable Sensor6
  Next SubScan
```

```
  SW12 (SW12_1,0) 'Turn off 12V power to Airmar sensor
  SW12 (SW12_2,0) 'Turn off 12V power to AV sensor and CLarivue
NextScan
EndProg
```

Appendix B – Data Collected from the Bridges

The entirety of data collected from each bridge is extensive and not suitable for plotting in multiple graphs in this report. The best is to visualize the data directly in spreadsheets. Therefore, all data is saved in spreadsheets in the following weblinks:

- Bridge over Blue Creek, on Meriwether Trail, (BIN 010738) near Lapine, Montgomery County, AL

Data can be accessed in the following weblink:
https://auburn.box.com/s/tp35caqo318mxi88u2mexky51daqlswp

- Bridge over Little Double Bridges Creek on County Road 606 near Enterprise, Coffee Co. (BIN 015002)

Data can be accessed in the following weblink:
https://auburn.box.com/s/9y3e85u9e6f0gphwizwp5ntxbkuv9m8l

- Bridge over Conecuh River, on County Road 2243, near Goshen, Pike Co. (BIN 013310)

Data can be accessed in the following weblink:
https://auburn.box.com/s/7yf7fzul1xfg0hfojkcad2rg111u2xnw

- Bridge over French Creek, on Arcola St, near Demopolis, Marengo Co. (BIN 007070)

Data can be accessed in the following weblink:
https://auburn.box.com/s/7jecegwnq7cdchn1kkltcgkik63iau0o

- Bridge over Chewacla Creek, on I85 Northbound Lane, near Tuskegee, Macon Co. (BIN 008598)

Data can be accessed in the following weblink:
https://auburn.box.com/s/j8pcwnqbxcxmgx9vgdpand9olebuym83

Appendix C – Turbidity Tests

Turbidity tests were conducted in the laboratory to understand how the EchoRange sensor performs under varying turbidity conditions.

The laboratory tests were conducted using a previous version of the Campbell Scientific Clarivue 10 sensor, designated as OBS3+. The manufacturer has discontinued this version. As a result, Clarivue10 sensors were purchased for field deployment.

OBS3+ measures turbidity in NTU (Nephelometric Turbidity Units), and Clarivue10 measures turbidity in FNU (Formazin Nephelometric Units). There is no reliable relationship between NTU and FNU, but the laboratory tests also included a test to determine a relationship between the OBS3+ and Clarivue10 sensors purchased by the research team. Figure C1 shows this relationship.

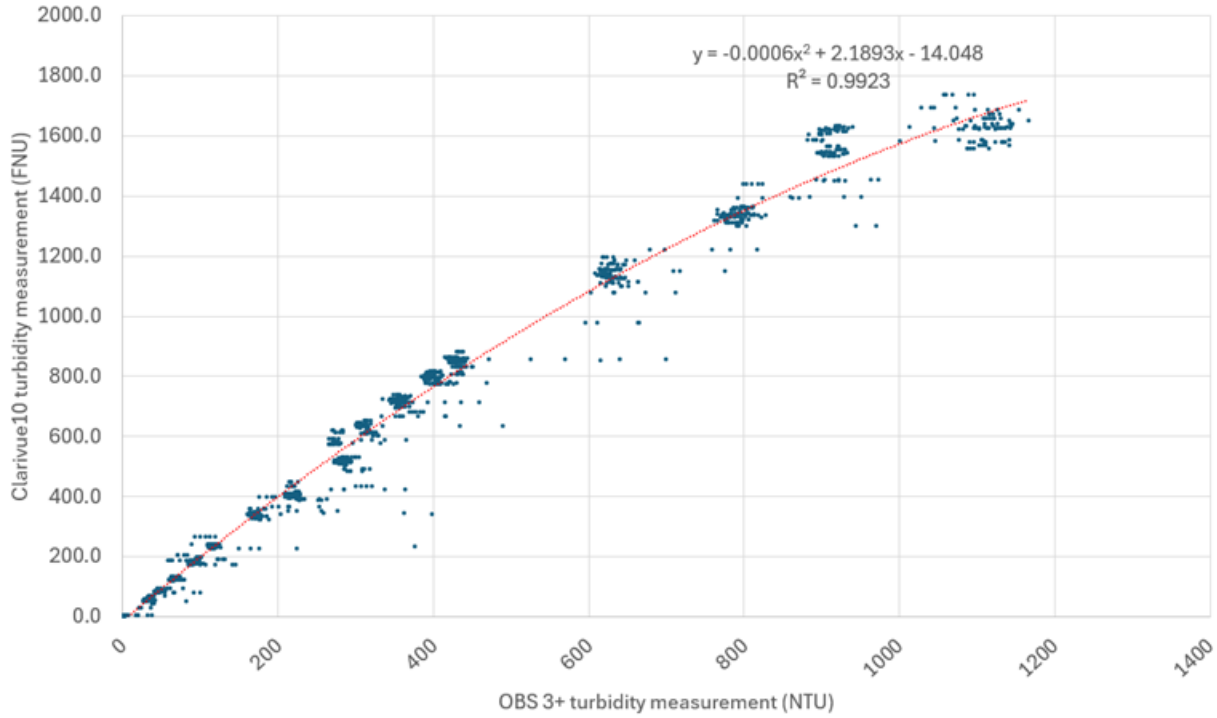

Figure C1. Relationship between turbidity measurements by Campbell Scientific sensors OBS3+ (NTU) and Clarivue10 (FNU).

The turbidity tests were conducted either in a 7-gallon bucket or in a 55-gallon barrel, as seen in Figure C2.

Figure C2. Turbidity tests were conducted in a 7-gallon bucket and a 55-gallon barrel.

The tests were conducted by applying a layer of sand 3 to 6 inches thick to the bottom of the container. The container walls were lined with layers of textured rubber. These were done to simulate the streambed conditions and to minimize reverberation in the EchoRange readings. A small aquarium pump was used to simulate the water flow.

The EchoRange underwent several programming modifications to enhance sensor accuracy in turbid and shallow environments. Soil was added in different amounts and frequencies to observe its impact on turbidity and sonar readings.

The test results were analyzed by comparing turbidity measurements to the "noise-to-signal ratio." This ratio is simply the amount of noise measured divided by true value measurements in any 1-minute time interval of the test.

A few different types of tests were conducted:

- "Quick" tests: A certain amount of soil was added to the container at given time intervals (10g of soil added every 10 minutes, or 50 g of soil added every 5 minutes).
- "Long" tests: A specified amount of soil was added daily for 3 consecutive days. The water pump was periodically turned on and off to observe any changes in measurements (50g/day, 200g/day, 500g/day, 1500g/day,

Examples of the tests are shown in the figures below.

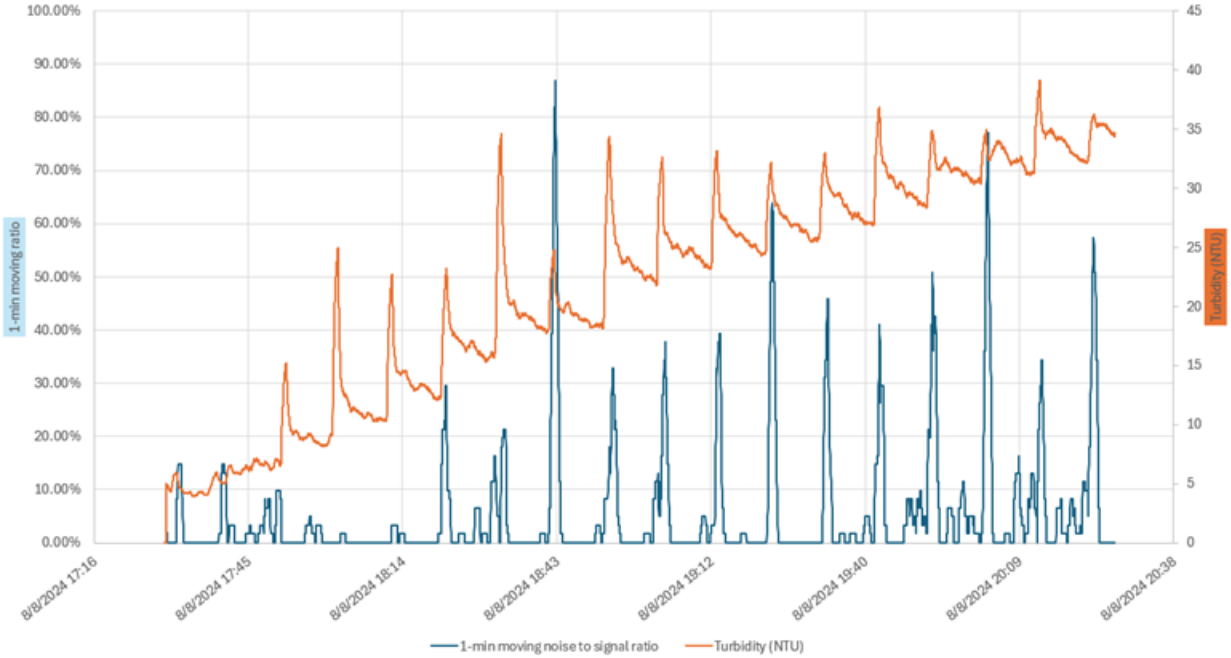

Figure C3. Turbidity test #26 (10g every 10 min). Sonar at ~50 cm height. Noise/signal ratio = 5%.

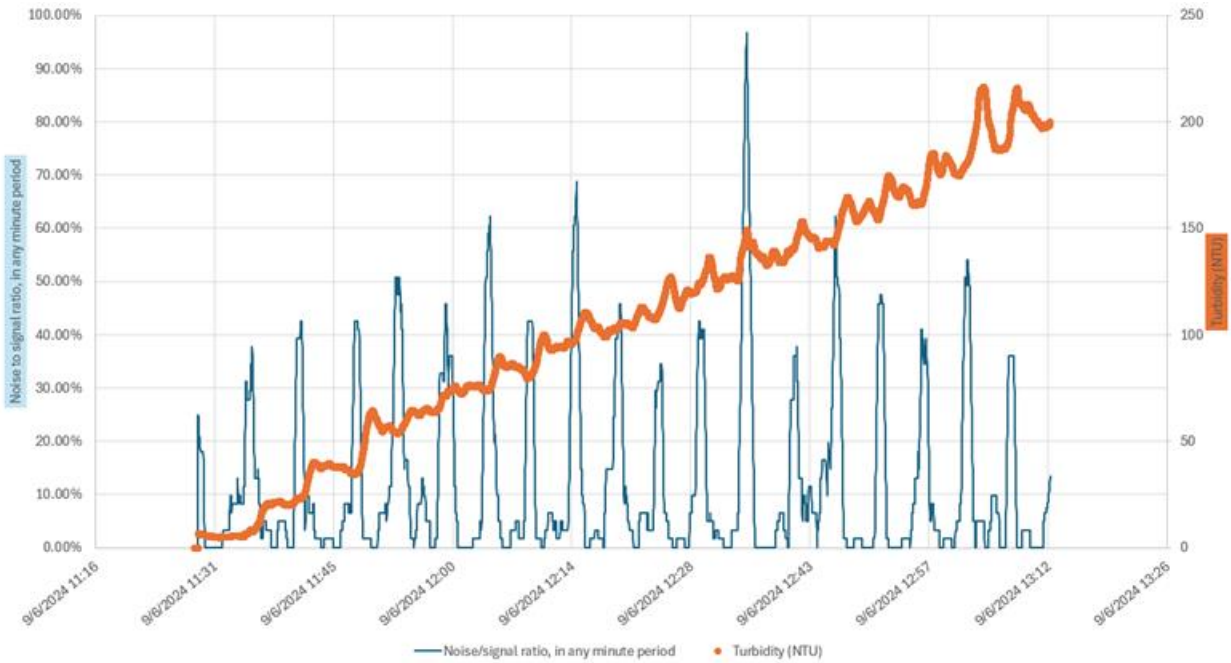

Figure C4. Turbidity test #29 (50g every 5 min). Sonar at ~60 cm height. Noise/signal ratio = 12%.

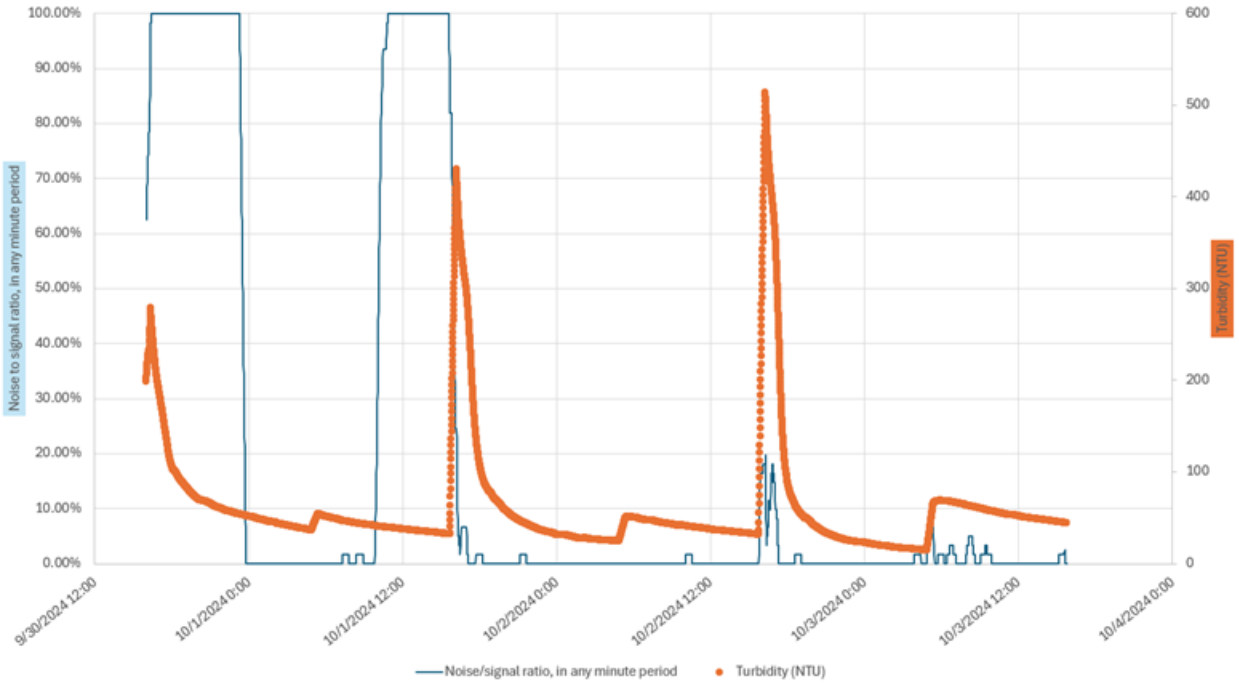

Figure C5. Turbidity test #34 (1500g/day). Sonar at ~60 cm height. Noise/signal ratio = 19%.

A few observations can be made:

- The periodic addition of small amounts (10g) of soil does have some influence on noise measurements. However, greater amounts of soil (50g) in shorter periods result in increased noise measurements.
- Lower amounts of soil addition resulted in a turbidity of approximately 35 to 40 NTU (or 55 to 65 FNU) at the end of the test. Greater amounts of soil addition resulted in higher turbidity, reaching around 200 NTU (or 320 FNU).
- In longer tests, the amount of noise was consistently greater on the first day, when the clear water received its first batch of 1,500 g of soil.
- In all tests, the greater amount of noise occurred when turbidity experienced a sudden spike (due to the addition of soil). As turbidity decreased and the coarser particles were washed away or settled, noise readings became less frequent.
- In long tests, especially when the soil amount was high, the simple act of turning on the water pump and agitating the finer particles still in suspension was enough to suddenly increase turbidity and, therefore, increase noise measurements. However, as time passed and the turbidity spike decreased, so did noise measurements.

From these tests, it was concluded that the EchoRange does suffer from increased turbidity. However, data trends can still be observed among the noise. Therefore, a proper filtering method may be enough to filter out the noise measurements in post-processing and observe the real data.

Many turbidity tests were conducted, and they can be accessed in the following weblink: https://auburn.box.com/s/bo7jv4wdyemdgeyzg49yg1mi5g06xr2p

Appendix D – Power Budgeting

The figure below shows the monitoring of power consumption. Battery voltage and charging voltage were measured over 3 months in 2023. It is possible to clearly distinguish the daytime periods (solar charging) and nighttime periods (no charge).

Based on the data, it is clear that, even with long periods of no charging, the battery's voltage never dropped below 12.6 V, which is approximately 90% of its capacity.

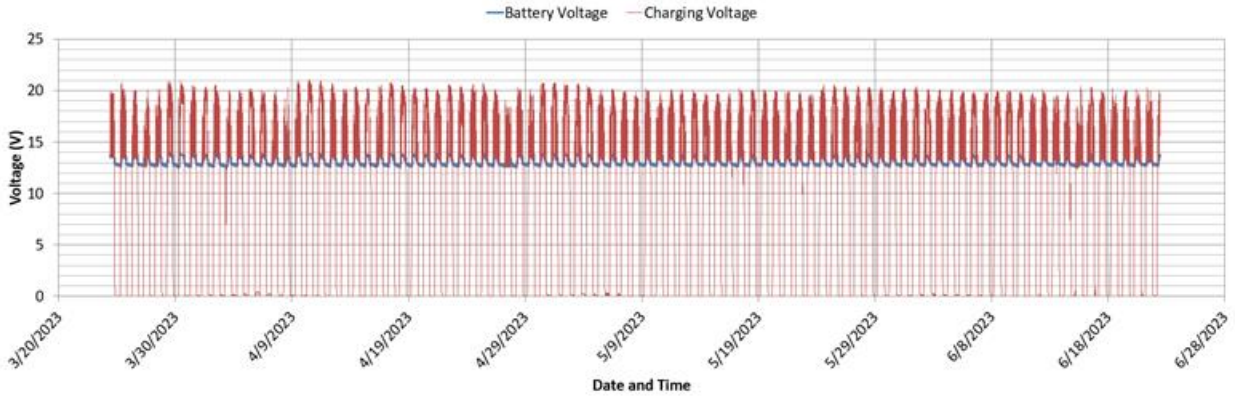

Figure D1. BIN 013310, Goshen, AL. Monitoring of power consumption.

Appendix E – Manuals

This appendix contains a weblink providing access to several manuals aiding in the understanding and operations of the several sensors and equipment used in this research:

- AIRMAR EchoRange (Sonar)
- BlueSiren AV sensor
- Campbell Scientific CH200 charging regulator
- Campbell Scientific CR6 Datalogger
- Campbell Scientific Clarivue10 Turbidity sensor

All manuals can be accessed in the following weblink:
https://auburn.box.com/s/z3bwvh0ws0qrbl1sxlerezv02kgcpxq3

Appendix F – Supporting material for Scour Calculations

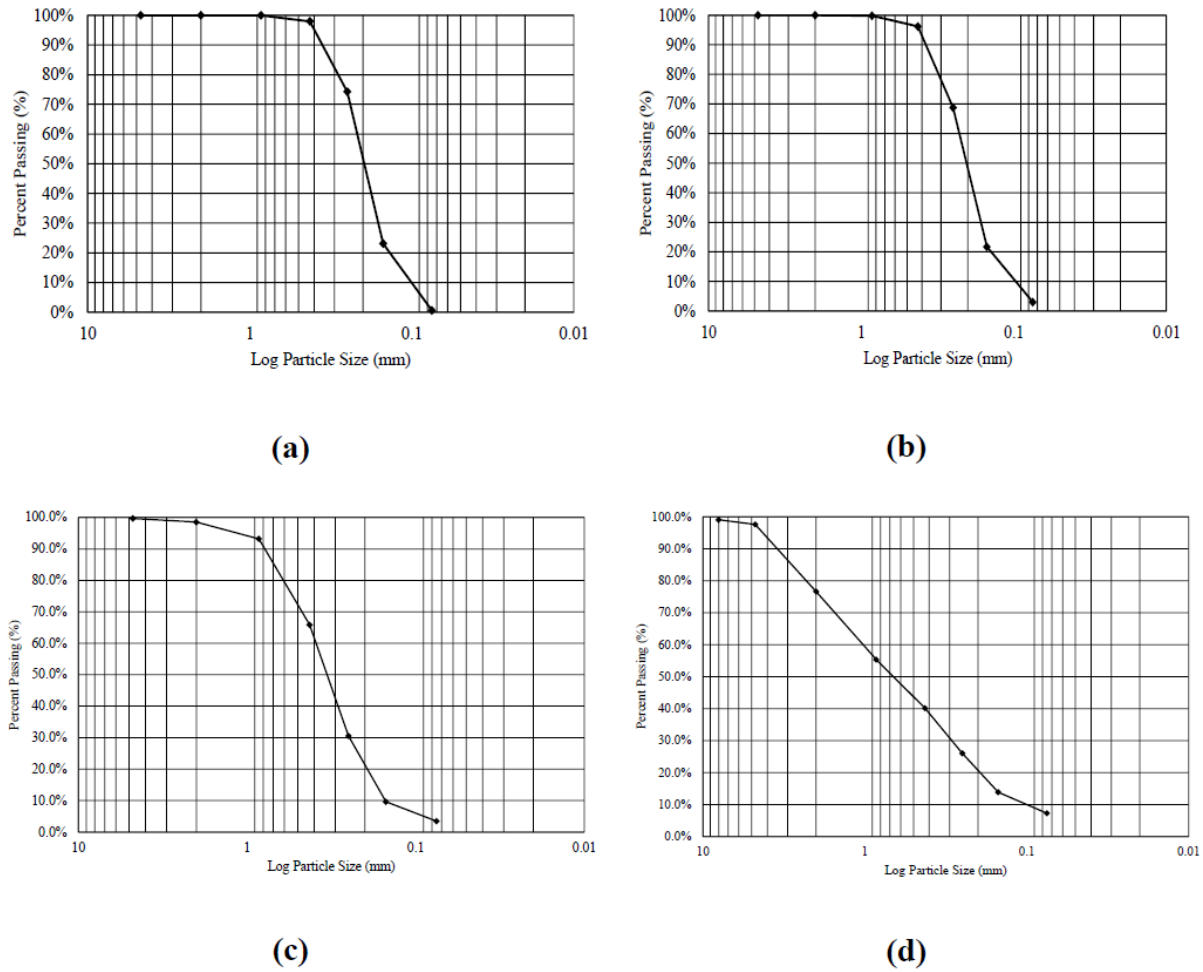

Figure F1. Particle site distribution for the analyzed bridges (a) BIN 015002, (b) BIN 010738, (c) BIN 013310, (d) BIN 007070

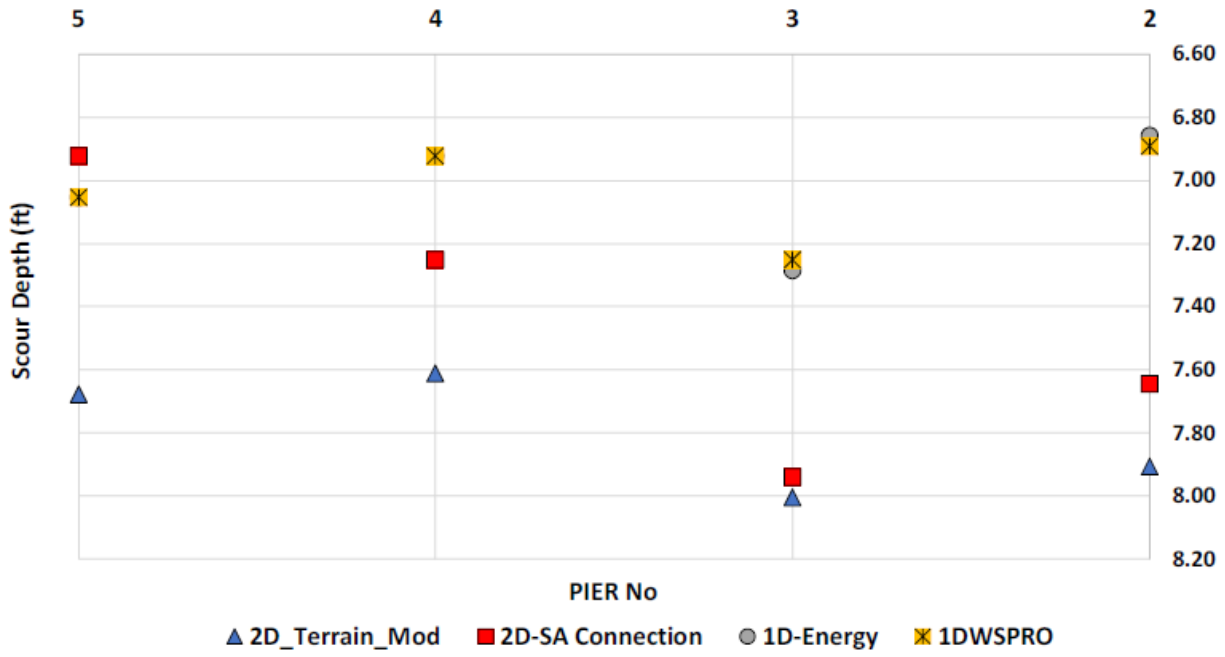

Figure F2. Scour results for BIN 015002 using HEC-18. Different Bridge modeling approaches. Peak Flow RRE

Table F1. Scour values for BIN 015002 using HEC-18. Different Bridge modeling approaches. Peak Flow RRE

PIER BrM	1D- WSPRO	1D- Energy	2D- SA Connection	2D_Terrain_Mod
2	6.9 ft	6.9 ft	7.6 ft	7.9 ft
3	7.3 ft	7.3 ft	7.9 ft	8.0 ft
4	6.9 ft	6.9 ft	7.3 ft	7.6 ft
5	7.1 ft	7.1 ft	6.9 ft	7.7 ft

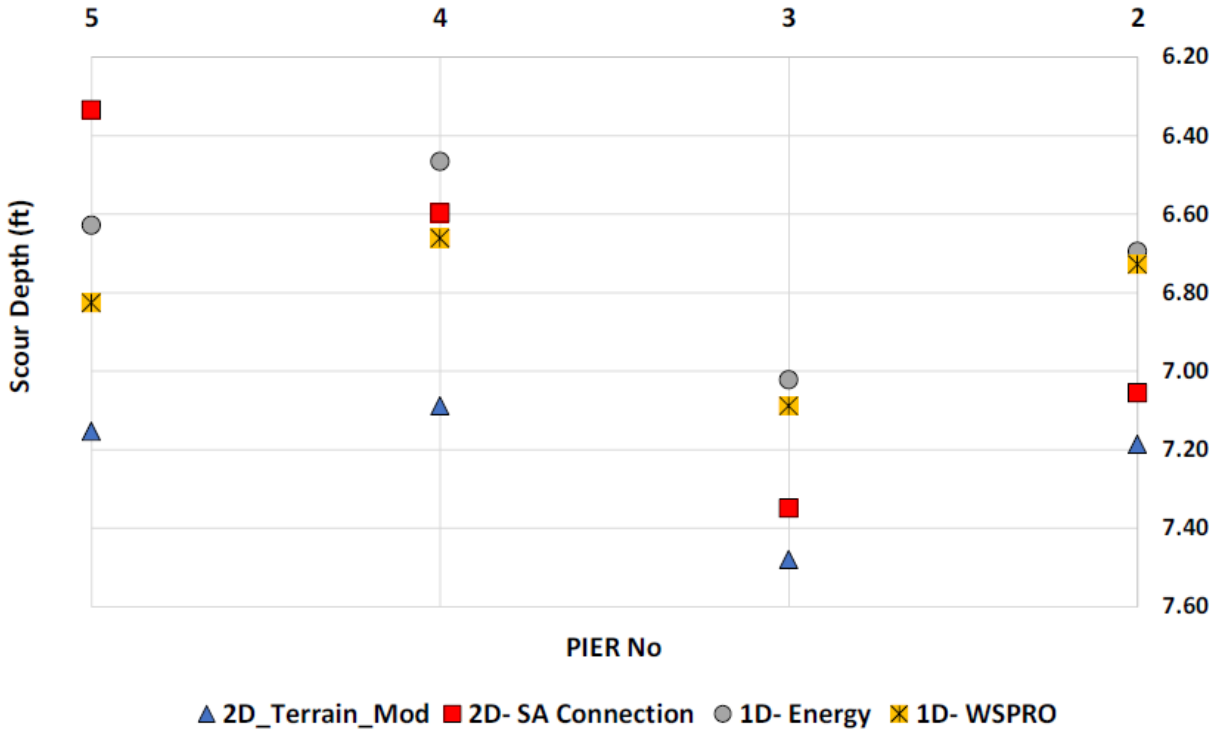

Figure F3. Scour results for BIN 015002 using HEC-18. Different Bridge modeling approaches. Peak Flow CNII

Table F2. Scour values for BIN 015002 using HEC-18. Different Bridge modeling approaches. Peak Flow CNII

PIER BrM	1D- WSPRO	1D- Energy	2D- SA Connection	2D_Terrain_Mod
2	6.7 ft	6.7 ft	7.1 ft	7.2 ft
3	7.1 ft	7.0 ft	7.3 ft	7.5 ft
4	6.7 ft	6.5 ft	6.6 ft	7.1 ft
5	6.8 ft	6.6 ft	6.3 ft	7.2 ft

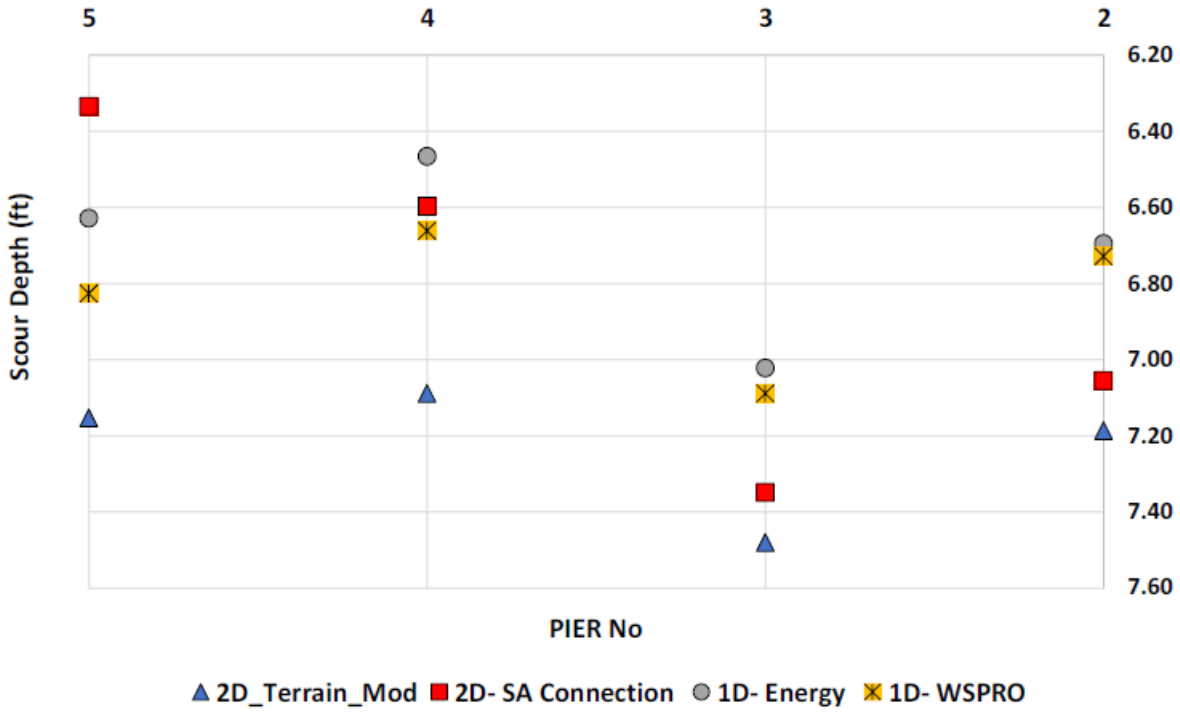

Figure F4. Scour results for BIN 015002 using HEC-18. Different Bridge modeling approaches. Peak Flow CNIII

Table F3. Scour values for BIN 015002 using HEC-18. Different Bridge modeling approaches. Peak Flow CNIII

PIER BrM	2D_Terrain_Mod	2D- SA Connection	1D- Energy	1D- WSPRO
2	8.3 ft	7.9 ft	7.6 ft	7.6 ft
3	8.5 ft	8.2 ft	7.8 ft	7.8 ft
4	8.1 ft	7.5 ft	7.5 ft	7.5 ft
5	8.1 ft	7.2 ft	7.6 ft	7.7 ft

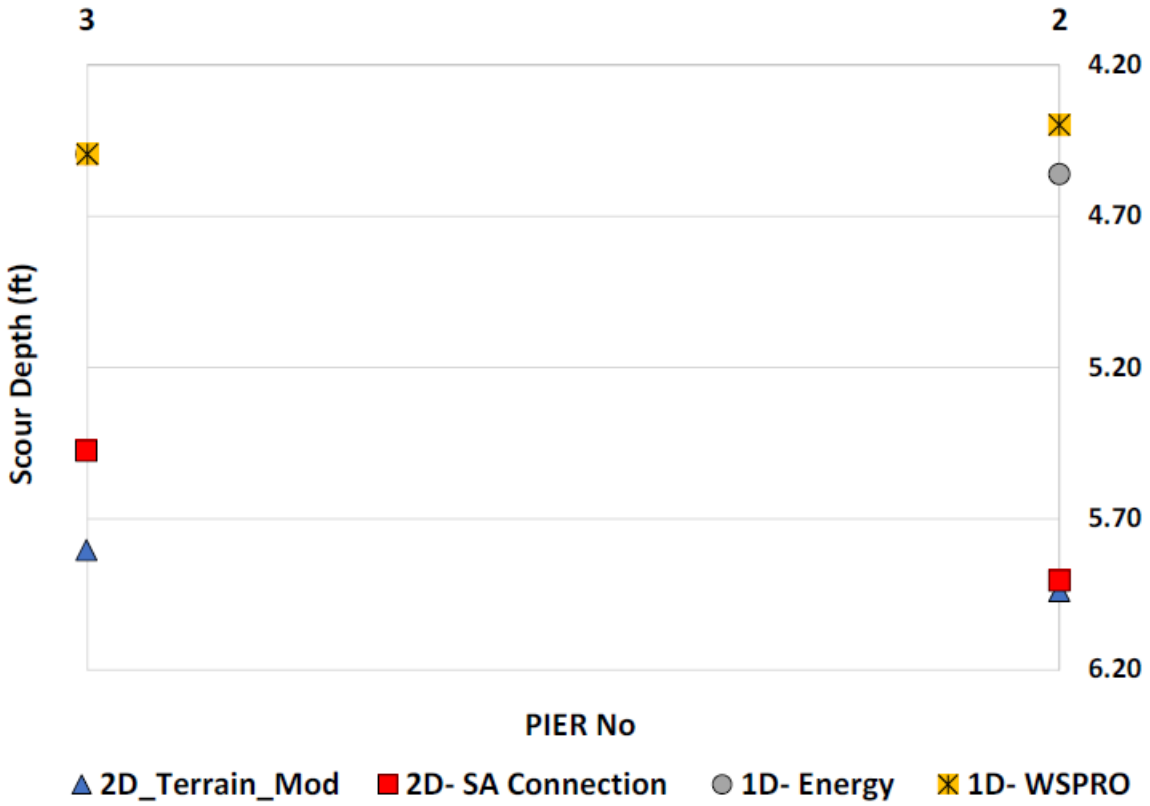

Figure F5. Scour results for BIN 010738 using HEC-18. Different Bridge modeling approaches. Peak Flow RRE

Table F4. Scour values for BIN 010738 using HEC-18. Different Bridge modeling approaches. Peak Flow RRE

Pier BrM	1D- WSPRO	1D- Energy	2D- SA Connection	2D_Terrain_Mod
2	4.4 ft	4.6 ft	5.9 ft	5.9 ft
3	4.5 ft	4.5 ft	5.5 ft	5.8 ft

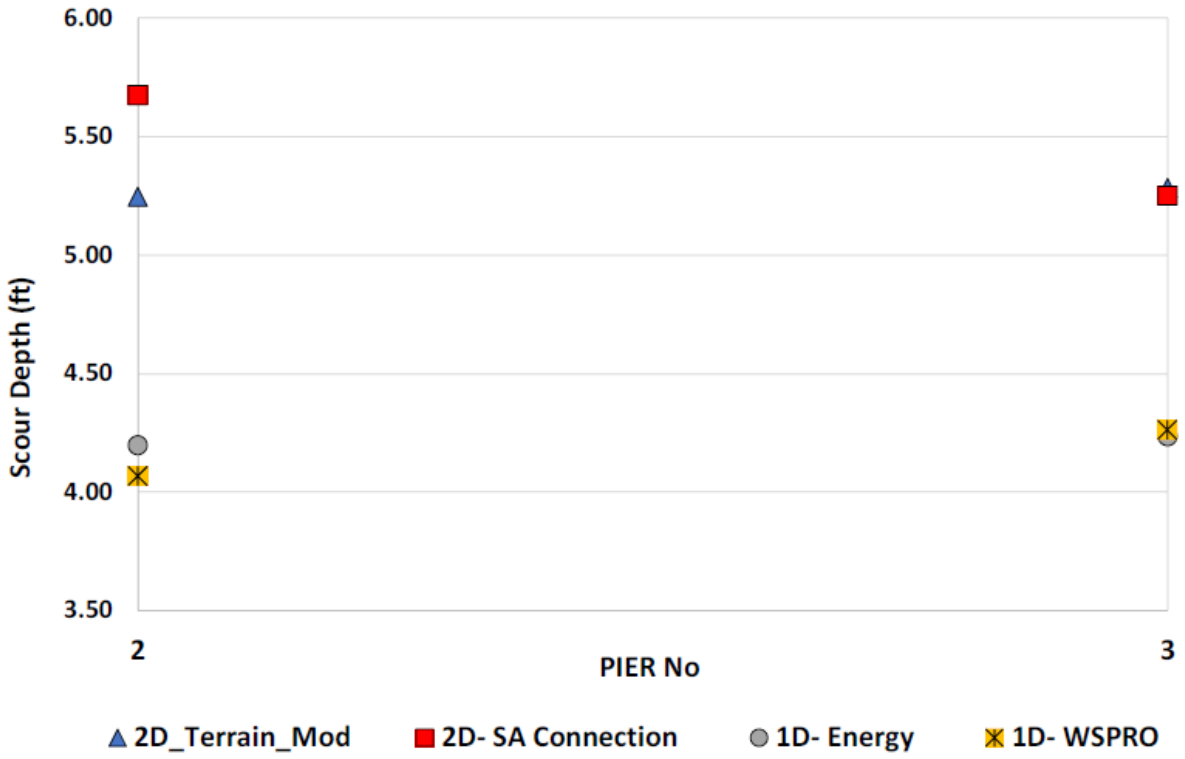

Figure F6. Scour results for BIN 010738 using HEC-18. Different Bridge modeling approaches. Peak Flow CNII

Table F5. Scour values for BIN 010738 using HEC-18. Different Bridge modeling approaches. Peak Flow CNII

Pier BrM	1D- WSPRO	1D- Energy	2D- SA Connection	2D_Terrain_Mod
2	4.1 ft	4.2 ft	5.7 ft	5.2 ft
3	4.3 ft	4.2 ft	5.2 ft	5.3 ft

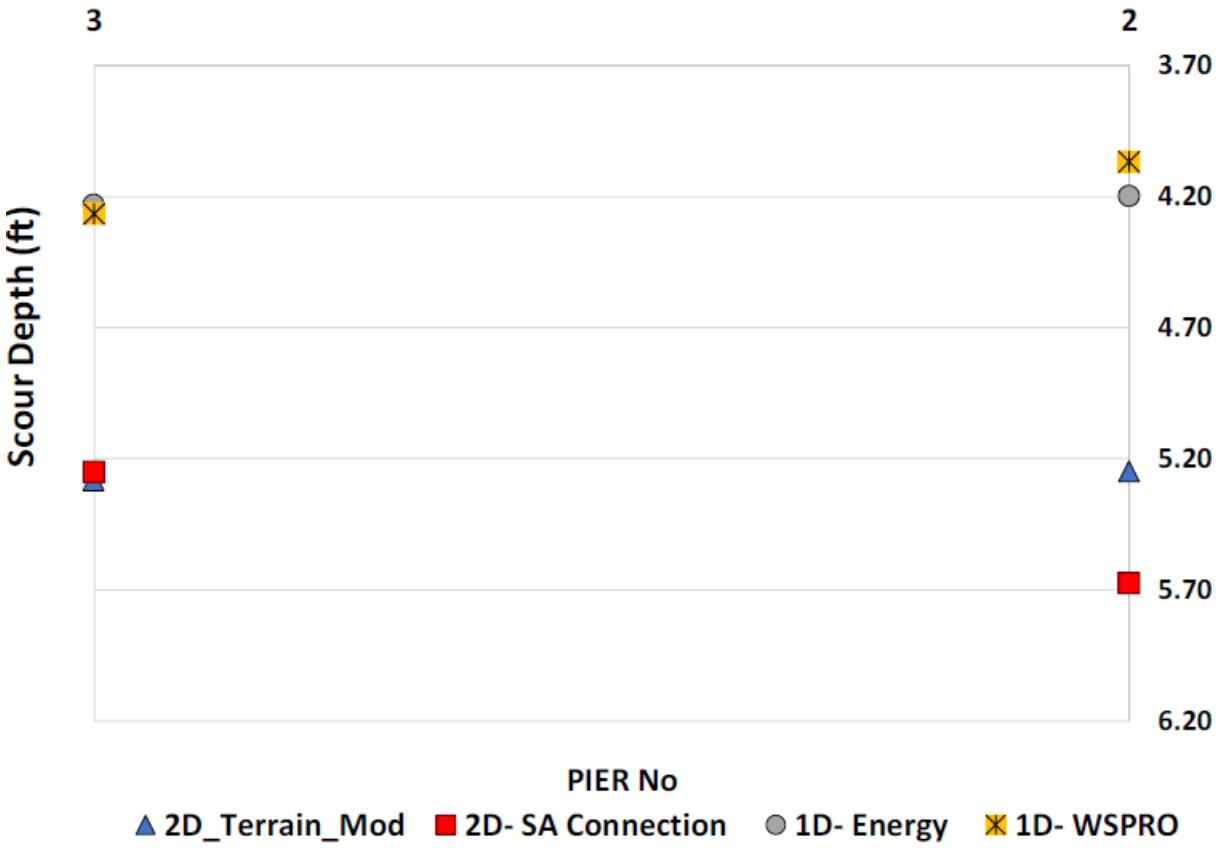

Figure F7. Scour results for BIN 010738 using HEC-18. Different Bridge modeling approaches. Peak Flow CNIII

Table F6. Scour values for BIN 010738 using HEC-18. Different Bridge modeling approaches. Peak Flow CNIII

Pier BrM	1D- WSPRO	1D- Energy	2D- SA Connection	2D_Terrain_Mod
2	4.3 ft	4.4 ft	5.4 ft	5.6 ft
3	4.3 ft	4.3 ft	5.9 ft	5.6 ft

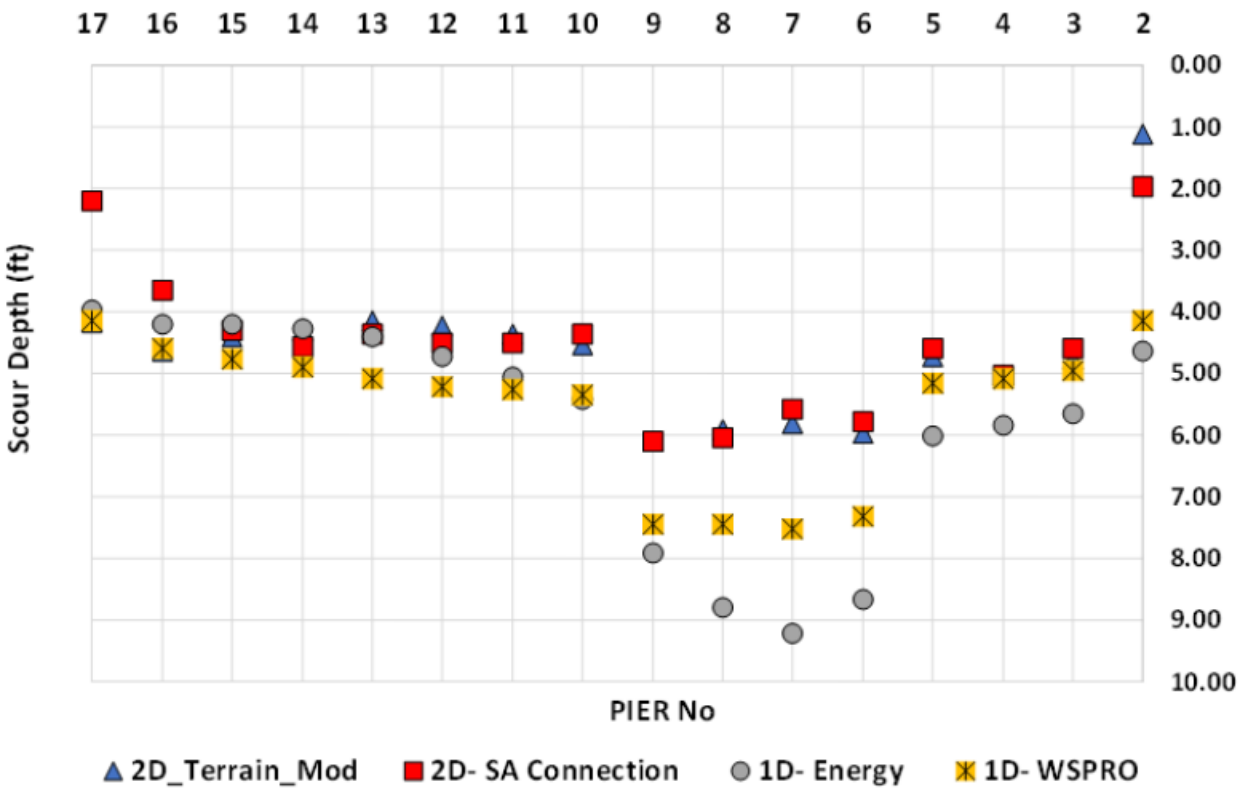

Figure F8. Scour results for BIN 013310 using HEC-18. Different Bridge modeling approaches. Peak Flow RRE

Table F7. Scour values for BIN 013310 using HEC-18. Different Bridge modeling approaches. Peak Flow RRE

Pier BrM	1D- WSPRO	1D- Energy	2D- SA Connection	2D_Terrain_Mod
2	2.9 ft	3.6 ft	0.0 ft	0.0 ft
3	4.6 ft	5.2 ft	4.8 ft	3.4 ft
4	4.6 ft	5.5 ft	4.3 ft	3.9 ft
5	4.8 ft	5.6 ft	3.9 ft	3.6 ft
6	6.8 ft	8.1 ft	4.9 ft	4.2 ft
7	7.0 ft	8.7 ft	4.7 ft	4.2 ft
8	7.0 ft	8.2 ft	5.1 ft	4.3 ft
9	7.0 ft	7.3 ft	5.2 ft	4.5 ft
10	5.0 ft	5.0 ft	3.8 ft	3.4 ft
11	4.9 ft	4.6 ft	3.9 ft	3.3 ft
12	4.8 ft	4.3 ft	3.8 ft	3.1 ft
13	4.7 ft	3.9 ft	3.6 ft	3.0 ft
14	4.5 ft	3.8 ft	3.8 ft	3.1 ft
15	4.3 ft	3.7 ft	3.7 ft	3.1 ft
16	4.2 ft	3.7 ft	2.8 ft	3.4 ft
17	3.7 ft	3.4 ft	1.9 ft	2.8 ft

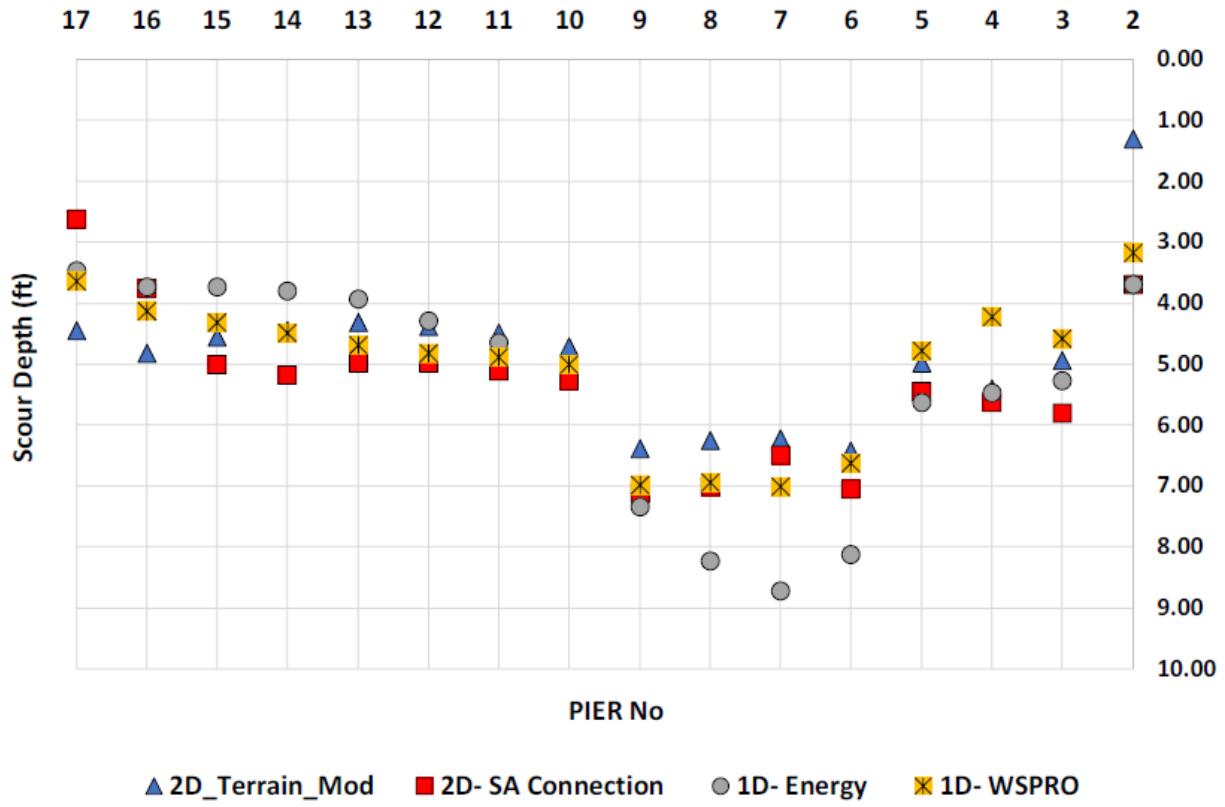

Figure F9. Scour results for BIN 013310 using HEC-18. Different Bridge modeling approaches. Peak Flow CNII

Table F8. Scour values for BIN 013310 using HEC-18. Different Bridge modeling approaches. Peak Flow CNII

Pier BrM	1D- WSPRO	1D- Energy	2D- SA Connection	2D_Terrain_Mod
2	3.2 ft	3.7 ft	3.7 ft	1.3 ft
3	4.6 ft	5.3 ft	5.8 ft	5.0 ft
4	4.2 ft	5.5 ft	5.6 ft	5.4 ft
5	4.8 ft	5.6 ft	5.4 ft	5.0 ft
6	6.6 ft	8.1 ft	7.1 ft	6.4 ft
7	7.0 ft	8.7 ft	6.5 ft	6.2 ft
8	7.0 ft	8.2 ft	7.0 ft	6.3 ft
9	7.0 ft	7.3 ft	7.1 ft	6.4 ft
10	5.0 ft	5.0 ft	5.3 ft	4.7 ft
11	4.9 ft	4.7 ft	5.1 ft	4.5 ft
12	4.8 ft	4.3 ft	5.0 ft	4.4 ft
13	4.7 ft	3.9 ft	5.0 ft	4.3 ft
14	4.5 ft	3.8 ft	5.2 ft	4.5 ft
15	4.3 ft	3.7 ft	5.0 ft	4.6 ft
16	4.1 ft	3.7 ft	3.8 ft	4.8 ft
17	3.6 ft	3.5 ft	2.6 ft	4.5 ft

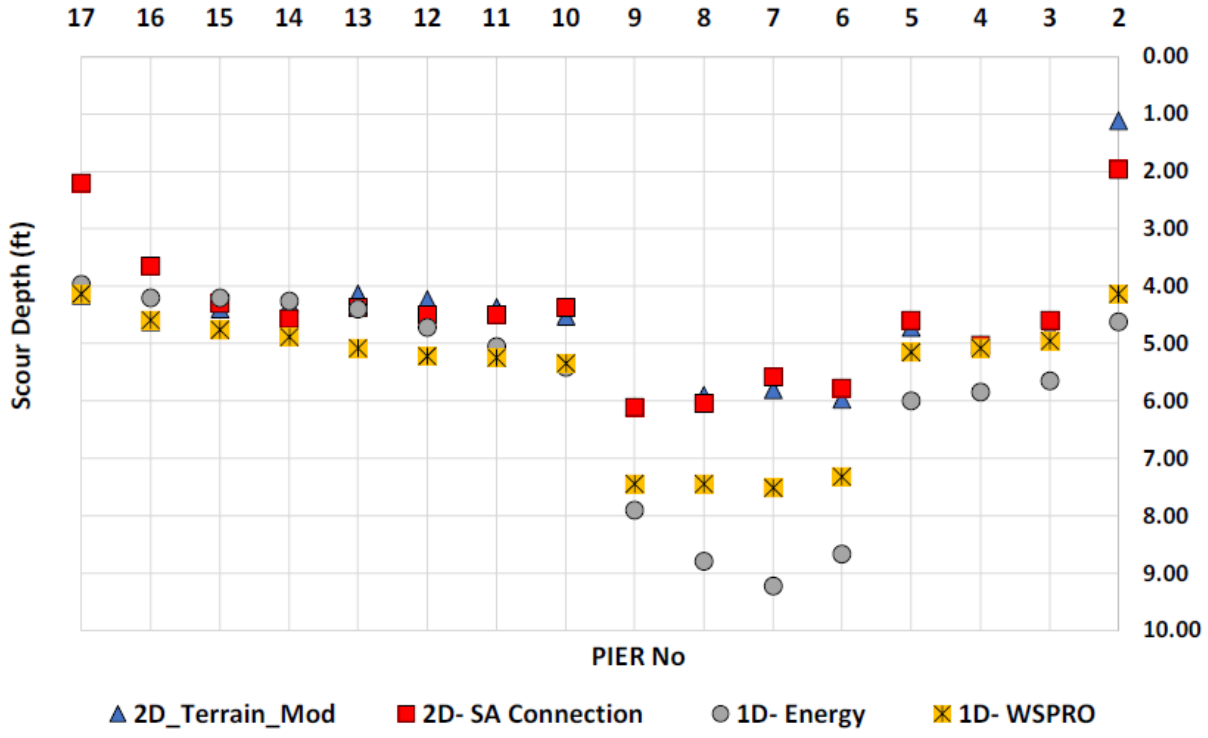

Figure F10. Scour results for BIN 013310 using HEC-18. Different Bridge modeling approaches. Peak Flow CNIII

Table F9. Scour values for BIN 013310 using HEC-18. Different Bridge modeling approaches. Peak Flow CNIII

Pier BrM	1D- WSPRO	1D- Energy	2D- SA Connection	2D_Terrain_Mod
2	4.13 ft	4.63 ft	1.97 ft	1.12 ft
3	4.95 ft	5.64 ft	4.59 ft	4.76 ft
4	5.09 ft	5.84 ft	5.02 ft	5.02 ft
5	5.15 ft	6.00 ft	4.59 ft	4.72 ft
6	7.32 ft	8.66 ft	5.77 ft	5.97 ft
7	7.51 ft	9.22 ft	5.58 ft	5.81 ft
8	7.45 ft	8.79 ft	6.04 ft	5.91 ft
9	7.45 ft	7.91 ft	6.10 ft	6.10 ft
10	5.35 ft	5.41 ft	4.36 ft	4.53 ft
11	5.25 ft	5.05 ft	4.49 ft	4.36 ft
12	5.22 ft	4.72 ft	4.49 ft	4.23 ft
13	5.09 ft	4.40 ft	4.36 ft	4.13 ft
14	4.89 ft	4.27 ft	4.56 ft	4.30 ft
15	4.76 ft	4.20 ft	4.30 ft	4.40 ft
16	4.59 ft	4.20 ft	3.64 ft	4.63 ft
17	4.13 ft	3.97 ft	2.20 ft	4.17 ft

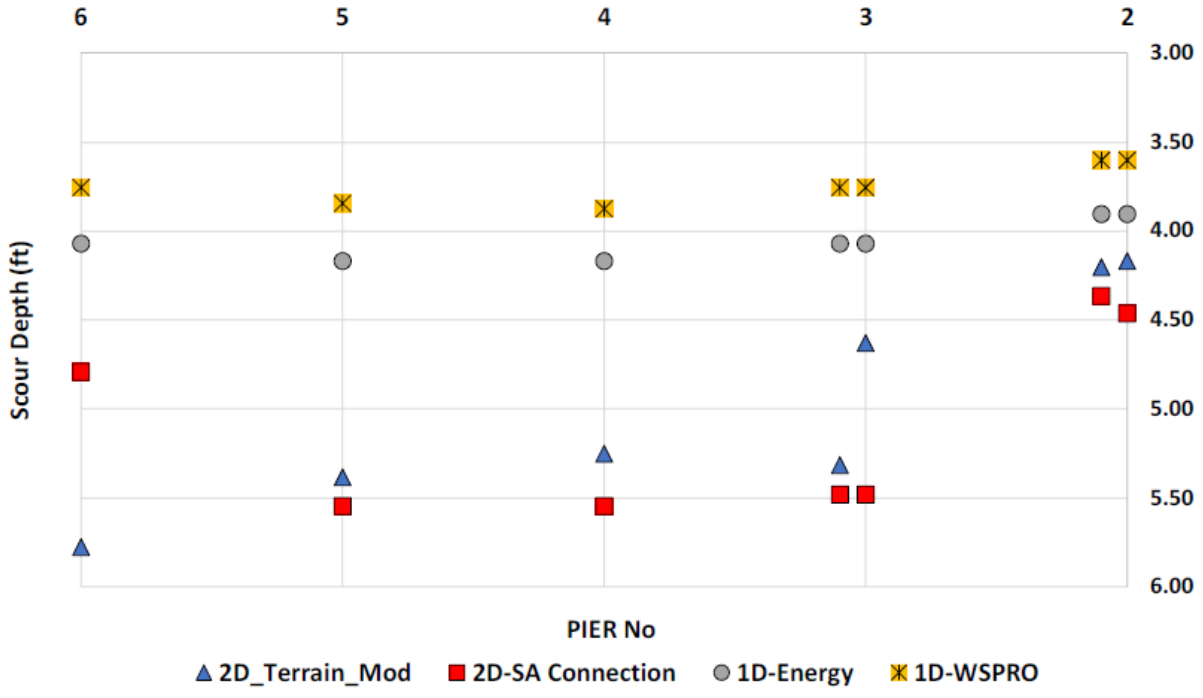

Figure F11. Scour results for BIN 007070 using HEC-18. Different Bridge modeling approaches. Peak Flow RRE

Table F10. Scour values for BIN 007070 using HEC-18. Different Bridge modeling approaches. Peak Flow RRE

Pier BrM	1D- WSPRO	1D- Energy	2D- SA Connection	2D_Terrain_Mod
2	3.6 ft	3.9 ft	4.5 ft	4.2 ft
2.1	3.6 ft	3.9 ft	4.4 ft	4.2 ft
3	3.8 ft	4.1 ft	5.5 ft	4.6 ft
3.1	3.8 ft	4.1 ft	5.5 ft	5.3 ft
4	3.9 ft	4.2 ft	5.5 ft	5.2 ft
5	3.8 ft	4.2 ft	5.5 ft	5.4 ft
6	3.8 ft	4.1 ft	4.8 ft	5.8 ft

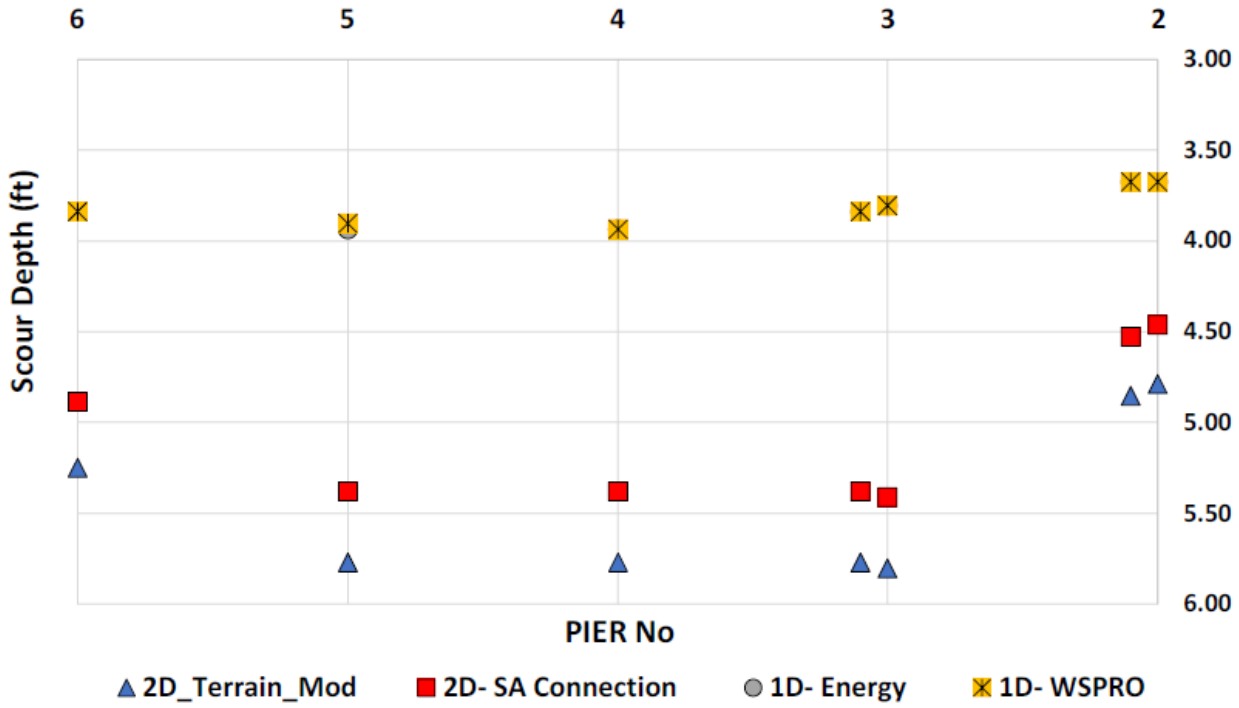

Figure F12. Scour results for BIN 007070 using HEC-18. Different Bridge modeling approaches. Peak Flow CNII

Table F11. Scour values for BIN 007070 using HEC-18. Different Bridge modeling approaches. Peak Flow CNII

Pier BrM	1D- WSPRO	1D- Energy	2D- SA Connection	2D_Terrain_Mod
2	3.7	3.7	4.5	4.8
2.1	3.7	3.7	4.5	4.9
3	3.8	3.8	5.4	5.8
3.1	3.8	3.8	5.4	5.8
4	3.9	3.9	5.4	5.8
5	3.9	3.9	5.4	5.8
6	3.8	3.8	4.9	5.2

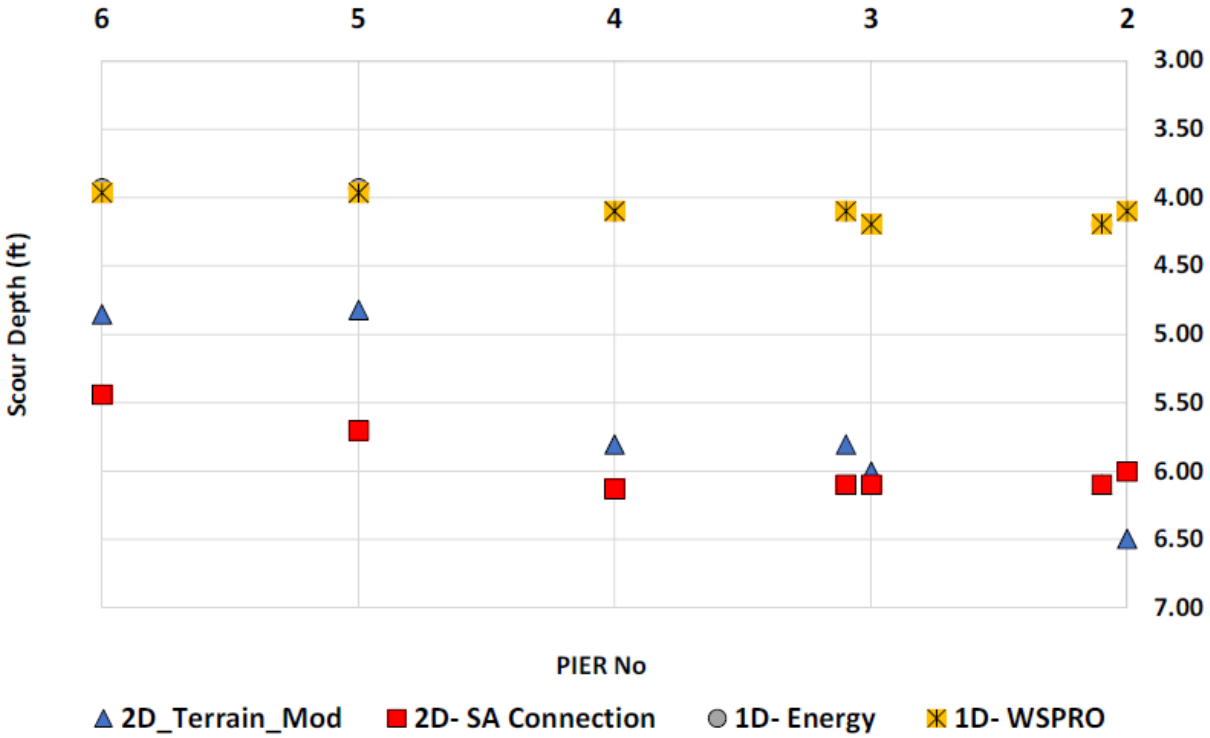

Figure F13. Scour results for BIN 007070 using HEC-18. Different Bridge modeling approaches. Peak Flow CNIII

Table F12. Scour values for BIN 007070 using HEC-18. Different Bridge modeling approaches. Peak Flow CNIII

Method	1D- WSPRO	1D- Energy	2D- SA Connection	2D_Terrain_Mod
2	4.1 ft	4.1 ft	6.0 ft	6.5 ft
2.1	4.2 ft	4.2 ft	6.1 ft	6.1 ft
3	4.2 ft	4.2 ft	6.1 ft	6.0 ft
3.1	4.1 ft	4.1 ft	6.1 ft	5.8 ft
4	4.1 ft	4.1 ft	6.1 ft	5.8 ft
5	4.0 ft	3.9 ft	5.7 ft	4.8 ft
6	4.0 ft	3.9 ft	5.4 ft	4.9 ft